



Thakur Educational Trust's (Regd.)

**THAKUR RAMNARAYAN
COLLEGE OF ARTS & COMMERCE**

ISO 21001:2018 Certified



List of Publications

Sr. No.	Particulars
1	Bubere V (2022), To study the future prospects of BSNL with respect to the bailout package of Rs. 1.64 lakh crore in the year 2022, Kanpur Philosophers, Page 89-91.
2	Singh R (2021), Size reduction of KLOPFENSTEIN-BALUN transformer for balanced antennas, Malaysian Journal of Science, Page 55-66.
3	Singh R (2020), Online signature verification using hybrid wavelet transform, International Journal of Electrical and Computer Engineering, Page 1823-1832.
4	Singh R (2018), Coplanar Stripline Loaded Reconfigurable Loop Antenna for WLAN and WiMAX Applications, Engineering Technology & Applied Science Research, Page 3479-3483.
5	Singh R (2018), Nonuniform C-Band Loop Antenna: A New Approach for Future UWB Applications, Engineering Technology & Applied Science Research, Page 3496-3501.
6	Singh R (2018), Multiband Printed Loop Antenna for UWB Applications, Helix The Scientific Explorer, Page 3481-3490.
7	Singh R (2018), Capacitive Gap Loaded Dual, Triple and Wide Band Loop Antenna, Helix The Scientific Explorer, Page 4580-4588.

NEW ARCHAEOLOGICAL AND GENOLOGICAL SOIETY KANPUR
A REGISTERED NON PROFIT ORGANISATIONERS
REGISTRATION NO. 346-2009-201 UNDER SOCIETIES ACT 21, 1860

KANPUR PHILOSOPHERS

An internationally peer reviewed and Refereed journal
of Humanities & Social Sciences, Law, Modernity,
Gender Studies and allied disciplines

Volume-X, Issue-I (E), 2023

KANPUR
PHILOSOPHERS

Chief Editor Atul Kumar Shukla

ISSN 2348 – 8301

Kanpur Philosophers

Volume X, Issue I(E), 2023

DOI: 10.13140/RG.2.2.13995.98084

**An internationally Peer Reviewed and Refereed Journal of History,
Archaeology, Indology, Epigraphy, Numismatics, Law, Literature
& allied disciplines of Arts, Humanities and Social Sciences**

**NEW ARCHAEOLOGICAL & GENOLOGICAL SOCIETY 125/L/89,
FF104, GOVIND NAGAR, KANPUR U.P. INDIA 208006
<https://sites.google.com/site/kanpurhistorian/>**

© Secretary, N.A.A.G.S. Kanpur India

Opinions expressed by the authors in the journal are not those of
N.A.A.G.S.

Secretary
New Archaeological & Genological Society
125/L/89, FF 104, Govind Nagar
Kanpur U.P. India -208006

Index
Kanpur Philosophers
Volume X, Issue I(E) : 2023

S.No.	TITLE	PAGE No
1	PRODUCTION RELIABILITY AND COMMON RISK TO CONTRACT FARMING	1
2	CONSTITUTIONAL ASPECTS OF INTELLECTUAL PROPERTY RIGHTS	8
3	THE LEGALITY OF CYBER SOCIALIZING AND THE BOOMING OF HI-TECH CRIMES AGAINST WOMEN	15
4	STUDY OF THE INDICATORS OF EFFECTIVENESS OF A COMPETITION LAW AND POLICY FOR A DEVELOPING COUNTRY	20
5	AN EXPERIMENTAL RESEARCH ON FAMILY INTERVENTION FOR DRUG ADDICTION TREATMENT AND REHABILITATION	30
6	A STUDY ON SPEECH RECOGNITION USING DEEP NEURAL NETWORK	39
7	EMPLOYER BRANDING: PERCEPTION & IMPORTANCE AMONG THEPOST-GRADUATE STUDENTS	42
8	CRIME BY AND AGAINST THE CHILDREN IN BROKEN FAMILIES	46
9	DOMESTIC VIOLENCE ACT AND-ITS ABUSE	52
10	MANAGING THE EMOTION IN BUSINESS ORGANISATIONS – A SUCCESS OR A FAILURE	60
11	MEASURING THE ENVIRONMENTAL DISCLOSURE SCORE (EDS) SCORE DIFFERENCES IN THE CEMENT COMPANIES OF INDIA	70
12	A COMPREHENSIVE STUDY ON THE IMPACT OF COVID -19 ON E-PAYMENT APPS	78
13	TO STUDY THE FUTURE PROSPECTS OF BSNL WITH RESPECT TO THE BAILOUT PACKAGE OF Rs. 1.64 LAKH CRORE IN THE YEAR 2022	89
14	A STUDY ON EXPLORING CHALLENGES FACED BY INSURANCE AGENTS IN MUMBAI REGION	92
15	MEASURING SATISFACTION OF THE RESPONDENTS FOR IMPACT OF INFLATION ACCOUNTING ON VARIOUS RATIOS	97
16	FUZZY JC IRRESOLUTE MAP IN FUZZY TOPOLOGICAL SPACES	104
17	MEASURING THE FINANCIAL PERFORMANCE OF LIC, SBI AND HDFC LIFE INSURANCE COMPANIES IN INDIA	111
18	NEW CLASS OF CLOSED AND OPEN MAPS IN SOFT TOPOLOGICAL SPACES	119
19	HUMAN RESOURCES AND INDUSTRIAL RELATIONS: COMMONALITIES AND DIFFERENCES	126
20	POLITICAL PARTICIPATION AND VOTER BEHAVIOUR: AN OVERVIEW	130



Kanpur Philosophers

CERTIFICATE OF PUBLICATION

This is to certify that the article entitled

**TO STUDY THE FUTURE PROSPECTS OF BSNL WITH RESPECT TO THE BAILOUT PACKAGE OF Rs. 1.64
LAKH CRORE IN THE YEAR 2022**

Authored By

Mr. Bubere Vaqar Athar

Asst. Professor Department of B.M.S., Thakur Educational Trust's Thakur Ramnarayan College of Arts &
Commerce

Published in

Kanpur Philosophers : **International Journal of humanities, Law and Social Sciences**

ISSN 2348-8301

Vol. X, Issue I (E) : 2023

UGC CARE Approved, Group I, Peer Reviewed and Referred Journal
by New Archaeological & Genealogical Society Kanpur India




Editor-in-Chief



TO STUDY THE FUTURE PROSPECTS OF BSNL WITH RESPECT TO THE BAILOUT PACKAGE OF Rs. 1.64 LAKH CRORE IN THE YEAR 2022

Mr. Bubere Vaqar Athar Asst. Professor Department of B.M.S., Thakur Educational Trust's
Thakur Ramnarayan College of Arts & Commerce : vaqar.bubere@trcac.org.in

Abstract

The paper highlights the phenomenon of bailout packages and why does Governments give bailout packages. Furthermore, the paper reviews and examines the literature available to find different aspects of bailout offered by the Government. Paper also puts forward neutrally professional arguments against and in favour of bailouts offered by the Government which seeks to give a new life to a sick company. This paper also tries to answer some vital questions as to why the Government gives out financial bailouts and why the current Government wants the BSNL to survive. It also explores different manners of bailout packages and whether the BSNL bailout package will work.

Key words: Bailout packages, Government, BSNL, Revival, Tax payer and Money.

Introduction: The Union Cabinet has approved a Rs 1.64-lakh crore revival package for the government-owned Bharat Sanchar Nigam Limited (BSNL), on July 27, 2022.

The package will have three main elements:

1. Improving the quality of BSNL services
2. Destress the balance sheet
3. Expand the company's fibre reach by merging Bharat Broadband Network Limited (BBNL)

The package will include a cash support of Rs 43,964 crore and non-cash support of Rs 1.20 lakh crore. The revival programme is for a four-year period, but most of it will be implemented in the first two years, he added.

The cash proponent will be used for spectrum allocation, capital expenditure and viability gap funding, the minister noted.

Funding for the same will come from three sources:

1. Issuance of Sovereign Guarantee Bonds
2. Conversion of AGR (Adjusted Gross Revenue) dues into equity
3. Issue of Preference Shares to the Government

Objectives:

1. To realise the motives behind the bailout packages offered by the Government
2. To understand the pros and cons related to bailout packages
3. To acknowledge why does Governments give out bailout packages
4. To know why does Government want BSNL to survive
5. To evaluate whether BSNL bailout packages work

Literature Review: Bailout is a general term for extending financial support to a company or a country facing a potential bankruptcy threat. It can take the form of loans, cash, bonds, or stock purchases. A bailout may or may not require reimbursement and is often accompanied by greater government oversight and regulations.

The reason for the bailout is to support an industry that may be affecting millions of people internationally and could be on the verge of bankruptcy due to prolonged financial crises.

Bailout policies come in various forms, the most common being direct loans or guarantees of third-party (private) loans to the rescued entity. These direct loans are often on terms favouring the entity being rescued. Sometimes even direct subsidies are provided to the parties concerned. Stock purchases are also not uncommon.

The government or the financing body places strict requirements such as restructuring of organisation, no dividend payment to shareholders, change of management and in some cases a cap on salaries of executives till a stipulated time period or the repayment of dues. This may also be followed by a temporary relaxation of rules that may impact the accounts of the rescued entity.

Why does the Government consider bailout packages?: A bailout could be done for profit motives, such as when a new investor resurrects a floundering company by buying its shares at fire-sale prices, or for social objectives, such as when a wealthy philanthropist reinvents an unprofitable fast food company into a non-profit food distribution network. However, the common use of the phrase occurs where government resources are used to support a failing company typically to prevent a greater problem or financial contagion to other parts of the economy.

These bailouts not only save the company but also help the economy and save jobs of thousands of people working for years in a company. Bailout support from the Government is cheap money (low cost of capital), which is easily available in abundance.

Pros and cons of the bailout packages:

Pros:

- The short term stability. Often bailouts are used on “too big to fail” companies. Companies that, if they fail, would cause a huge ripple effect in the economy. The consideration is that a lot of people would be laid off, and so by saving the company the jobs are also saved. So it seems like it's good for the working class.
- For the business owners, usually large corporations, it's a huge benefit. They can continue “business as usual” knowing full well that if they screw up badly, then the government will come and save them.

Cons:

- You are taking tax payer money and spending it on failing businesses. This money was supposed to go to other things. Or rather, the money is borrowed from future taxes, meaning you would have to keep taxes higher than needed.
- You are keeping failing businesses alive artificially. This creates a problem within a free-market, as better suited businesses cannot take the place of the “too big to fail” companies, and thus the market is no longer free.
- You aren't fixing the core issue. Failing is a great way to avoid something happening again later. Bailing out companies will only reinforce their bad behavior without removing the people who made it happen in the first place from their positions. The problem here is every bailout, every safety net, just makes the next problem and need for bailout that much bigger. Bailouts create the “too big to fail” scenarios.
- It helps the “big guys” and hurts the little guys. Very rarely are small businesses given bailouts. They aren't “too big to fail”.

Why does the Government want BSNL to survive?: The fresh infusion of funds this month is specifically aimed at conversion of the company's dues into equity, providing financial support and allocation of spectrum to provide 4G services. The intent clearly is to get the telco, which has been

losing market share over the years, back on its feet at a time when private players, such as Jio and Bharti Airtel, are already working on rolling out 5G services.

For one, the view is that India needs an efficient state-run telco in a world where digital boundaries have blurred and cyber security has taken precedence. The government needs a secured state-run network for high security communication. Also, private telecom operators tend to focus on high revenue markets, and fail to meet communication needs in remote areas.

Further, the telecom space is evolving in a manner that could leave only two big players standing. A third entity is needed to ensure healthy competition and for the benefit of consumers at large. However, BSNL will need a complete overhaul to stand a chance to emerge as the third big player. The public sector enterprise will need to imbibe a competitive spirit, upskill its employees and come up to speed in a fast-evolving and investment-heavy industry. Still bound by socialist era principles of doing business, BSNL's hiring policies are unlike that of the private players: salaries are thought to be inflated and employee morale has been down for a while.

Findings:

- Providing financial support to the company
- Allocation of 4G spectrum
- Having an efficient state-run telco for the integrity of our country
- Government need a secured state-run network for high security and cyber security communication
- Want to break the duopoly of private run telco in free and fair market

Conclusion: It's pertinent to note that BSNL's first Rs 70,000 crore bailout package in 2019 didn't deliver. Though it addressed the excess workforce issue, reducing losses by half and total expenditure by 24%, it's the other and most crucial part of the package that didn't yield. In 2019, the government had provided Rs 24,000 crore for 4G services, but BSNL wasn't technology-ready, which led to declining revenues. Even today, it lacks 4G connectivity on a pan-India basis—a decade after 4G services first began and just when competitors are moving towards 5G. Worse, BSNL even surrendered unutilised 2G spectrum last year, where most operators have subscribers.

BSNL has a distinctive presence in far-flung areas, improving rural teledensity considered un-viable by private operators. But profits from a social objective are always slim.

Meaning BSNL needs autonomy and separation from bureaucracy to make commercial decisions for the wireless and broadband segment, where its market share is a pitiful 9.7% and 2.9%, respectively. Both BSNL's topline and subscriber base aren't improving, and the government may have to keep bailing it out unless revenues increase.

References:

1. *Cash bailout alone can't help BSNL.* (2022, July 30). Retrieved from The New Indian Express: <https://www.newindianexpress.com/opinions/editorials/2022/jul/30/cash-bailout-alone-cant-help-bsnl-2482143.html>
2. Ludvigsen, M. (n.d.). *What are the pros and cons of government bailouts?* Retrieved from Quora: <https://www.quora.com/What-are-the-pros-and-cons-of-government-bailouts>
3. Prabhakar, B. (2022, July 28). *Cabinet approves Rs 1.64 lakh crore revival package for BSNL.* Retrieved from MoneyControl: <https://www.moneycontrol.com/news/business/cabinet-approves-rs-1-64-lakh-crore-re-vival-package-for-bsnl-8899191.html>
4. Punj, S. (2022, August 04). *Why a bailout package alone cannot revive BSNL.* Retrieved from India Today: <https://www.indiatoday.in/india-today-insight/story/why-a-bailout-package-alone-cannot-revive-bsnl-1983746-2022-08-04>
5. *What is 'Bailout'.* (n.d.). Retrieved from The Economic Times: <https://economictimes.indiatimes.com/definition/bailout>

SIZE REDUCTION OF KLOPFENSTEIN-BALUN TRANSFORMER FOR BALANCED ANTENNAS

Shailendra P. Shastri^{1a}, Ravish R. Singh^{2b} and Sandeep Y. Pawar^{3c}

^aFaculty of Engineering, Pacific Academy of Higher Education and Research University, Udaipur, Rajasthan-313003, INDIA. Email: shastri_shailendra@rediffmail.com

^bAcademic Advisor, Thakur Educational Trust, Mumbai-400068, INDIA. Email: ravishrsingh@yahoo.com

^cDepartment of Electronics and Telecommunication Engineering, Vidyavardhini's College of Engineering and Technology, Vasai, Maharashtra-401202, INDIA. Email: sandeepyp@yahoo.co.in

Corresponding author: shastri_shailendra@rediffmail.com

Received: 7th May 2019

Accepted: 11th Mar 2020

Published: 28th Feb 2021

DOI: <https://doi.org/10.22452/mjs.vol40no1.5>

ABSTRACT A compact broadband BALUN transformer is designed using the Klopfenstein taper line transformer approach to transform a 50 Ω impedance into 100 Ω . To reduce the length of the conventional BALUN, a straight microstrip (MS) line is modified as a curved MS line. The proposed compact BALUN is 56.7%–73% smaller w.r.t the straight conventional BALUN but at the cost of a 4.5%–13% reduction in the overall band. The conventional BALUN has a measured % bandwidth of 165, while the compact BALUN has a result of 159. The measured results agree with the simulated results.

Keywords: Unbalanced line, BALUN, balanced line, coplanar stripline, % bandwidth and tapered microstrip line.

1. INTRODUCTION

R. W. Klopfenstein proposed an improved design of tapered transmission lines in 1956, and since then, this technique has been used to improve the performance of high-frequency devices. It is an impedance matching transmission line to keep the reflection coefficient at the minimum over a particular passband (Klopfenstein, 1956). This tapered line is an important part of a BALUN transformer when it comes to the transformation of impedance and conversion from an unbalanced line into a balanced one. The BALUN transformer is one of the most important elements when it is required to feed a balanced antenna using an unbalanced feed. Unfortunately, the high-frequency line available to feed balanced antennas is unbalanced in nature. Therefore, when an unbalanced feed is directly

connected to a balanced antenna, the current entering the antenna and the current returning from the antenna differ. This action changes the antenna impedance seen by the feed line and is different from the designed impedance of the antenna. The problem can be resolved using a BALUN transformer between the antenna feed point and the single-ended transmission line.

There are many printed BALUNs proposed in the literature. A broadband coplanar waveguide (CPW) to coplanar strip (CPS) transmission line transition exhibited very good performance up to 55 GHz (Anagnostou et al., 2008). A wide band from 1.1 GHz to 10.5 GHz was achieved using a transition from a multisection microstrip (MS) line to a CPS line terminated with a quarter wavelength radial stub (Tu & Chang, 2006). A tapered Klopfenstein line was used to match

impedances between a Ka-band pillbox window and a Helix-TWT. The designed transformer gives excellent performance across 30 GHz to 34 GHz (Resley & Song, 2012). The performance of the Klopfenstein taper line for various loads and lengths was investigated to reduce the maximum group delay with an acceptable variation of the impedance bandwidth (Ruvio & Ammann, 2008). BALUNs have also been designed to feed slot antennas, and one such BALUN was a fourth-order modified Marchand BALUN covering a band from 0.5 GHz to 5.5 GHz. This wideband performance was achieved using a slot line to MS line transition with radial stubs (Maksimovitch et al., 2007). A dipole antenna with both arms on opposite sides of a substrate was excited using an asymmetric MS line BALUN transformer. This BALUN comprised a taper ground plane connected to one arm of the dipole and the MS line of the BALUN connected to the other arm of the dipole present on the other side of the substrate (Bah, 2016). Impedance transformation using a taper transmission line technique is not restricted to printed technology but also extends to the coaxial transmission line (Vega et al., 2011). A larger band of 30:1 can be achieved using multiple transitions from MS to coplanar waveguide and back to the MS line (Meng et al., 2016).

All the previously designed BALUNs or taper transformer structures are geometrically straight, and thus, occupy relatively large onboard space. Here, we propose a technique that can reduce the size of straight BALUNs or taper line

transformer structures. The proposed broadband BALUN is much smaller compared with conventional BALUNs. The conventional straight structure is modified with an equivalent curved structure, and onboard space is saved. The complete design of the conventional BALUN is discussed along with the design technique of the proposed BALUN. The conventional and proposed BALUNs are compared in terms of bandwidth and size. The BALUN is designed to transform an impedance of 50Ω to 100Ω , but the solution can also be applied to other impedances.

The remainder of the paper proceeds as follows: Section 2 introduces a conventional way of designing a wideband BALUN using the Klopfenstein taper line technique. Section 3 is dedicated to modification in the conventional taper BALUN to reduce its size. Finally, Section 4 provides the results and discussion for the implemented BALUN transformers.

2. DESIGN OF A TAPERED BALUN

To design a tapered BALUN, the FR-4 substrate is used with a thickness of 0.8 mm. Figure 1 is a representation of a taper transmission line loaded with a load Z_L ; in the figure, $Z(z)$ is the characteristic impedance variation of the taper line, and Z_0 is the characteristic impedance or reference impedance. The design of the BALUN is based on the Klopfenstein taper transformer, which is derived from a stepped Chebyshev transformer.

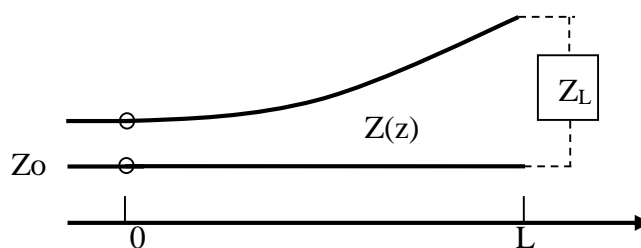


Figure 1. Taper transmission line loaded with load Z_L and driven by reference impedance Z_0

The taper line transformer of length L is divided into n sections of different impedances to transform Z_L into Z_0 . The following Klopfenstein taper relation is

used to determine the characteristic impedance variation of the taper section (Pozar, 1998):

$$Z(z) = \frac{1}{2} \ln Z_0 Z_L + \frac{\Gamma_0}{\cosh A} A^2 \phi \left(\frac{2z}{L} - 1, A \right), \tag{1}$$

where $0 \leq z \leq L$ (length of the taper line), $Z(z)$ is the characteristic impedance variation along the line and $Z_0 = 50 \Omega$ and $Z_L = 100 \Omega$.

The function $\phi(x, A)$ is defined as

$$\phi(x, A) = -\phi(-x, A) = \int_0^x \frac{I_1(A\sqrt{1-y^2})}{A\sqrt{1-y^2}} dy, \tag{2}$$

where $I_1(x)$ is the modified Bessel function, and

$$A = \cosh^{-1} \left\{ \frac{\Gamma_0}{\Gamma_m} \right\}, \tag{3}$$

$$\Gamma_0 = \frac{Z_L - Z_0}{Z_L + Z_0}, \tag{4}$$

$$\Gamma_m = \frac{\Gamma_0}{\cosh A}, \tag{5}$$

where Γ_m is the maximum ripple in the passband of the transformer and is assumed by the designer. Moreover, Γ_0 is the reflection coefficient at zero frequency, and it is given by (4). The passband of the transformer is defined for $\beta L \geq A$.

The following equation is used to produce the relation between Γ and βL , as shown in Figure 2:

$$|\Gamma| = \frac{1}{2} \ln \left[\frac{Z_L}{Z_0} \right] \left[\frac{\sin \left(\frac{\beta L}{2} \right)}{\frac{\beta L}{2}} \right]^2. \tag{6}$$

Here, $|\Gamma|$ is the magnitude of the reflection coefficient along the taper line and β is the phase constant.

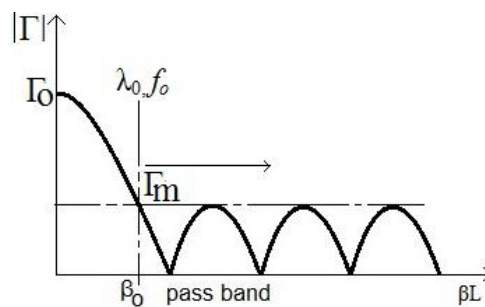


Figure 2. Reflection coefficient as a function of βL for an n section Tchebycheff transformer

In Figure 2, β_0 is the phase constant for the largest wavelength λ_0 or the smallest frequency f_0 for which the reflection coefficient is Γ_m . It can be

$$\beta L = A = \beta_0 L. \tag{7}$$

β_0 is expressed as

$$\beta_0 = \frac{2\pi}{\lambda_0}. \tag{8}$$

Equation (7) also shows that the maximum operating wavelength of the taper line depends on the taper length L . A larger L ensures a lower operating frequency in the passband for which the maximum reflection coefficient is Γ_m . Therefore, to have a lower operating frequency, the length of the taper line should be larger. Further discussion and

observed that Γ_m is the maximum reflection coefficient in the passband. The largest wavelength is found using the relation for a known L :

simulations elaborate on the relations among Γ_m , L and β . Figure 3 shows the behaviour of the reflection coefficient along the taper line for the assumed values of Γ_m ranging from 0.01 to 0.03. The taper line lengths were chosen as 3 cm and 5 cm. From the figure, it can be observed that the variation in Γ_m affects the least frequency in the passband.

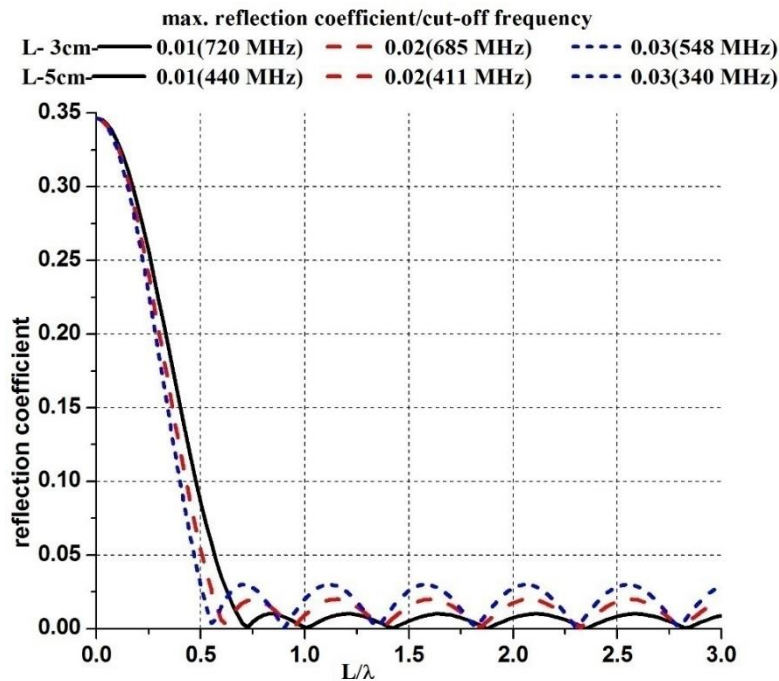


Figure 3. Behaviour of the reflection coefficient of taper line through calculation

The complete analysis of Figure 3 is tabulated in Table 1(a), and a summary of similar analysis for the taper line of length

5 cm is tabulated in Table 1(b). The conclusions drawn from Figure 3 and Table 1 are as follows:

- 1) A larger value of Γ_m reduces the minimum frequency in the passband. The minimum frequency in the passband can be calculated using

$$f_0 = \frac{3 * 10^8}{\lambda_0 \sqrt{\epsilon_r}}, \tag{9}$$

Where $\sqrt{\epsilon_r}$ is relative dielectric constant of the dielectric material FR-4. Therefore, the minimum frequency f_0 in the passband is inversely proportional to the length of L . This frequency can be calculated by selecting L and using relations (3), (7), (8) and (9).

- 2) The operating frequency f is much smaller than f_0 for the reflection coefficient Γ of about -10 dB, as shown in the last column of Table 1. Furthermore, f can be calculated from (6) and (9).

Table 1 (a). Summary of relations among Γ_m, L and β

$Z_L = 100, Z_0 = 50, L = 3 \text{ cm}, \Gamma_0 = 0.333$					
Sr. No	Γ_m	A	f_0 GHz	Γ_m (dB)	$f_{@ -10 \text{ dB}}$
1	0.01	4.23	3.7	-40	800 MHz
2	0.02	3.54	3.0	-34	690 MHz
3	0.04	2.85	2.5	-28	550 MHz

Table 1 (b). Summary of relations among Γ_m, L and β

$Z_L = 100, Z_0 = 50, L = 5 \text{ cm}, \Gamma_0 = 0.333$					
Sr. No	Γ_m	A	f_0 GHz	Γ_m (dB)	$f_{@ -10 \text{ dB}}$
1	0.01	4.23	2.2	-40	430 MHz
2	0.02	3.54	1.85	-34	410 MHz
3	0.04	2.85	1.49	-28	340 MHz

In this section, a taper line transformer is designed using data from Table 1a; this is summarised in Table 2. The same transformer is modified to have a compact size in the next section.

The taper line transformer under consideration has a -40 dB (Γ_m) reflection coefficient from 3.7 GHz onwards, whereas the -10 dB frequency is at 800 MHz.

Table 2. Assumed design data and simulated results of taper line.

Z_L	Z_0	Γ_m	f_0	$f_{@ -10 \text{ dB}}$	L
100 Ω	50 Ω	0.01 / -40 dB	3.7 GHz	800 MHz	3 cm
Simulated results		-21.7 dB	3.7 GHz	624 MHz	3 cm

The complete BALUN structure comprising the taper line transformer and a CPS line is shown in Figure 4. The taper line is the MS line, and it is unbalanced in nature, whereas the CPS line is balanced. In this section, a taper line is simulated to transform 50 Ω to 100 Ω impedance. The same taper line transformer is added with a CPS line of 100 Ω to complete the BALUN transformer.

The length of the taper line is 30 mm, and it is divided into 20 sections, each of which is 1.5 mm long. The width of each section is different as these small lines represent different impedances along the taper line. The impedance of the first section is 51 Ω , marked as ‘1’ in Figure 4. The impedance of the last section is 98.9 Ω , marked as ‘20’. The width of the first section is 1.44 mm and that of the last section is 0.32 mm. Section ‘0’ in Figure 4

is a 50 Ω MS line of 5 mm in length; and it is used to accommodate SMA connectors. The electrical behaviour of the taper line is shown in Figure 5, and the results are summarised in Table 2. The passband is available from 3.7 GHz with a reflection

coefficient of -21.7 dB. The -10 dB frequency is available at 624 MHz. The simulated response of the taper line for the reflection coefficient in Figure 5 is similar to the calculated response in Figure 3, with a difference in Γ_m .

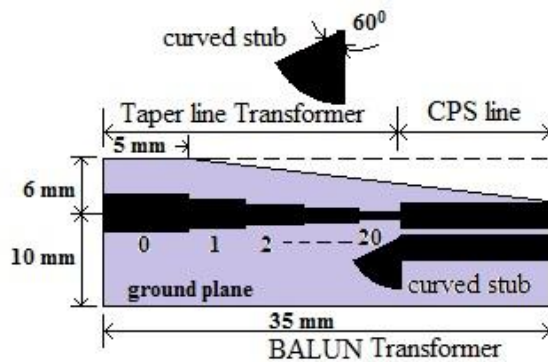


Figure 4. Structure of BALUN transformer using a taper line

To change the taper geometry into a BALUN, a CPS line of 100 Ω is added. The gap between the CPS lines is 0.25 mm, and the width of the CPS is 1.44 mm. The CPS line is added with a broadband radial stub which also plays an important role in changing the orientation of the electric field (Tu & Chang, 2006). The band considered for the analysis is 1 GHz to 9 GHz. Therefore, the calculated radius of the curved stub is approximately 8.5 mm, which is 1/4th of the wavelength at the centre frequency of the assumed band. The radius of the radial stub is changed to

$$\text{MS line} + \text{taper line} + \text{CPS line} = 5 + 30 + 11 = 46 \text{ mm}$$

3. DESIGN OF PROPOSED COMPACT BALUN

To reduce the size of the BALUN,

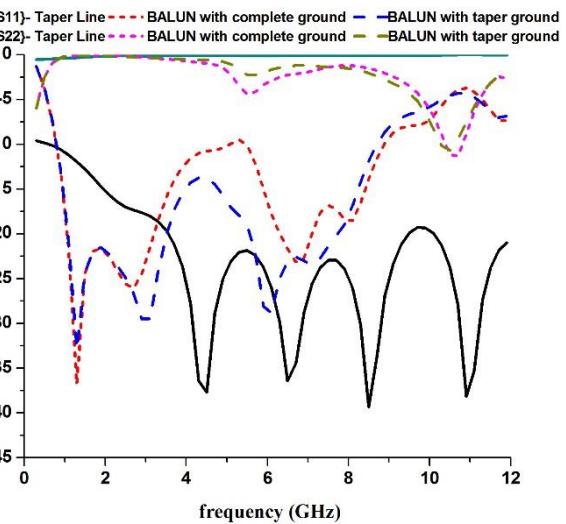


Figure 5. Frequency V/S reflection coefficient of taper line, and BALUN transformer

7.5 mm only after multiple simulations to obtain optimum performance from the BALUN for the assumed band. Figure 5 shows that the electrical band spans from 800 MHz to 8.7 GHz with an insertion loss of -3.2 dB at 6.1 GHz. The inclusion of taper ground improves S_{21} and is less than -3 dB for the band. The shape of the taper ground plane is shown in Figure 4. The CPS length is found to influence the performance of the BALUN significantly, and the % bandwidth of 166 is obtained only for the CSP line of length 11 mm. The total length of the BALUN is

the tapered section comprising 20 small MS lines is changed into a curved structure. The proposed structure of the tapered transmission line is shown in Figure 6 and

is compared with the straight taper line. The complete proposed reduced size BALUN is shown in Figure 7. It comprises an MS line, taper-curved MS line and CPS line. The input is applied to the MS line and is expressed as input port-1, while the output is taken at the balanced port (i.e. at the CPS line), which is expressed as output port-2. The dimensions of the proposed structure and the shape of the ground plane are shown in Figure 7. The first and the last two sections of the tapered line are kept as they are to avoid any abrupt change in the entire structure between the MS and CPS lines. The total length of the remaining 17 sections is 27 mm. This length is changed into a curved structure whose outer radius is equal to $27 / \pi$ (i.e. 8.2 mm) as it is half of a complete circle. Since one end of the

taper line is wider than the other end, the structure of the curved line is also kept tapered and width W_1 is larger than the width W_2 , Figure 6. The width W_2 is taken as 0.34 mm, which is equal to the width of the 19th section of the taper line. The width W_1 is kept equal to the width of the second section and is 1.4 mm. The first section is kept as it is and is aligned with the MS line shown in Figure 7. The radius of the stub is kept at 7.5 mm. The proposed compact BALUN with a curved MS line of radius 8.2 is simulated for an 8.5 mm radius for analysis purposes. It is observed in Fig. 8 that the reflection coefficient is very poor from 5.5 GHz to 6.2 GHz. It is observed that not only the reflection coefficient but also the insertion loss is larger than -3 dB from 5.7 GHz to 6.3 GHz.

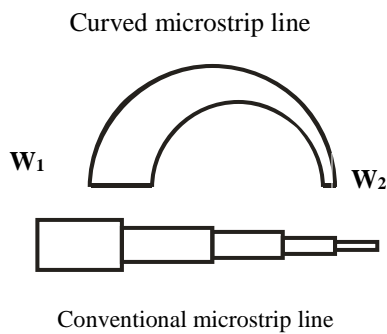


Figure 6. Proposed taper curved MS line and conventional taper line

It can be observed in Figure 4 that all the taper sections are connected along a straight line and there is a smooth transition in the cross-sectional dimension of the taper line. To have a smooth transition from section '1' to '2' in the proposed BALUN, section '1' is slightly tapered; its impact on the BALUN performance is shown in Figure 8. There is no change in the insertion loss with this taper section, but a small

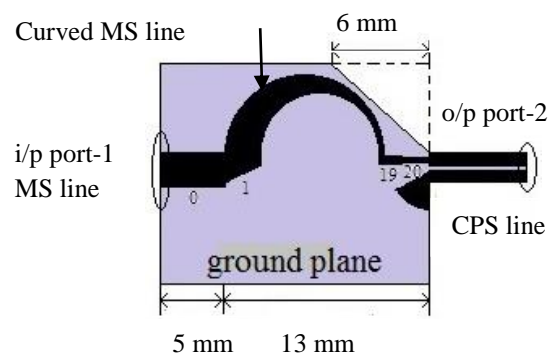


Figure 7. The proposed BALUN transformer with a tapered ground plane

improvement is observed in the reflection coefficient from 5.5 GHz to 6.2 GHz. To have a smooth transition of the electric field from the MS line to CPS line, the upper part of the ground plane is also tapered, as shown in Figure 7. This also ensures the similarity between structures of the conventional BALUN shown in Figure 4 and the proposed BALUN shown in Figure 7.

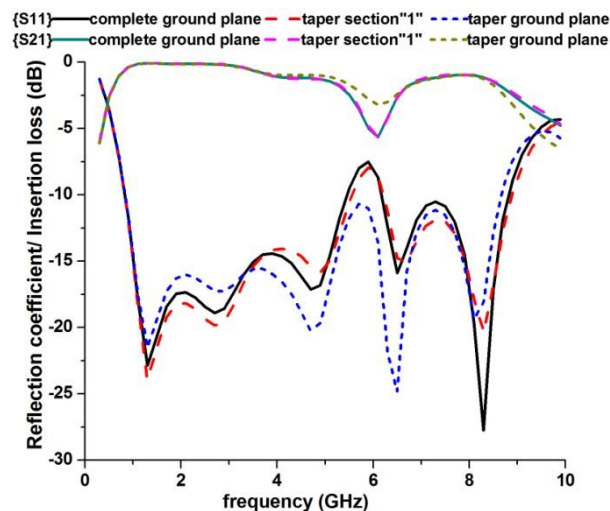


Figure 8. Result of frequency V/S reflection coefficient/insertion loss for a radius of MS line of 8.5 mm

It can be observed in Figure 8 that the taper ground structure influences the overall performance significantly. The reflection coefficient is well below -10 dB from 0.844 GHz to 8.66 GHz. The taper ground plane also improves the insertion loss, and the maximum insertion loss observed is -3.18 dB at 6.1 GHz. The proposed structure with a tapered section ‘1’ and ground plane works well as a BALUN transformer. It is observed only after multiple simulations that the CPS length can be reduced to 10 mm while maintaining the optimum performance of the proposed BALUN.

To analyse the impact of the outer radius of the curved MS line on the performance of the proposed structure, different outer radii of the curved MS line are taken for simulation, keeping widths W_1 and W_2 , the stub radius and the CPS length constant. The reflection coefficient and insertion loss of the proposed BALUN for the different outer radii of the curved MS line are shown in Figure 9. It can be observed that, when the radius of the MS line is 3 mm, there are two bands available, one from 1.21 GHz to 5.41 GHz, and the other from 6 GHz to 9.2 GHz. The insertion loss for this band is less than -3 dB. The reflection coefficient from 5.41 GHz to

6 GHz is -9.7 dB, and if it is considered approximately equal to -10 dB, then there is a complete -10 dB band available from 1.21 GHz to 9.2 GHz with a % bandwidth of around 154. The % bandwidth improves to 157 when the radius increases to 4 mm. There is an increase in the insertion loss from 9.1 GHz to 9.6 GHz. Therefore a -10 dB bandwidth with insertion loss less than -3 dB is available from 1.06 GHz to 9.1 GHz. The further increase in the outer radius of the curved MS line to 5 mm improves the % bandwidth to 161.5 with insertion loss less than -2.2 dB. The curved MS line with a radius of 5 mm gives the widest bandwidth for minimum insertion loss.

Reduction in the radius of the curved MS line below 3 mm reduces the bandwidth of the BALUN and increases the insertion loss. A summary of the electrical performance under different radii of the curved MS line of the compact BALUN is tabulated in Table 3. The length of the CPS line is taken as 10 mm for all the cases covered, and this provides the optimum result. The total length of the proposed BALUN is curved MS line + length of two end sections of tapered line + CPS length, that is, $10 + 3 + 10 = 23$ mm. In contrast, the conventional BALUN has length

(tapered line 20*1.5) 30 + 11 (CPS line) = 41 mm. A 5 mm length of MS line

accommodating the SMA connector was discarded in both cases.

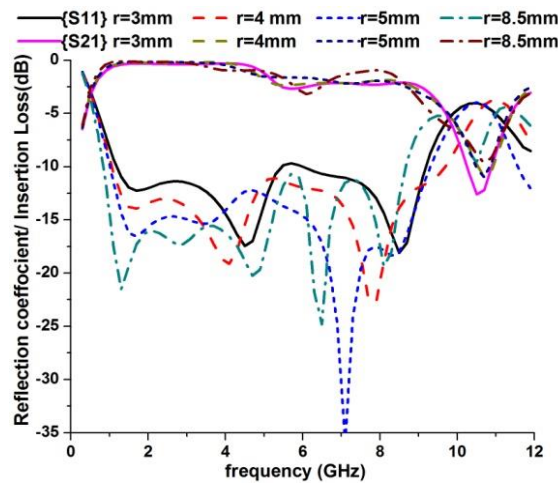


Figure 9. Result of frequency V/S reflection coefficient/insertion loss for different radius of MS

Table 3. Comparative analysis of the proposed BALUN for different radius of curved MS line

Radius (MS Line) mm	f_u-f_l GHz (-10 dB)	BW GHz	% BW	S ₂₁ dB
8	8.66–0.84	7.82	165	-3.18
5	9.3–0.99	8.31	161.5	-2.2
4	9.6–1.06	7.66	157	-4.7
3	5.41–1.21	4.2	127	-2.7
	9.2–6	3.2	42	

To design the proposed BALUN transformer, the following steps apply once the length of taper line is fixed:

- Using the Klopfenstein taper relation to determine the impedance of the first two and last two sections of a taper line and calculate the width of these sections.
- The radius of the outer curved MS line = (Length of taper line – length of three sections of taper line) / π . Choosing W_1 as the width of the N_2 section and W_2 as the width of the (N-1) section. N_2 is the second section of tapered line and N is total sections.
- Choosing CPS line length can be chosen for maximum bandwidth and minimum insertion loss.

- Further reducing the radius of the curved MS line to have the smallest possible size of the overall BALUN.

4. RESULTS AND DISCUSSION

The conventional and proposed compact BALUNs were simulated using CST STUDIO and developed on FR-4. Both the BALUNs were measured using a vector network analyser. There were four different cases of proposed BALUNs, but the BALUN with a curved MS line with a 5 mm radius was manufactured. The BALUN with this radius gives the largest bandwidth and the smallest insertion loss. Figure 10 shows a photograph of the BALUNs. Both were loaded with a 100 Ω SMD resistor at

the output port. The measured results of both the BALUNs, along with the simulated results, are shown in Figure 11. The conventional BALUN shows complete band coverage from 0.87 GHz to 9 GHz. S_{21} is not included because BALUNs are

designed as a single port device. The % bandwidth for the conventional BALUN is 165. The measurement of the proposed BALUN shows that the % bandwidth was 159% for the frequency range from 1.1 GHz to 9.65 GHz.

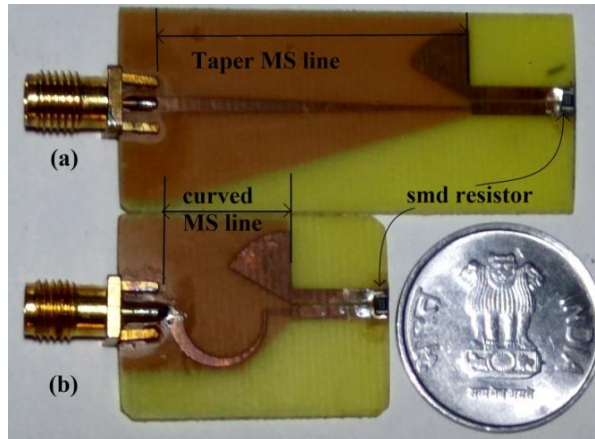


Figure 10. Photograph of (a) conventional BALUN and (b) proposed compact BALUN

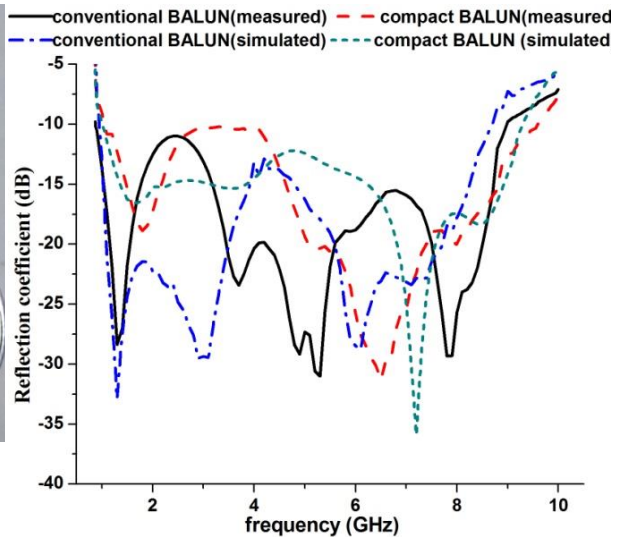


Figure 11. Measured and simulated results of conventional and compact BALUNs

Table 4 compares the simulated results of all the proposed BALUNs with the conventional BALUN in terms of % bandwidth and length. The comparison was done only for the taper lines from conventional and proposed BALUNs. It can be observed that, when the length of the taper MS line of the proposed BALUN (curved $L = 19$ mm) is equal to the taper

length of the conventional BALUN (straight $L = 30$ mm), the length of the proposed BALUN reduces to only 36% w.r.t. the conventional BALUN. The % bandwidth of the proposed BALUN is 165 and the % bandwidth of the conventional BALUN is 166. The maximum reduction in taper line length is 73% but at the cost of a % bandwidth reduction of 13.

Table 4. Comparison of taper line length from conventional and proposed BALUNs

BALUN parameters	Conventional BALUN	Proposed length of curved taper line (mm)			
Length (L)	30	9	11	13	19
Bandwidth (GHz)	7.9	7.99	7.66	9.31	7.82
% Bandwidth	166	153	157	161.5	165
% Size Reduction	-----	73	63	56.7	36

The comparison between the proposed BALUN and other existing BALUNs is included in Table 5. In the table, the length of the proposed BALUN represents the length of the taper line only.

When a CPS line of length 10 mm is added to the curved taper line, the total length of the BALUN is extended by 10 mm. It can be observed that the proposed structure of the BALUN outperforms all the BALUNs

in terms of size and % bandwidth, excluding the BALUNs given by Bah (2016), Lin et al. (2015) and Lee et al. (2018). These three BALUNs are smaller than the proposed curved BALUN. The proposed curved BALUN outperforms the

BALUN proposed by Lee et al. (2018) in terms of % bandwidth. Another advantage of the proposed BALUN over these three BALUNs is that it does not require vias and is simple to manufacture.

Table 5. Performance comparison of proposed BALUN with existing BALUNs

Author	P	P	Tu and Chang (2006)	Bah (2016)	Shao et al. (2013)	Hong (2013)	Lin (2010)	Lin et al. (2015)	Zhu et al. (2012)	Lee et al. (2018)
f_l - f_h	1.1	0.84	2.7–10.4	0.7–15	0.72	0.5–5	2.4–6	3.6–10.7	3.1–10.6	6–40
GHz	9.6	8.66	5		2.05					
%B	15	165	118	175	96	164	86	99.3	110	148
W	9									
L	13	19	23.3	25.5	71	34.1	25.8	10.5	20	13
mm										
Year	----	-----	2006	2016	2013	2013	2010	2015	2012	2018
	---	--								

f_l , lower cut-off frequency; f_h , upper cut-off frequency; BW, bandwidth, P, proposed

5. CONCLUSION

The Klopfenstein taper line is already a compact line used to transform impedance, but the proposed technique can be used to reduce this line further. It is found that the proposed method reduces the size of the BALUN by 56.7% at the cost of 4.5% reduction in the bandwidth of the proposed BALUN as compared to the conventional BALUN. The size of the BALUN can be reduced to 73% w.r.t. the conventional BALUN at the cost of % bandwidth. The % bandwidth drops by 13% for the maximum reduction of 73% in the size of the BALUN. This technique can be applied to other existing straight BALUNs, and a further reduction in size can be achieved. This product can be helpful for feeding any balanced antenna without occupying much area on the PCB.

6. ACKNOWLEDGEMENTS

The authors are very thankful to Mr Shivraj for providing the measurement facility for the designed products.

7. REFERENCES

Anagnostou, D. E., Morton, M., Papapolymerou, J., & Christodoulou C. G. (2008). A 0–55GHz coplanar waveguide to coplanar strip transition. *IEEE Transactions on Microwave Theory and Techniques*, 56, 1–6.

Bah, A. O. (2016, September). An extremely wideband tapered balun for application in tightly coupled arrays. In *6th IEEE-APS Topical*

- Conference on Antennas and Propagation in Wireless Communications* (pp. 162–165). IEEE>
- Hong Y.-P. (2013). Fat dipole antenna with broadband balun using CPW-to-slotline field transformation. *Electronics Letters*, 49, 635–636.
- Klopfenstein, R. W. (1956, January). A transmission line of improved design. In *Proceedings of the I.R.E.* (pp. 31–35).
- Lee, H. G., Mohyuddin, W., Choi C. H., & Kim K. W. (2018). Asymmetric ultra-wideband microstrip-to-coplanar stripline transition. *IEEE Microwave and Wireless Components Letters*, 28(5).
- Lin, S., Wang, J., Deng, Y., & Zhang, G. (2015). A new compact ultra-wideband balun for printed balanced antennas. *Journal of Electromagnetic Waves and Applications*, 29, 1570–1579.
- Lin, S.-C. (2010). Wideband series-fed dipole antenna with balun integrated. *Journal of Electromagnetic Waves and Applications*, 24, 2463–2477.
- Maksimovitch, Y., Mikhnev, V., & Vainikainen, P. (2007, September). Step-by-Step modification of Printed Wideband Balun for GPR Antennas. In *17th International Conference on Microwave and Telecommunication Technology* (pp. 427–428). IEEE.
- Meng, X., Wu, B., Huang, Z., & Wu, X. (2016). Compact 30:1 bandwidth ratio Balun for printed balanced antennas. *Progress in Electromagnetics Research C*, 64, 125–132.
- Pozar, D. M. (1998). *Microwave engineering*. John Wiley & Sons.
- Resley, L., & Song, H. (2012). Ka-band Klopfenstein tapered impedance transformer for radar applications. *Progress in Electromagnetics Research*, 27, 253–263.
- Ruvio, G., & Ammann, M. J. (2008, July). Effects of Klopfenstein tapered feedlines on the frequency and time domain performance of planar monopole UWB antennas. In *IEEE Antennas and Propagation Society, International Symposium* (pp. 1–4). IEEE.
- Shao, J., Zhou, R., Chen, C., Wang, X., Kim, H., & Zhang, H. (2013). Design of a wideband Balun using parallel strips. *IEEE Microwave and Wireless Components Letters*, 23, 125–127.
- Tu, W.-H., & Chang, K. (2006). Wide-band microstrip-to-coplanar stripline/slotline transitions. *IEEE Transactions on Microwave Theory and Techniques*, 54, 1084–1089.
- Vega, F., Mora, N., & Rachidi, F. (2011, September). Design and simulation of a coaxial exponential transmission line for a half impulse radiating antenna. In *2011 XXXth URSI General Assembly and Scientific Symposium* (pp. 1–4). IEEE.
- Zhu, F., Hong, W., Chen, J., & Wu, K. (2012). Ultra-wideband single and dual Baluns based on substrate integrated coaxial line technology. *IEEE Transactions on Microwave Theory and Techniques*, 60, 3062–307.

Online signature verification using hybrid wavelet transform

Manoj Chavan¹, Ravish R. Singh², Vinayak Bharadi³

¹Department of Electronics and Telecommunication Engineering, Thakur College of Engineering and Technology, India

²Academic Advisor, Thakur Educational Trust, Mumbai, India

³Information Technology Department, Finolex Academy of Management and Technology, India

Article Info

Article history:

Received Dec 22, 2017

Revised Oct 18, 2019

Accepted Oct 30, 2019

Keywords:

HMM

HWT

Left Right Model

Online Signature Verification

ABSTRACT

Online signature verification is a prominent behavioral biometric trait. It offers many dynamic features along with static two dimensional signature image. In this paper, the Hybrid Wavelet Transform (HWT) was generated using Kronecker product of two orthogonal transform such as DCT, DHT, Haar, Hadamard and Kekre. HWT has the ability to analyze the signal at global as well as local level like wavelet transform. HWT-1 and -2 was applied on the first 128 samples of the pressure parameter and first 16 samples of the output were used as feature vector for signature verification. This feature vector is given to Left to Right HMM classifier to identify the genuine and forged signature. For HWT-1, DCT HAAR offers best FAR and FRR. For HWT-2, KEKRE 128 offers best FAR and FRR. HWT-1 offers better performance than HWT-2 in terms of FAR and FRR. As the number of states increase, the performance of the system improves. For HWT-1, KEKRE 128 offers best performance at 275 symbols whereas for HWT-2, best performance is at 475 symbols by KEKRE 128.

Copyright © 2020 Institute of Advanced Engineering and Science.
All rights reserved.

Corresponding Author:

Manoj Chavan,

Department of Electronics and Telecommunication Engineering,

Thakur College of Engineering and Technology,

Thakur Village, Kandivali East Mumbai-400101 Maharashtra, India.

Email: prof.manoj@gmail.com

1. INTRODUCTION

Handwritten Signatures have been used for centuries for identification and authentication of a person as well as documents [1, 2]. In biometrics classification, it is part of behavioral characteristics like voice, gait etc. whereas physical characteristics include fingerprint, palm print, face, iris, retina etc. [3]. Biometric characteristics are universal, unique and measurable and are better than personal ID cards, PIN or passwords [4-6]. Biometric system for signatures can operate in two ways. First Verification, in which the individual's signature will be compared with his stored signature in a database to verify that the individual is the same who he says to be. Second Identification, in which the signature will be compared with the many signatures in the database to identify an individual out of many unknowns.

Automating the process of Handwritten Signature Verification will be useful for document verification in various sectors such as banking, legal documentation etc. There are two types of Signature Verification; offline (static) or online (dynamic). Offline signatures offer two dimensional image of the signatures whereas online signatures have added advantage that it also measures pressure applied by the user, speed of writing, inclination of pen along with the two dimensional signature image [7]. Dr. Kekre proposed Hybrid Wavelet Transform (HWT) which is formed by combining the two orthogonal transforms using Kronecker product. It has the ability to analyze the signal at global as well as local level like wavelet transform [8]. HWT is of two types and are explained below. Consider matrices X and Y as shown below.

$$X = \begin{bmatrix} x_{11} & x_{12} & \dots & x_{1a} \\ x_{21} & x_{22} & \dots & x_{2a} \\ \dots & \dots & \dots & \dots \\ x_{a1} & x_{a2} & \dots & x_{aa} \end{bmatrix} \quad Y = \begin{bmatrix} y_{11} & y_{12} & \dots & y_{1b} \\ y_{21} & y_{22} & \dots & y_{2b} \\ \dots & \dots & \dots & \dots \\ y_{b1} & y_{b2} & \dots & y_{bb} \end{bmatrix}$$

HWT-1 matrix ‘T_{XY}’ of size (N×N), as shown in Table 1, can be formed by the Kronecker product of two orthogonal transform matrices X and Y respectively, with sizes (a x a) and (b x b), such that N=a x b. For HWT-1, first ‘b’ number of rows of the HWT matrix are calculated as the product of each element of first row of the orthogonal transform X with each of the columns of the orthogonal transform Y. For next ‘b’ number of rows of HWT matrix the second row of the orthogonal transform matrix X is shift rotated after being appended with zeros. Similarly the other rows of HWT matrix are generated as set of b rows each time for each of the ‘a-1’ rows of orthogonal transform matrix X starting from second row up to last row.

Table 1. HWT-1 Matrix

y11x11	y11x12	...	y11x1a	y12x11	y12x12	...	y12x1a	y1bx11	y1bx12	...	y1bx1a
y21x11	y21x12	...	y21x1a	y21x12	y22x12	...	y22x1a	y2bx11	y2bx12	...	y2bx1a
...
yb1x11	yb1x12	...	yb1x1a	yb2x11	yb2x12	...	yb2x1a	yb1x11	yb1x12	...	yb1x1a
x21	x22	...	x2a	0	0	...	0	0	0	...	0
0	0	...	0	x21	x22	...	x2a	0	0	...	0
...
0	0	...	0	0	0	...	0	x21	x22	...	x2a
x31	x32	...	x3a	0	0	...	0	0	0	...	0
0	0	...	0	x31	x32	...	x3a	0	0	...	0
...
0	0	...	0	0	0	...	0	x31	x32	...	x3a
...
...
xa1	xa2	...	xaa	0	0	...	0	0	0	...	0
0	0	...	0	xa1	xa2	...	xaa	0	0	...	0
...
0	0	...	0	0	0	...	0	xa1	xa2	...	xaa

HWT-2 matrix of size (N×N) is also formed by the Kronecker product of two orthogonal transform matrices X and Y. First N/2 rows of the matrix are formed by product of each element of first a/2 rows of the matrix X with each of the columns of the matrix Y. For next ‘b’ number of rows of matrix, the ‘a/2+1’th row of the orthogonal transform matrix X is shift rotated after being appended with zeros. Next N/2 rows are generated as set of b rows each time for each of the ‘a/2’ rows of orthogonal transform matrix X starting from ‘a/2+1’th row up to last row.

HWT offers better performance in image compression than the orthogonal transforms used to generate them [9, 10]. HWT is also used for water marking [11] and to convert color image to gray image [12]. Various classifiers based on KNN, SVM and NN [13, 14] have been used for verification of signatures. In [15], KNN classifier was used with, HWTs of the pressure map of online signatures as feature vector. It offered an EER of 30%. In [16], SVM classifier was used with, a kernel function of online signature time series, based on LCSSs detection, as a feature vector. It offered an EER of 6.84%. Using SVM in conjunction with HMM offered FAR of 1.96% and FRR of 60.43%. In [17], neural network classifier was used with, the approximation and detail component of DWT of the pen position and pen movement angle as feature vector. Using all coefficients of DWT, success rate was 100% with trained signature, 90% with untrained signatures and FRR of 24%. Using selected 25 coefficients of DWT, success rate was 100% with trained signature, 95% with untrained signatures and FAR of 8%.

In this paper, we propose a method for online signature verification using Hybrid Wavelet Transform and Hidden Markov Model classifier. The proposed method is shown in Figure 1. We have used SVC2004 database which is a large database containing signatures from 40 individuals. It has total of 1,600 signatures, obtained using a Wacom Intuos tablet. It consists of 20 genuine and 20 forgery signatures collected for each person. Genuine signatures are collected in two different sessions. Forgeries for each person are provided by at least four other individuals from the database. The performance results of various signature verification systems that participated in the SVC2004 competition is available. The best performance for 40 available users is average EER 6.90% with standard deviation of 9.45%, minimum value of 0.00 and maximum value of 50.00%. The best performance for 60 other users is average EER 2.89% with standard deviation of 5.69%, minimum value of 0.00 and maximum value of 30.00% [18]. Every signature sample consist of X-coordinate-scaled cursor position along the x-axis, Y-coordinate-scaled cursor position along the y-axis,

Time stamp-system time at the time of signing, Button status-current button status (0 for pen-up and 1 for pen-down), Azimuth-clockwise rotation of cursor about the z-axis, Altitude-angle upward toward the +ve z-axis, Pressure-normal pressure applied by hand. Pressure applied by the tip of the pen on the pressure sensitive pad is used for generating the feature vector. We have used Discrete Cosine transform (DCT), Discrete Hartley transform (DHT), Discrete Walsh transform (DWT) and Discrete Kekre transform (DKT) to form the HWT-1 and HWT-2 matrix. The output of HWT is given to HMM for classification.

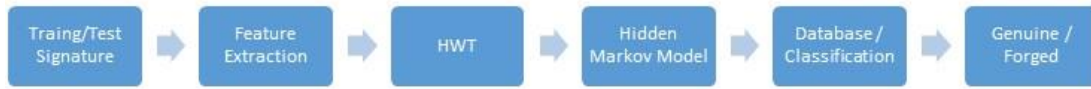


Figure 1. Proposed System

2. RESEARCH METHOD

Signature database of 1600 signatures, provided by The First International Signature Verification Competition (SVC 2004) is used. It has signatures of 40 users. Every user has 40 signatures, out of which, 20 are genuine and 20 are skilled forgeries. The first 128 samples of every signature is used to find HWT. The signatures, having samples less than 128, will be padded with zeroes. The first 16 samples of the HWT output are used as feature vector. Discrete Cosine transform (DCT), Discrete Hartley transform (DHT), Discrete Walsh transform (DWT) and Discrete Kekre transform (DKT) are used to form the HWT [19, 20]. There are many topologies of HMM such as Left to Right, Ergodic and Ring. Left to Right topology as shown in Figure 2, is found to be best suited for the Signature modelling [21, 22].

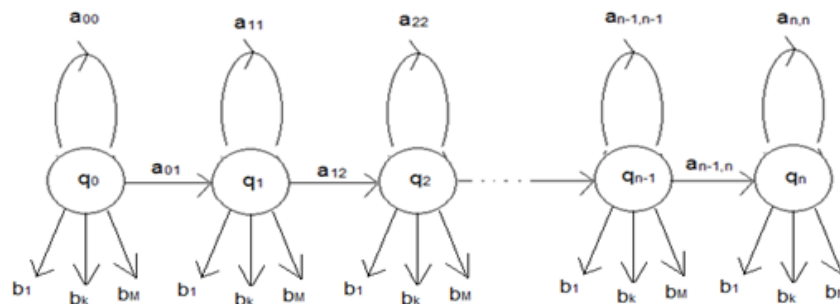


Figure 2. Left to Right HMM model

HMM is represented by the transition probability matrix (A), Observation matrix (B) and initial probability distribution matrix (π). [23, 24] Consider a system which is in a distinct state (S_1, S_2, \dots, S_N) at any point of time. In this experiment the number of states (N) of the model are varied from 2 to 5. As the number of states increase, the time needed for training increases. The number of observations (M) corresponding to each state are varied from 200 to 750 in the increments of 25. The output of HWT is a matrix of dimension $[1 \times 128]$. The matrix elements from 1 to 16 are chosen as a feature vector. Feature vectors are scaled into M number of observations.

Initial Probability Distribution (π): $\pi_i = P(q_1 = S_i); 1 \leq i \leq N$. We assume the initial probability of the first state is 1 and the others are 0 which implies that in the beginning HMM is always in state 1. State transition probability (a_{ij}): $a_{ij} = P(S_t = j / S_{t-1} = i)$. For the left-to-right HMM, $a_{ij} = 0$ when $i > j$. we are using the HMM of first order so that $a_{ij} = 0$ when $j > i + 1$. Initially, the state transition matrix is generated using the random numbers such that $\sum_{j=1}^N a_{ij} = 1; 1 \leq i \leq N$. Observation probability (b_j): $b_j(k) = P(V_k \text{ at } t / q_t = S_j); 1 \leq j \leq N; 1 \leq k \leq M$; the probability of generating a symbol V_k in state j .

Statistics and machine learning toolbox of the MATLAB 13 was used for implementation of HMM. Initially a randomly generated transition probability Matrix (A) is generated using MATLAB. We assume observation probability matrix (B) to have equal probability for every symbols and HMM to be in state 1. HMM is trained using the function 'hmmtrain' for 3 to 20 genuine training signature samples, number of states from 2 to 5 and symbols from 200 to 750. After HMM is trained, it is used to test 20 genuine and 20 forged signatures of 40 users.

3. RESULTS AND DISCUSSION

Performance of the system will be measured on the basis of False Rejection Ratio (FRR) and False Acceptance Ratio (FAR). FRR refers to false rejection of genuine signature and FAR refers to false acceptance of forged signature [25]. FRR is computed as ratio of the number of signatures detected as forged to the total number of genuine signatures tested. FAR is computed as ratio of the number of signatures detected as genuine to the total forged signatures tested. Testing has been carried out for 40 users and then the average FRR and FAR are calculated. In FRR-FAR plot shown in Figure 3, the point where two graphs cross each other is referred as Equal Error Rate (EER). At this point the value of FRR and FAR is minimum. The results obtained by the first 1–16 samples of HWT-1 and 2 for DCT, DHT, HAAR, HADAMARD and KEKRE combinations is shown in the Tables 2-4.

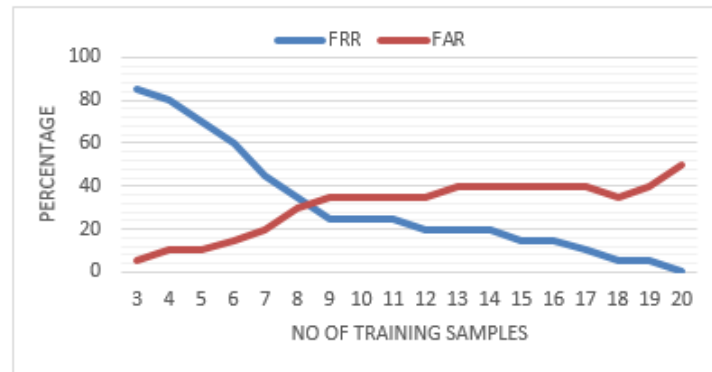


Figure 3. FRR – FAR plot

The comparison of HWT-1 and 2 for 1–16 bit for DCT combinations is shown in the Tables 2-4.

- Best FRR–FAR: FRR–FAR should be as low as possible. For HWT-1, DCT HAAR offers best performance with FRR & FAR of 0 %. For HWT-2, DCT KEKRE offers best performance with FRR & FAR of 9%. The performance offered by DCT HAAR HWT for HWT-1 is better than HWT-2. The performance offered by DCT combinations for HWT-1 is better than HWT-2. For HWT-1, the performance offered by DCT combinations except DCT DHT is better than Orthogonal DCT transform. For HWT–2, only DCT KEKRE offers better performance than DCT combinations than Orthogonal DCT transform.
- Best Number of Training Samples: The number of training samples should be as low as possible. For HWT–1, DCT DHT offers best performance of 12 compared to 15 training samples for Orthogonal DCT transform. For HWT–2, Orthogonal DCT transform offers best performance of 4 training samples compared to all combinations of DCT HWT. The performance offered by DCT combinations for HWT-2 is better than HWT-1.
- Best state wise FRR–FAR: FRR–FAR should be as low as possible for the given state from 2 to 5. For HWT-1, DCT HAAR offers best performance for 2, 4 and 5 states, DCT KEKRE for state 3 and DCT HAAR for state 5 compared to orthogonal DCT transform. For HWT-2, DCT KEKRE offers best performance for 2 to 5 states compared to orthogonal DCT transform. The performance offered by DCT combinations for HWT-1 is better than HWT-2.
- Best Number of Symbol: It should be as low as possible. Testing was carried out for number of symbols from 200 to 750. It evident that the best performance in terms of FRR–FAR, AAR–ARR, EER is offered by 275-325 symbols for HWT-1 and 450–500 symbol for HWT-2. The performance offered by DCT combinations for HWT-1 is better than HWT-2.

The comparison of HWT-1 and 2 for 1–16 bit for DHT combinations is shown in the Table 2-4.

- Best Number of Training Samples: For HWT-1, DHT KEKRE offers best performance with FRR & FAR of 5 %. For HWT-2, DHT KEKRE offers best performance with FRR 13% & FAR of 19%. The performance offered by DHT KEKRE HWT for HWT-1 is better than HWT-2. The performance offered by DHT combinations for HWT-1 is better than HWT-2. For HWT–1, the performance offered by DHT DCT, DHT KEKRE is better than Orthogonal DHT transform. For HWT–2, only DHT KEKRE offers better performance than Orthogonal DHT transform.

- Best Number of Training Samples: For HWT-1, DHT HADAMARD offers best performance of 10 training samples compared to 13 training samples for Orthogonal DHT transform. For HWT-2, DHT HADAMARD offers best performance of 5 training samples compared to 7 training samples for Orthogonal DHT transform. DHT combinations offer better performance for HWT-2 than HWT - 1.
- Best state wise FRR-FAR: For HWT-1, DHT KEKRE offers best performance for 2, 3 and 4 states and DHT DCT for state 5 compared to orthogonal DHT transform. For HWT-2, DHT KEKRE offers best performance for 2 to 5 states compared to orthogonal DHT transform. DHT combinations offer better performance for HWT-1 than HWT-2.
- Best Number of Symbol: Testing was carried out for number of symbols from 200 to 750. It evident that the best performance in terms of FRR-FAR, AAR-ARR, EER is offered by 275 symbols for HWT-1 and 450-500 symbols for HWT-2. DHT combinations offers better performance for HWT-1 than HWT-2.

The comparison of HWT-1 and 2 for 1-16 bit for HAAR combinations is shown in the Tables 2-4.

- Best FRR-FAR: For HWT-1, HAAR DCT and HAAR KEKRE offers best performance with FRR & FAR of 0 %. For HWT-2, HAAR KEKRE offers best performance with FRR 11% & FAR of 12%. The performance offered by HAAR DCT and HAAR KEKRE HWT for HWT-1 is better than HWT-2. The performance offered by HAAR combinations for HWT-1 is better than HWT-2. For HWT-1, the performance offered by all combinations of HAAR is better than Orthogonal HAAR transform. For HWT-2, HAAR DHT and HAAR KEKRE offers better performance than Orthogonal HAAR transform.
- Best Number of Training Samples: For HWT-1, HAAR DHT offers best performance of 12 training samples with FRR, FAR of 15%, 15% respectively compared to 13 training samples with FRR, FAR of 10%, 30% respectively for Orthogonal DHT transform. For HWT-2, HAAR HADAMARD offers best performance of 5 training samples compared to 6 training samples for Orthogonal HAAR transform. HAAR combinations offer better performance for HWT-2 than HWT-1.
- Best state wise FRR-FAR: For HWT-1, HAAR KEKRE offers best performance for 2 to 5 states. HAAR DCT offers best performance for state 5 compared to orthogonal HAAR transform. For HWT-2, HAAR KEKRE offers best performance for 2 to 5 states compared to orthogonal HAAR transform. HAAR combinations offer better performance for HWT-1 than HWT-2.
- Best Number of Symbol: Testing was carried out for number of symbols from 200 to 750. It evident that the best performance in terms of FRR-FAR, AAR-ARR, EER is offered by 275 symbols for HWT-1 and 450-500 symbols for HWT-2. HAAR combinations offer better performance for HWT-1 than HWT-2.

The comparison of HWT-1 and 2 for 1-16 bit for HADAMARD combinations is shown in the Table 2-4.

- Best FRR-FAR: For HWT-1, HADAMARD KEKRE offers best performance with FRR & FAR of 0%. For HWT-2, HADAMARD KEKRE offers best performance with FRR 25% & FAR of 22%. The performance offered by HADAMARD KEKRE HWT for HWT-1 is better than HWT-2. The performance offered by HADAMARD combinations for HWT-1 is better than HWT-2. For HWT-1, the performance offered by all combinations of HADAMARD except HADAMARD DCT is better than Orthogonal HADAMARD transform. For HWT-2, the performance offered by all combinations of HADAMARD is better than Orthogonal HADAMARD transform
- Best Number of Training Samples: For HWT-1, Orthogonal HADAMARD transform offers best performance of 8 training samples compared to all combinations of HADAMARD HWT. For HWT-2, Orthogonal HADAMARD transform offers best performance of 5 training samples compared to all combinations of HADAMARD HWT. HADAMARD combinations offer better performance for HWT-2 than HWT-1.
- Best state wise FRR-FAR: For HWT-1, HADAMARD KEKRE offers best performance for 2 and 5 states. HADAMARD DHT offers best performance for state 4 and 5 compared to orthogonal HADAMARD transform. For HWT-2, HADAMARD KEKRE offers best performance for 2 to 5 states compared to orthogonal HADAMARD transform. HADAMARD combinations offer better performance for HWT-1 than HWT-2.
- Best Number of Symbol :Testing was carried out for number of symbols from 200 to 750. It evident that the best performance in terms of FRR-FAR, AAR-ARR, EER is offered by 275-300 symbols for HWT-1 and 500 symbols for HWT-2. HADAMARD combinations offer better performance for HWT-1 than HWT-2.

- The comparison of HWT-1 and 2 for 1–16 bit for KEKRE combinations is shown in the Tables 2-4.
- Best FRR–FAR: For HWT-1, KEKRE DCT, KEKRE HAAR and KEKRE128 offers best performance with FRR & FAR of 0 %. For HWT-2, KEKRE 128 offers best performance with FRR 5% & FAR of 2%. The performance offered by KEKRE DCT, KEKRE HAAR and KEKRE128 HWT for HWT-1 is better than HWT-2. The performance offered by KEKRE combinations for HWT-1 is better than HWT-2. For HWT–1, the performance offered by KEKRE 128 is better than all combinations of KEKRE HWT. For HWT–2, the performance offered by KEKRE 128 is better than all combinations of KEKRE HWT.
 - Best Number of Training Samples: For HWT–1, KEKRE DHT offers best performance of 11 training samples compared to 20 training samples for Orthogonal KEKRE transform. For HWT–2, KEKRE HADAMARD offers best performance of 6 training samples compared to 16 training samples for Orthogonal KEKRE transform. KEKRE combinations offer better performance for HWT-2 is better than HWT-1.
 - Best state wise FRR–FAR: For HWT-1, KEKRE 128 offers best performance for 2 TO 5 states compared to combinations of KEKRE HWT. For HWT-2, KEKRE 128 offers best performance for 2 TO 5 states compared to combinations of KEKRE HWT. KEKRE combinations offer better performance for HWT-1 is better than HWT-2.
 - Best Number of Symbol: Testing was carried out for number of symbols from 200 to 750. It evident that the best performance in terms of FRR–FAR, AAR–ARR, EER is offered by 275 symbols for HWT-1 and 450-500 symbols for HWT-2. KEKRE combinations offer better performance for HWT-1 is better than HWT-2.

Table 2. Best FRR FAR for HWT-1 and 2

Combinations	HWT-1					HWT-2					
	States	Symbols	Training samples	FRR	FAR	Combinations	States	Symbols	Training samples	FRR	FAR
DCT 128	2	300	16	5	10	DCT 128	5	475	11	27	32
DCT DHT	3	300	13	10	10	DCT DHT	5	400	10	31	34
DCT Haar	5	325	18	0	0	DCT Haar	4	425	9	30	33
DCT Hadamard	5	300	17	0	5	DCT Hadamard	5	400	10	30	42
DCT Kekre	3	300	17	5	5	DCT Kekre	5	500	18	9	9
DHT 128	4	350	15	5	10	DHT 128	5	500	12	24	30
DHT DCT	5	275	18	5	5	DHT DCT	4	500	9	31	37
DHT Haar	5	275	17	5	10	DHT Haar	5	500	10	29	37
DHT Hadamard	4	300	14	10	15	DHT Hadamard	5	500	11	31	28
DHT Kekre	4	275	20	0	5	DHT Kekre	5	475	16	13	19
Haar 128	2	275	13	10	30	Haar 128	5	475	13	24	28
Haar DCT	5	275	20	0	0	Haar DCT	5	500	11	31	24
Haar DHT	5	300	15	5	15	Haar DHT	5	450	11	26	21
Haar Hadamard	2	300	14	5	10	Haar Hadamard	5	425	10	30	33
Haar Kekre	3	275	19	0	0	Haar Kekre	5	500	17	11	12
Hadamard 128	5	350	14	5	15	Hadamard 128	5	475	9	32	32
Hadamard DCT	5	300	17	10	10	Hadamard DCT	5	500	12	27	26
Hadamard DHT	4	300	14	5	5	Hadamard DHT	5	500	10	29	29
Hadamard Haar	4	275	16	5	5	Hadamard Haar	4	500	10	31	30
Hadamard Kekre	5	275	20	0	0	Hadamard Kekre	5	500	14	25	22
Kekre 128	2	275	20	0	0	Kekre 128	4	475	19	5	2
Kekre DCT	5	275	20	0	0	Kekre DCT	5	500	13	27	27
Kekre DHT	5	275	18	5	5	Kekre DHT	4	350	8	30	36
Kekre Haar	2	525	20	0	0	Kekre Haar	5	500	14	21	21
Kekre Hadamard	2	550	19	100	0	Kekre Hadamard	5	500	13	23	21

Table 3. Best No. of training samples for HWT-1 and 2

HWT-1						HWT-2					
Combinations	States	Symbols	Training samples	FRR	FAR	Combinations	States	Symbols	Training samples	FRR	FAR
DCT 128	3	300	15	15	15	DCT 128	2	275	4	35	63
DCT DHT	2	300	12	15	25	DCT DHT	3	325	7	33	50
DCT Haar	3	300	13	5	20	DCT Haar	3	375	6	33	47
DCT						DCT					
Hadamard	2	275	12	30	30	Hadamard	4	325	6	30	51
DCT Kekre	3	300	17	5	5	DCT Kekre	2	450	11	22	30
DHT 128	2	350	13	10	20	DHT 128	2	375	7	32	40
DHT DCT	4	275	15	5	10	DHT DCT	2	500	8	33	43
DHT Haar	2	275	13	20	20	DHT Haar	2	350	6	34	46
DHT						Dht Hadamard	4	275	5	29	52
Hadamard	2	300	10	20	25	DHT Kekre	2	475	12	23	27
DHT Kekre	2	275	19	5	5	Haar 128	2	325	6	32	57
Haar 128	2	275	13	10	30	Haar DCT	4	350	7	32	52
Haar DCT	2	275	13	15	0	Haar DHT	2	375	6	37	49
Haar DHT	3	275	12	15	15	Haar					
Haar	3	275	13	10	20	Hadamard	3	275	5	32	57
Hadamard						Haar Kekre	3	400	12	20	33
Haar Kekre	3	275	19	0	0	Hadamard 128	2	475	5	38	52
Hadamard 128	2	275	8	35	30	Hadamard DCT	2	375	6	30	45
Hadamard	2	275	11	20	15	Hadamard					
DCT						DHT	3	300	6	31	49
Hadamard	2	275	11	15	20	Hadamard					
DHT						Haar	2	425	8	34	37
Hadamard	2	275	14	5	15	Hadamard					
Haar						Kekre	2	500	11	34	31
Hadamard	2	275	18	10	10	Kekre 128	2	450	16	11	16
Kekre	2	275	20	0	0	Kekre DCT	2	425	9	31	37
Kekre 128	2	275	13	10	15	Kekre DHT	4	350	8	30	36
Kekre DCT	2	275	11	15	25	Kekre Haar	2	500	10	33	38
Kekre DHT	2	275	11	15	25	Kekre					
Kekre Haar	2	525	20	0	0	Hadamard	2	375	6	34	49
Kekre	2	550	19	100	0						
Hadamard											

Table 4. Best Statewise FRR FAR for HWT-1 and 2

HWT-1						HWT-2					
Combinations	States	Symbols	Training samples	FRR	FAR	Combinations	States	Symbols	Training samples	FRR	FAR
DCT Haar	2	300	14	5	10	DCT Kekre	2	450	11	22	30
DCT Kekre	3	300	17	5	5	DCT Kekre	3	450	13	19	20
DCT Haar	4	275	15	10	10	DCT Kekre	4	450	15	17	18
DCT Haar	5	325	18	0	0	DCT Kekre	5	500	18	9	9
DHT Kekre	2	275	19	5	5	DHT Kekre	2	475	12	23	27
DHT Kekre	3	275	19	5	5	DHT Kekre	3	500	13	22	20
DHT Kekre	4	275	20	0	5	DHT Kekre	4	450	15	15	14
DHT DCT	5	275	18	5	5	DHT Kekre	5	475	16	13	19
Haar Kekre	2	275	19	5	5	Haar Kekre	2	450	12	21	35
Haar Kekre	3	275	19	0	0	Haar Kekre	3	400	12	20	33
Haar Kekre	4	275	20	0	5	Haar Kekre	4	475	16	14	22
Haar Kekre	5	275	20	0	0	Haar Kekre	5	500	17	11	12
Hadamard						Hadamard					
Kekre	2	275	18	10	10	Kekre	2	500	11	34	31
Hadamard						Hadamard					
DHT	3	275	12	10	10	Kekre	3	500	15	16	44
Hadamard						Hadamard					
DHT	4	300	14	5	5	Kekre	4	500	13	25	27
Hadamard						Hadamard					
Kekre	5	275	20	0	0	Kekre	5	500	14	25	22
Kekre 128	2	275	20	0	0	Kekre 128	2	450	16	11	16
Kekre 128	3	275	20	0	0	Kekre 128	3	500	17	10	11
Kekre 128	4	275	20	0	0	Kekre 128	4	475	19	5	2
Kekre 128	5	275	20	0	0	Kekre 128	5	475	19	5	2

From Tables 2-4, we get following important results.

- FRR–FAR: For HWT-1, DCT HAAR offers best performance with FRR and FAR of 0 %. For HWT-2, KEKRE 128 offers best performance of FRR 5 % and FAR 2 %. HWT-1 offers better performance than HWT-2.
- Number of training samples: For HWT–1, Orthogonal HADAMARD transform offers best performance of 8 training. For HWT–2, Orthogonal DCT transform offers best performance of 4 training samples. HWT-2 offers better performance than HWT-1.
- State wise FRR–FAR: For HWT-1, KEKRE 128 offers best performance for 2 to 5 states. For HWT-2, KEKRE 128 offers best performance for 2 to 5 states. HWT-1 offers better performance than HWT-2. As the number of states increase, the performance of the system improves. HWT-1 found to offer better performance for 3 to 5 states and HWT-2 for 5 states.
- Number of Symbol: For HWT-1, KEKRE 128 offers best performance at 275 symbols whereas for HWT-2, best performance is at 475 symbols by KEKRE 128.

The proposed system is compared with existing systems in Table 5. The proposed system offers better performance than the existing systems.

Table 5. Comparison of proposed system with existing systems

Paper	FAR (%)	FRR (%)
[13]	30	30
[14]	1.96	60.93
[15]	0	8
Proposed system	0	0

4. CONCLUSION

In the proposed system for online signature verification with pressure as feature vector, HWT-1 offers better performance than HWT-2 for various combinations of DCT, DHT, Haar and Hadamard orthogonal transform. But Kekre transform offers better performance than its various combination of HWT-1 and HWT-2. Comparing KNN, SVM and NN classifier with various dynamic parameters as feature vector, HMM offers better performance. This findings show that the HWT with HMM has been a feasible method for feature vector extracton of online signature vector based biometric systems.

REFERENCES

- [1] R. Plamondon, "A kinematic theory of rapid human movements: Part I: Movement representation and generation," *Biological Cybernetics*, vol. 72, no. 4, pp. 295-307, 1995.
- [2] R. Plamondon, "A kinematic theory of rapid human movements: Part II: Movement time and control," *Biological Cybernetics*, vol. 72, no. 4, pp. 309-320, 1995.
- [3] A. K. Jain, A. Ross and S. Prabhakar, "An Introduction to Biometric Recognition," *IEEE Transactions on Circuits and Systems for Video Technology*, vol. 14, no. 1, p 4-20, Jan 2004.
- [4] K. Veeramacheni, L. A. Osadciw and P. K. Varshney, "An adaptive multimodal biometric management algorithm," *IEEE Trans. Systems, Man and Cybernetics*. Part C, vol. 35, no. 3, p. 344–356, Aug 2005.
- [5] K. Huang and H. Yan, "Signature verification using fractal transformation," *Proc. 15th Int. Conf. Pattern Recog. (ICPR-15)*, Barcelona, Spain, Sept 2000.
- [6] S. Nanavati, M. Thieme, and R. Nanavati, "Biometrics: Identity Verification in a Networked World," New York: Wiley, p 123–131, 2002.
- [7] T. Ohishi, Y. Komiya, H. Morita, and T. Matsumoto, "Pen-input online signature verification with position, pressure, inclination trajectories," in *Proc. 15th Int. Parallel Distrib. Process. Symp. (IPDPS-15)*, San Francisco, CA, p. 170, Apr. 2001.
- [8] H. B. Kekre, T. K. Sarode and S. D. Thepade, "Inception of HWT using Two Orthogonal Transforms and It's use for Image Compression," (*IJCSIS*) *International Journal of Computer Science and Information Security*, vol. 9, no. 6, p 80-87, Jun 2011.
- [9] H. Kekre, T. Sarode and P. Natu, "Colour Image Compression using DKT-DCT Hybrid Wavelet Transform in Various Colour Spaces," *International Journal of Signal Processing, Image Processing and Pattern Recognition*, vol. 7, no. 5, pp. 105-124, 2014.
- [10] H. Kekre, T. Sarode and N. Prachi, "Image Compression Using Real Fourier Transform, Its Wavelet Transform and Hybrid Wavelet with DCT," *International Journal of Advance Computer Science and Application*, vol. 4, no. 5, 2013.
- [11] H. Kekre, T. Sarode and S. Natu, "Robust Watermarking Technique using Hybrid Wavelet Transform Generated from Kekre Transform and Discrete Cosine Transform," *International Journal of Scientific and Research Publications*, vol. 4, no. 2, Feb 2014.

- [12] G. B. Atkar and S. Gore, "Enhanced Performance of Color To Gray and Back by Using Hybrid Wavelet Transforms," *International Journal of Emerging Technology and Advanced Engineering*, vol. 3, no. 4, April 2013.
- [13] M. Singhal, M. Trikha, M. Dutta, "Time Independent Signature Verification using Normalized Weighted Coefficients," *International Journal of Electrical and Computer Engineering (IJECE)*, vol. 6, no. 6, p 2658-2664, December 2016.
- [14] M. Singhal, M. Trikha, M. Dutta, "Signature Verification using Normalized Static Features and Neural Network Classification," *International Journal of Electrical and Computer Engineering (IJECE)*, vol. 6, no. 6, p 2665-2673, December 2016.
- [15] V. A. Bharadi, V. I. Singh and Bhushan Nemade, "Hybrid Wavelets based Feature Vector Generation from Multidimensional Data set for On-line Handwritten Signature Recognition" *Proc. 5th Int. Conf. Confluence The next Generation Information Technology Summit (Confluence) Noida, India, Nov 2014.*
- [16] C. Gruber, T. Gruber, S. Krinninger, and B. Sick, "Online Signature Verification With Support Vector Machines Based on LCSS Kernel Functions," *IEEE Transactions on Systems, MAN, And Cybernetics–Part B: Cybernetics*, vol. 40, no. 4, p 1088-1100, Aug 2010.
- [17] Maged M.M. Fahmy, "Online handwritten signature verification system based on DWT features extraction and neural network classification," *Ain Shams Engineering Journal*, vol. 1, no. 1, p 59-70, Sept 2010.
- [18] SVC2004 Home. <http://www.cse.ust.hk/svc2004/>. Accessed 02 Dec 2011.
- [19] M. Chavan, R. R. Singh and V. A. Bharadi, "Online Signature Verification using HWT with Hidden Markov Model" in *Proc 4th International Conference on Computing, Communication, Control And Automation (ICCUBEA)*, Pune, India Aug 2017.
- [20] M. Chavan, R. R. Singh and V. A. Bharadi, "Handwritten Signature Verification using Hidden Markov Model with HWT" in *Proc 4th International Conference on Computing, Communication, Control And Automation (ICCUBEA)*, Pune, India Aug 2017.
- [21] S. Garcia-Salicetti and B. Dorizzi, "On using the Viterbi path along with HMM likelihood information for online signature verification," *IEEE Trans. Syst., Man, Cybern. B*, vol. 37, no. 5, p 1237–1247, Oct 2007.
- [22] L. Rabiner, "A tutorial on hidden Markov models and selected applications in speech recognition," *Proceedings of IEEE*, vol. 77, no. 2, p 257-286, Feb 1989.
- [23] M. M. Shafiei and H. R. Rabiee, "A New On-line Verification Algorithm Using Variable length Segmentation and Hidden Markov Models," in *Proc 7 th International Conference on Document Analysis and Recognition (ICDAR'03)*, Singapore, 2003.
- [24] H. S. Yoon, J. Y. Lee and H. S. Yang, "An on-line signature verification system using hidden Markov model in polar space," in *Proc. 8th Int. Workshop Front. Handwriting Recognit. (IWFHR-8)*, Ontario, Canada, Aug. 2002.
- [25] D. Impedovo and G. Pirlo, "Automatic Signature Verification: The State of the Art," *IEEE Transaction on Systems, MAN and Cybernetics Part C: Application and Reviews*, vol. 28, no.5, Sept 2008.

BIBLIOGRAPHIES OF AUTHORS



Manoj Chavan received the B.E. degree from the Vidyavardhini's College of Engineering and Technology, University of Mumbai, Maharashtra, India, in 2001, the M.E. degree from the Shivaji University, Kolhapur, India, in 2012, and currently he is doing Ph.D. from Pacific University, Udaipur, India. From 2001 to 2005, He worked as lecturer in the department of Electronics and Telecommunication Engineering at St. Francis Institute of Technology, Borivali, Mumbai-400103, India. He has been working as Assistant Professor in Thakur College of Engineering and Technology, Mumbai, since 2005. He is life member of ISTE, India. His area of interest is Pattern recognition and Machine Learning.



Dr. Ravish R. Singh received B.E. from K.J. Somaiya College of Engineering, Mumbai, University of Mumbai, July 1991 and M. Tech. (Communication Engineering), I.I.T. Bombay, January 2001. He did his Ph.D. (Technology), from Sardar Patel College of Engineering, Mumbai, University of Mumbai, November 2013. He worked as Associate Professor in Electronics and Telecommunication in Thakur College of Engineering and Technology from 1st January, 2006 to 4th July, 2014. He also worked as Assistant Professor in Electronics and Telecommunication Engineering from 20th July, 2002 to 31st December 2005 and as Senior Lecturer in Electronics and Telecommunication Engineering from 8th August, 2001 to 19th July 2002. Now he is holding chair of Academic Advisor at Thakur Educational Trust, Mumbai. He has authored and co-authored several books including Electrical Engineering (McGraw Hill Education, India, 2016), Engineering Mathematics (McGraw Hill Education, India, 2016) Numerical and Statistical Methods for Computer Engineering (McGraw Hill Education, India, 2016), Complex Variables and Numerical Methods (McGraw Hill Education, India, 2015), and Linear Algebra and Vector Calculus (McGraw Hill Education, India, 2014). He is life member of IETE and ISTE, India.



Dr. Vinayak Ashok Bharadi received the B.E. degree in Electronics from Finolex Academy of Management and Technology, University of Mumbai, in 2002. M.E. degree in Electronics and Telecommunication in 2007 and PhD in engineering in 2011 from NMIMS University, Mumbai, India. Presently he is working as Associate Professor with Department of Information Technology of Finolex Academy of Management and Technology He is life member of ISTE and area of interest are cloud computing, big data analytics, biometrics and DSP.

Coplanar Stripline Loaded Reconfigurable Loop Antenna for WLAN and WiMAX Applications

S. P. R. Shastri

Pacific Institute of Technology, Pacific
University, Rajasthan, India
shailendra.shastri@thakureducation.org

R. R. Singh

Thakur Educational Trust,
Mumbai, India
ravishrsingh@yahoo.com

K. V. Ajetroa

K. J. Somaiya College of Engineering,
Mumbai, India
kiranjetrao@somaiya.edu

Abstract—In this paper, a loop antenna loaded with coplanar strip (CPS) line is proposed as a multiband antenna. The CPS line is added with two switches to vary the antenna perimeter to cover seven different bands. The CPS line introduced into the loop is not only useful in reconfiguring antenna dimensions but also provides stationary radiation patterns for the all the covered bands. The proposed antenna works in single and dual-band modes. When the proposed antenna works as a single band antenna, it produces a band from 4.2GHz to 5.7GHz. Under dual-band operation, it produces bands from 3.75GHz to 4.7GHz and from 6.4GHz to 7.8GHz. The other dual-band mode ranges from 3.5GHz to 3.8GHz and from 5.58GHz to 7.4 GHz. The simulated and measured results are in good agreement and the proposed antenna can be used satisfactorily for W-LAN and WiMax applications. The proposed technique can also be used for size reduction of loop antennas.

Keywords—coplanar stripline; loop antenna; multiband; wideband; wavelength

I. INTRODUCTION

UWB band allocation ranges from 3.1GHz to 10.6GHz. There are 12 different bands, each 528MHz wide [1]. The center frequency of each band from [1] is used as reference below. The electrical behavior of the wire loop antenna is examined in [2]. For a fixed radius of the loop, the impedance of the antenna depends on the wire thickness. The relation between the wire thickness and loop radius is referred to as thickness factor (Ω). The thickness factor is defined in (1):

$$\Omega = 2\ln(2\pi r/b) \quad (1)$$

where Ω is the thickness factor, r is the radius of the loop in meters and b is the wire radius in meters, used to construct the loop antenna. The impedance variation of the loop as a function of the thickness factor and the loop circumference can also be seen in [2]. As the thickness factor decreases, antenna impedance also decreases. Therefore by varying thickness of the loop antenna, the impedance of the antenna can be varied easily. The loop antenna is categorized as thin or thick loop. The thin antenna has $\Omega > 9$ and resonates at more than one frequencies [2]. The thick antenna is capacitive in nature with the advantage of almost uniform resistance. The loop antenna is also categorized as small or large loop antenna. When the circumference of the loop is equal to or larger than the

operating wavelength, the loop is called a large loop and small otherwise. In general, the small loop antenna has a circumference less than $\lambda/10$, where λ is the wavelength at which the antenna is designed. The small loop is a poor radiator while the large loop antenna is a good radiator as shown in [2]. The loop antenna resonates at a wavelength equal to the circumference of the loop. The circumference of the loop is calculated using (2) and (3):

$$C = 2\pi r = \lambda \quad (2)$$

$$\lambda = c/f \quad (3)$$

where C is the circumference of the loop antenna (m), r is the radius of the loop (m), c is the speed of light in free space (m/s), f is the design frequency of the loop (Hz).

A multiband antenna should operate at different frequencies with stable radiation patterns. Since a thin and large loop antenna resonates at different frequencies [2], it can be used to operate at different frequencies. It is observed that the pattern at a smaller wavelength is different from the pattern at a larger wavelength for the specified band of operation. This happens due to the variation in the current distribution along the loop due to variation in the operating wavelength. A thin loop with $\Omega=12$ resonates at $C/\lambda=1.1$ i.e. $C=1.1\lambda$ or $C=2.2\lambda$. The second resonant wavelength is twice the first. Therefore we can design a loop to have the two desired bands using (2). But this technique suffers from poor stability in radiation patterns. Figure 1 explains this very well. A simple wire loop whose circumference is $C=\lambda$ radiates normal to its plane as shown in Figure 1(a). When the same loop is excited at a wavelength double to that of the previous case, then the pattern does not remain the same (Figure 1(b)). The radiation pattern at 2λ is too random. Such an antenna cannot be claimed as a multiband antenna. A simple solution to this problem is that the circumference of the loop should vary in accordance with the desired wavelength. This arrangement will keep the circumference $C=\lambda$ or near to λ .

II. RESEARCH METHOD

Since mechanical changes in the entire structure of the antenna are not possible to hold $C=\lambda$ true for different wavelengths, the loop structure in Figure 2 is proposed. The proposed loop is square in shape and a coplanar strip (CPS)

line is added to it. The CPS line is added with multiple electronic switches that can be turned ON and OFF to change CPS line length. The change in the CPS line length finally changes the overall circumference of the loop.

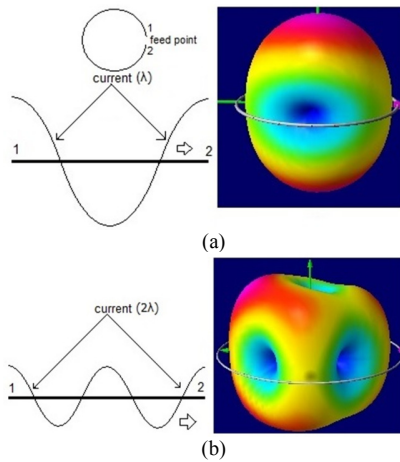


Fig. 1. The loop antenna showing radiation patterns at (a) λ , (b) 2λ .

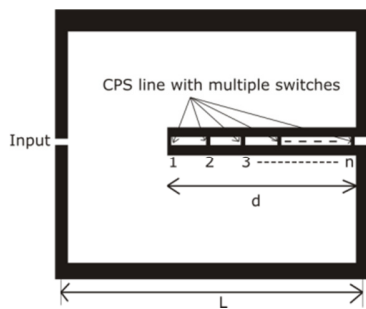


Fig. 2. Proposed loop antenna with CPS line along with the arrangement of switches.

The total length of the loop is $4 \times L$, L representing the arm length of the loop. When switch 1 is closed and the others are open, the length of the loop is $4 \times L + 2d$, where d is the length of the CPS line. Therefore, the loop length can be varied from $4 \times L$ to $4 \times L + 2d$. The loop length can be varied in small steps if the switches are placed close to each other. It is known that the transmission line only carries electrical energy from one point to another but does not radiate significantly. Therefore the four sides of the loop are the only radiating components of the proposed structure. The role of the CPS line is to only vary the overall length of the structure and eventually the generation of multiple bands. This structure ensures that the current distribution along the radiating portion will remain the same, therefore uniform radiation pattern is expected. A square loop of 16mm outer length and 0.7mm and 1mm width is simulated using CST Studio software in order to know the availability of possible bands with the corresponding antenna impedance as shown in Figure 3. It can be observed in Figure 4 that the antenna behaves differently for the two widths. There can be two bands available only after proper impedance matching. The larger width ensures larger bands since the antenna impedance is uniform. It can be observed in Figure 5 that the width of the loop antenna affects its impedance. When antenna width is

0.7mm, the loop resonates at 4.55GHz. The resistance at this frequency is about 125Ω . The resistance drops to about 96Ω for 1mm width. The loop with 1mm width shows minimum reactance at 5.1GHz and the resistance at this frequency is about 176Ω . The loop resistance is more than 270Ω for the same frequency when the width is 0.7mm. The antenna impedance for these frequencies is larger than the reference impedance of 50Ω , therefore there is poor reflection coefficient at these frequencies (Figure 4). Since the magnitude of the reflection coefficient is more than -8dB at the lower frequency, the band availability cannot be ignored. Another possible location for the availability of the band is at 7.6GHz and 7.9GHz for a loop with width 0.7mm and 1mm respectively. The reactance is larger at these frequencies. The loop with 1mm width has less variation in reactance than the loop with 0.7mm width.

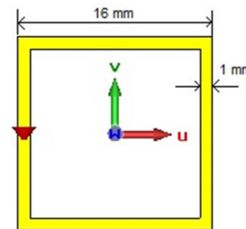


Fig. 3. Proposed loop antenna with CPS line along with the arrangement of switches.

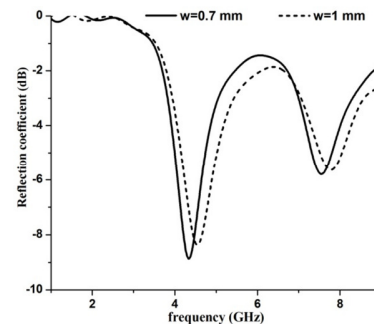


Fig. 4. Frequency v/s reflection coefficient of the loop antenna for different widths.

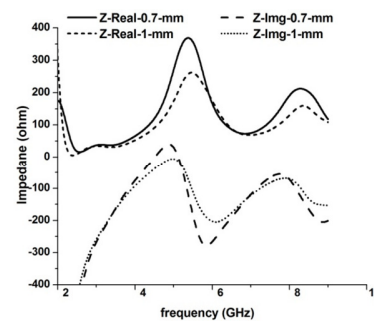


Fig. 5. Loop impedance as a function of width and frequency.

In order to solve the impedance mismatch problem, a printed BALUN transformer can be used to feed the antenna. The inclusion of the BALUN increases antenna size and if possible should be avoided. Here, we are providing a simple

solution to bring antenna impedance down to the reference impedance of 50Ω. Above, it was demonstrated that the loop impedance can be varied by varying the loop width. Therefore, instead of having a uniform width the loop can be made to have non uniform width. The proposed loop antenna contains non uniform width which changes gradually from 1mm to 1.5mm and then to 2mm towards feed end. Since there is no standard technique to introduce nonlinearity in the loop antenna, the dimension for the different arms of the loop is chosen only after multiple simulations. The different dimensions are given to the loop for reducing antenna impedance so that the loop can be directly fed with a 50Ω source. The dimensional information of the loop is shown in Figure 6. The feed is connected to the broader width of the antenna since it offers low impedance while the narrow width offers high impedance. Here the broader width helps converting loop antenna to a thick antenna which has low resistance with high capacitive reactance. The narrow dimension of the loop is present at the opposite of the feed and is 1mm wide. The narrow dimension of the loop converts the loop to a thin antenna which has high resistance and inductive and capacitive reactance. Therefore this combination brings overall antenna impedance to a uniform level. Finally, a folded coplanar strip line (CSP) feed is added to the loop. The folded CSP feed not only helps in lowering antenna impedance to 50Ω but also it saves the onboard space as most of the part of the folded CSP is within the loop area as shown in [1]. The proposed feed can be useful in feeding the antenna directly with a coaxial feed. The dimensional details of the folded CSP line are shown in Figure 7.

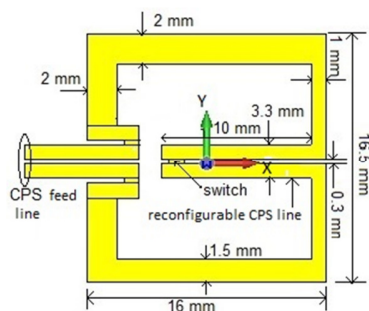


Fig. 6. The proposed loop with dimensional details.

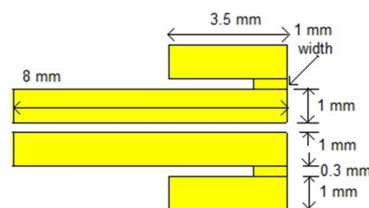


Fig. 7. The dimensional details of the feed.

The CSP line not only plays important role in the transformation of impedance but also converts an unbalanced coaxial cable to balanced feed [3]. The proposed loop is added with additional CSP line of 10mm length exactly opposite to the feed as shown in Figure 6. Therefore the inclusion of the CSP line can increase the length of the loop by 20mm. The CSP length can be increased or decreased by turning ON and

OFF the switches and the overall length of the loop can be varied to obtain different frequencies.

III. LOOP RESPONSE ANALYSIS

In this section, the proposed reconfigurable loop is analyzed for different switching conditions of the switches along CSP line. The ON state of the switch is realized by the short circuit and the OFF state by the open circuit. The switch is operated from the left of the CPS line towards the thin arm of the loop and the response of the loop is tabulated in Table I. It can be observed from Table I that there are two distinct modes of antenna operation: single and dual band modes. The antenna works as dual band antenna when the switch at locations 0mm and 3mm is ON from the left end of the CPS line. The bands covered are Band-6, Band-7, and Band-2, Band-8 respectively. Only one switch is ON at a time while the others are OFF.

TABLE I. BANDS GENERATED UNDER SWITCH ON STATE

Mode	Switch Location	f_1 - f_2 10dB BW (GHz)	Available band [1]	Center frequency (GHz)	% Band-width
A	0mm	3.5-3.8	No Band	3.65	8.2
		5.6-6.85	Band-6, 7	6.23	20
B	3mm	3.7-4.5	Band-2	4.1	19.5
		6.8-7.43	Band-8	7.12	9
C	8mm	4.17-5.9	Band-3, 4, 5	5	34.4
D	All Off	4.2-5.75	Band-3, 4, 5	4.975	31.2

A, B = dual band and C, D = single band, f_1 and f_2 are the lower and upper cut-off frequency respectively. The switch location is measured from the left of the CPS line shown in Figure 6.

It can be observed in Table I that when the switch at 8mm (near to the thin arm of the loop), is ON, the loop generates a wider band from 4.17GHz to 5.9GHz. The loop produces Band-3, Band-4 and Band-5 for this particular position of the switch. The loop generates the same bandwidth when all the switches present along the CPS line are OFF. Therefore to get the maximum number of bands at the minimum expense of switches, switch at location 8mm can be discarded. If we operate the switch at 0mm, and 3mm, we can easily get 7 different bands. It is also observed that the loop antenna generates larger bandwidth when it is operated under single mode (mode C and mode D). The maximum % bandwidth under C mode, CPS line is almost completely removed from the loop as the switch is closed. The lowest frequency observed under this mode of operation is 4.17GHz. When the switch at 0mm is ON, complete CPS line is added in series with the loop. The lowest frequency under this mode, i.e. mode A, is 3.5GHz. Since the area occupied by the proposed antenna is the same for the two frequencies, this technique can also be used to reduce antenna size. The different bands under the influence of the operating switches are shown in Figure 8, which gives a good idea of how well the proposed technique covers a wider band from 3.5GHz to 7.43GHz. In order to check the stability of the radiation pattern for claiming multiband operation, the radiation pattern at the center frequency of each band listed in Table I is analyzed. The radiation patterns are orthogonal to the plane of the loop and are shown in Figures 9(a) and 9(b). The patterns are plotted at the center frequencies of each obtained band listed in Table I. The plane of the proposed loop is aligned with X-Y plane for all radiation patterns. An antenna

having such a stable radiation pattern for different frequencies must have a uniform current distribution.

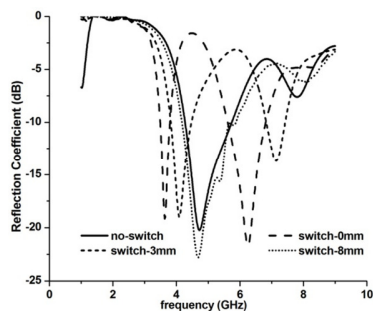


Fig. 8. The reflection coefficient v/s frequency for different switches.

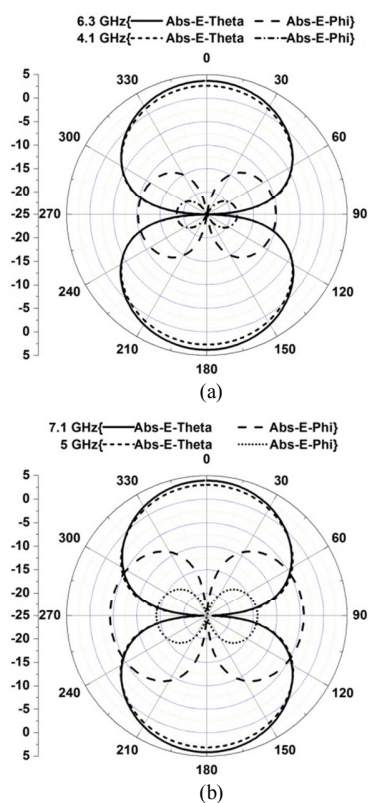


Fig. 9. The simulated radiation patterns at the center frequency of the bands listed in Table I.

In order to verify this relation, current distribution for all the plotted radiation patterns is reproduced and analyzed in Figure 10. The current distribution in the proposed antenna can be divided into two parts: a) Current in vertical arms, parallel to Y-axis and b) Current in horizontal arms, parallel to X-axis. The variation in the magnitude of current along the antenna is shown with a dashed line and the direction of current is shown with a continuous line (Figure 12(a)-(b)). It can be observed that the current distribution along Y-arms is in phase, while out of phase along X-arms. X-arms radiations are mutually canceled. On the other hand, the current from Y-arms contributes to radiation. The inclusion of the CPS line is completely justified here, as it only helps in reconfiguring the

antenna dimension and keeps the current distribution uniform along the loop for all the frequencies. A comparison of the proposed loop is done with other recent existing reconfigurable antennas. The summary of the comparison is shown in Table II.

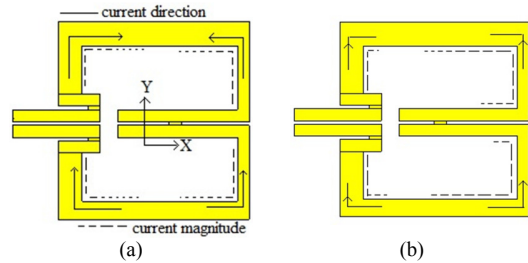


Fig. 10. The current distribution along the loop for different center frequencies. (a) $f=3.9\text{GHz}$, (b) $f=7.1\text{GHz}$

TABLE II. PROPOSED ANTENNA COMPARATIVE ANALYSIS

Reference	Bands	Frequency (GHz)	Number of switches	Number of antennas
[4]	2	1.8, 2.4	8	1
[5]	2	8.2, 10.4	1, MEM capacitor	1
[6]	2	15.95, 17.1	1, MEM capacitor	1
[7]	2	2.4, 5.8	Motor	2
[8]	3	1.58, 2.38	2	1
	5	1.51, 2.28	4	1
[9]	5	2.16-9	4	1
[10]	3	2.4, 3.5, 5.2	6	1
[11]	4	2.45, 3.49, 5.13, 5.81	2	1
Proposed	7	3.9-7.4	2	1

The antenna given in [4] generates two distinct bands centered at 1.8GHz and 2.4GHz. These two bands are generated using eight different switches. The antennas proposed in [5, 6] are multiband antennas generating two bands at 8.2GHz, 10.4GHz and 15.95GHz, 17.1GHz respectively. Both antennas use MEM switch for reconfiguration. There are four antennas proposed in [7]. The two antennas are used to generate two different bands and the others are used to change pattern and polarization. The two antennas used to generate different bands are selected using a rotating mechanism so the reconfiguration is controlled mechanically. The antenna proposed in [8] is operated with two switches and depending on the ON and OFF states of diodes, the antenna generates three different bands from 1.58GHz to 2.38GHz. When the same antenna is added with four diodes and is made ON or OFF in a particular sequence then it generates five different bands from 1.51GHz to 2.28GHz. The antenna proposed in [9] uses 4 switches and depending on the ON and OFF state of switches, it is operated as single, double and triple band antenna generating a total of 5 different bands. The antenna proposed in [10] uses 3 pairs of the diode and generates six different bands under single, dual and triple band modes. A single monopole antenna with two optical switches generates four different bands in [11]. The proposed antenna uses only two switches and can be operated as single and dual band antenna. When both switches are OFF, the loop works as a wideband antenna. The total bands generated by the proposed antenna are seven and is higher than all the antennas compared

in Table II. The proposed antenna uses a lesser number of switches. Other than this the antenna profile is very compact.

IV. RESULTS AND ANALYSIS

The proposed reconfigurable antenna is manufactured and tested using Vector Network Analyzer N9926A. A photograph of the entire four proposed antennas is shown in Figure 11. A comparison between the simulated and measured reflection coefficient is shown in Figure 12.

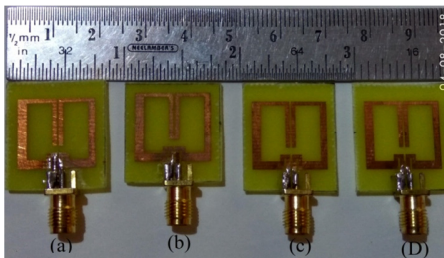


Fig. 11. Photograph of the reconfigurable square loops for (a) no switch, (b) switch at 0mm, and (c) switch at 3mm and (d) switch at 8mm.

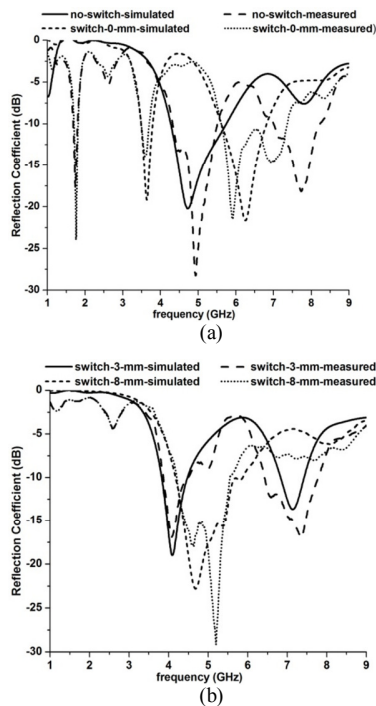


Fig. 12. Comparison between simulated and measured reflection coefficient.

TABLE III. SIMULATED AND MEASURED RESULT COMPARISON

Switch Location	Simulated f_1 - f_2 (GHz)	Measured f_1 - f_2 (GHz)	Bands Available	Center frequency (GHz)
0 mm	3.5-3.8	3.5-3.8	No Band	3.65
	5.6-6.85	5.58-7.4	Band-6,-7	6.23
3 mm	3.7-4.5	3.75-4.7	Band-2	4.1
	6.8-7.43	6.4-7.8	Band-8	7.12
All Off	4.2-5.75	4.2-5.7	Band -3, -4,	4.975
		6.8-8.3	-5	7.55

f_1, f_2 lower and upper cut off frequencies respectively

The simulated and measured results are in good agreement and are summarized in Table III. Measured results justify the importance of folded CPS feed and the role of the non-uniform loop arms with inner CPS line for frequency reconfigurability. It also shows that the inclusion of two switches is sufficient to cover seven different bands.

V. CONCLUSION

The proposed structure shows that a loop antenna can be designed to have multiple bands. The included CPS line within the antenna ensures the reconfigurability in antenna structure to get multiple bands with uniform radiation pattern. Since the CPS line does not contribute to radiation, the patterns generated for different lengths of CSP line have the same orientation. The proposed loop can be operated as single and dual band antenna and generates a total of seven bands using minimum number of switches. Since the proposed antenna covers Band-2, Band-3, Band-4, Band-5 Band-6, Band-7 and Band-8 ranging from 3.5GHz to 7.8GHz, it can be useful in WLAN 802.11 a/n and WiMAX applications. The proposed structure has the smallest dimensional profile. The proposed technique can be used for size reduction of the loop antenna.

REFERENCES

- [1] S. P. Shastri, R. R. Singh, K. V. Ajetroa, "Multiband Printed Loop Antenna For UWB Applications", Helix, Vol. 8, No. 4, pp. 3481-3490, 2018
- [2] C. A. Balanis, "Small Circular Loop: Loop Antennas", in: Antenna Theory: Analysis and Design, John Wiley & Sons, 2010
- [3] K. Wei, Z. Zhang, Z. Feng, "Design of a Wideband Horizontally Polarized Omnidirectional Printed Loop Antenna", IEEE Antennas And Wireless Propagation Letters, Vol. 11, pp. 49-52, 2012
- [4] P. Tilanthe, P. C. Sharma, "A New Frequency Reconfigurable Antenna", Journal of Active and Passive Electronic Devices, Vol. 9, pp. 133-140, 2014
- [5] K. Topalli, E. Erdil, O. A. Civi, S. Demir, S. Koc, T. Akin, "Tunable dual-frequency RF MEMS rectangular slot ring antenna", Sensors and Actuators A: Physical, Vol. 156, No. 2, pp. 373-380, 2009
- [6] K. Topalli, E. Erdil, O. A. Civi, "Reconfigurable Antenna Structures Using Mems Technology", IEEE Transactions on Antennas and Propagation, Vol. 55, No. 4, pp. 392-395, 2007
- [7] F. Alsharif, S. Safi, T. Aboufoul, M. Abu Nasr, S. A. Nasser, "Mechanical Reconfigurable Microstrip Antenna", International Journal of Microwave and Optical Technology, Vol. 11, No. 3, pp. 153-160, 2016
- [8] S. Sharma, C. C. Tripathi, "Frequency Reconfigurable U-Slot Antenna for SDR Application", Progress In Electromagnetics Research Letters, Vol. 55, pp. 129-136, 2015
- [9] X. Liu, X. Yang, F. Kong, "A Frequency-Reconfigurable Monopole Antenna with Switchable Stubbed Ground Structure", Radioengineering, Vol. 24, No. 2, pp. 449-454, 2015
- [10] H. I. Idris, M. R. Hamid, M. H. Jamaluddin, M. K. A. Rahim, J. R. Kelly, H. A. Majid, "Single-, Dual- and Triple-band Frequency Reconfigurable Antenna", Radioengineering, Vol. 23, No. 3, pp. 805-811, 2014
- [11] S. A. A. Shah, M. F. Khan, S. Ullah, A. Basir, U. Ali, U. Naeem, "Design and Measurement of Planar Monopole Antennas for Multiband Wireless Applications", IETE Journal of Research, Vol. 63, No. 2, pp. 194-204, 2017

Nonuniform C-Band Loop Antenna

A New Approach for Future UWB Applications

S. P. Shastri

Faculty of Engineering
Pacific University,
Rajasthan, India

shailendra.shastri@thakureducation.org

R. R. Singh

Thakur Educational Trust,
Mumbai, India
ravishrsingh@yahoo.com

K. V. Ajetroo

Electronics and Telecommunication
Department, K. J. Somaiya College of
Engineering, Mumbai, India
kiranjetrao@somaiya.edu

Abstract—Antenna design becomes very difficult at very small wavelengths and a special lab is required to manufacture a small antenna which costs a lot. A new approach is proposed to enhance the bandwidth of the loop antenna which can be designed at very high frequency using conventional PCB design technique. The proposed antenna is a nonuniform loop and covers UWB frequency range. The nonuniform structure of the loop is designed using the concept of both thin and thick loop antenna together which leads to an improvement in the antenna bandwidth. The proposed nonuniform loop antenna covers a band of 91.4% which is higher than any existing printed loop antenna. The frequency ranges from 3.54GHz to 9.5GHz and the measured result is in agreement with the simulated result. This technique can be very helpful in designing UWB antennas in the range of Ku band or higher than this.

Keywords—coplanar stripline; thin loop antenna; thick loop antenna; wire antenna; ultra wide band; nonuniform loop antenna

I. INTRODUCTION

UWB is a need of present and future communication systems as demand for more data is increasing. High-speed data transfer requires the availability of a larger band. In order to fulfill the need of larger bandwidth, broadband antennas are used as transmitting and/or receiving elements. Other UWB applications include location tracking and ground penetrating radars. So far monopole antennas appeared as strong candidates to fulfill the requirements of UWB applications. In order to improve gain and other electrical and radiation characteristics, metamaterials or EBG structures were added to monopole antennas. Dipole printed antennas fed with coplanar stripline (CPS) cover bandwidth from 3.1GHz to 11.4GHz. This structure has too many dimensional parameters in the antenna design [1]. A closed loop structure provides larger scope for the researchers to contribute. A square printed loop with L shape portion to its arm offers excellent performance at the lower-band of UWB system, ranging from 3.1GHz to 5.1GHz [2]. The antenna exhibits a -10dB return loss bandwidth over the entire frequency band. It is found that the lower band depends on the L portion of the loop antenna however the upper frequency limit is decided by the taper transmission line. The percentage of the bandwidth of the antenna is 48.78%. A printed loop antenna fed with coplanar waveguide can produce bandwidth of 1GHz and 1.14GHz. This antenna is suitable for

applications in PCS and IMT 2000 systems. The antenna has high gain with omnidirectional radiation pattern [3]. A small size loop antenna fed with CPW line produces a 70% bandwidth. The small size of the antenna makes it useful for array applications [4]. A single loop antenna has a narrow circular polarized bandwidth. When this antenna is added with another loop antenna as a passive element, then a second band is created and the combination of the antennas produces a larger bandwidth with circular polarization [5]. The band enhancement technique [2] was extended to a circular loop and bandwidth of 88.6% was achieved. The proposed work failed to give any justification on the enhancement of bandwidth and the impact of proposed shape on the antenna radiation pattern was not considered.

II. PROPOSED NONUNIFORM LOOP ANTENNA

A circular loop antenna with a thickness factor larger than 9, is called a thin loop antenna, otherwise it is called a thick loop antenna. The thin loop has multiple resonating frequencies and larger resistance with fluctuating characteristic. On the contrary, a thick loop antenna is capacitive in nature with low and uniform resistance [6]. The thickness factor is defined in (1), where Ω is the thickness factor, r is the radius of the loop in m and b is the wire radius in m:

$$\Omega = 2 \ln(2\pi r/b) \quad (1)$$

A loop antenna is basically a narrow band antenna. The bandwidth of the antenna can be improved when both thin and thick loop antennas are added together to have a uniform standing wave ratio (SWR) [7]. Its loop is comprised of a thick loop with 8.8 thickness factor and a thin loop with 11.7 thickness factor and covers 88.6% bandwidth. A wire loop antenna can be modified into a printed loop antenna using (2) as given in [8]. The thickness factor can be calculated using (1) and (2), where w is the width of the printed loop and b is the wire radius:

$$b = w/4 \quad (2)$$

In order to further improve the loop antenna bandwidth, a new geometry is proposed and is shown in Figure 1. The proposed geometry has a gradual increase in the width of the loop to have thin and thick loop properties together, unlike the

geometry in [7], which also has a step change in the width of the loop.

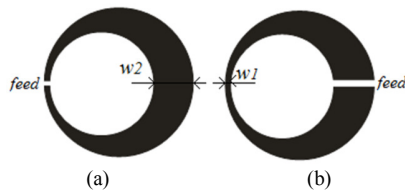


Fig. 1. Nonuniform loop with (a) feed at narrow width W1 (b) feed at wide width W2.

A loop antenna falls under two categories: 1) A large loop whose circumference is equal to or larger than a wavelength at a chosen frequency, 2) a small loop with circumference smaller than $\lambda/10$. A large loop is a good radiator while a small loop is a good receiver [9]. In order to cover the least frequency of 2GHz, the approximate radius of the loop using (3) and (4) is 24mm and the width of the loop is 1mm. Ω of the loop is 12.76 so it is thin in nature. The same antenna for 12mm width has Ω of 7.26 and is, a thick loop.

$$C = 2\pi r = \lambda \quad (3)$$

$$\lambda = c/f \quad (4)$$

where C is the circumference of the loop, r is the radius of the loop in m, λ is the wavelength in m, f is the frequency in Hz and c is the speed of light in m/s in free space. The antenna is simulated using CST STUDIO. The substrate used is FR-4 with a height of 0.8mm.

III. FEED LOCATION AND WIDTH IMPACT ON THE PERFORMANCE OF THE PROPOSED ANTENNA

The proposed geometry has minimum width $W1$ and maximum width $W2$ to give a nonuniform dimension. The outer radius of the loop is taken as 24mm. In order to analyze the characteristics of the nonuniform loop and the effect of this geometry on feed location, a feed is applied at one width and the same or other width of the loop varies.

A. Feed Impact at Narrow Width $W1$ with Varying Width $W2$

The possible advantage of the proposed structure is that there can be infinite locations for antenna excitation. This is because at different locations the feed will experience different loop width. Therefore the loop electrical properties will be different for different locations of the excitation due to its nonuniform structure. Nonuniform loop with thin width $W1$ of 1mm and thick width $W2$ of different values ranging from 6mm to 12mm is simulated. The feed to the loop is placed at the thin end $W1$. The result of the proposed nonuniform loop is compared with 1) a thin loop of 23.5mm radius with 1mm width having $\Omega=12.76$ and 2) a thick loop of 18mm radius with 12mm width having a thickness factor of 7.26. In order to have the same loop size, i.e. thin loop, thick loop and nonuniform loop, the outer radius is kept 24mm. Since the proposed nonuniform loop has $W1=1$ mm and width $W2$ varying from 6mm to 12mm, it is a combination of thin and thick loop. A thin loop of thickness factor of 12.76 shows a huge variation in resistance value. It ranges from 80Ω to more than 400Ω as is

observed in Figure 2(a). The thin loop resonates at about 1.9GHz as shown in Figure 2(b). The thick loop of 7.26 thickness factor, as observed in Figure 2(b), has stable resistance and resonates at 6GHz.

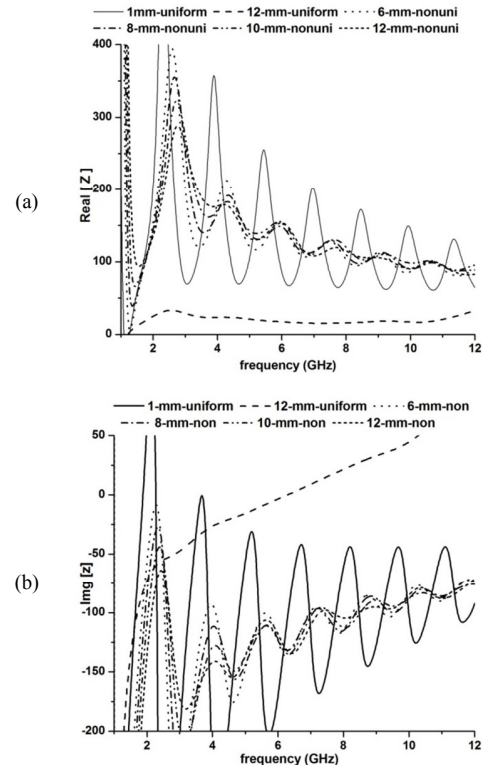


Fig. 2. Comparison of impedances of uniform and nonuniform loop when feed is applied at narrow width $W1$ and varying width $W2$.

It can be observed in Figure 2(a) that the resistance variation of the proposed loop antenna is reduced to a greater extent but it is larger than the resistance of the thick loop for all simulated cases. Similarly, the reactance of the nonuniform loop shows less variation when compared to the reactance of the thin antenna but it is larger than the reactance of the thick loop antenna as shown in Figure 2(b).

B. Feed Impact at Wide width $W2$ with Varying Width $W2$

In order to analyze the effect of feed locations on the characteristic of the nonuniform loop antenna, the feed is placed at wide end $W2$ as shown in Figure 1(b). The width $W2$ varies from 6mm to 12mm, while $W1$ is kept constant to 1mm. The behavior of the impedance of the nonuniform loop is shown in Figures 3(a) and 3(b). It is observed that the resistance of the nonuniform loop approaches the resistance of the thick loop antenna of uniform width of 12mm with $\Omega=7.26$. The resistance varies between 24Ω to 75Ω from 3GHz onwards. In Figure 3(b), it can be observed that as $W2$ increases from 6mm to 12mm, the reactance of the nonuniform loop decreases and approaches the reactance of the thick loop ($\Omega=7.26$) of 12mm width. The reactance of the nonuniform loop ranges from -75Ω to $+50\Omega$ for frequencies from 3.4GHz and onwards. The impedance of the proposed nonuniform loop under this case is smaller than in the previous case. The overall

impedance of the proposed loop for all cases is much smaller than the impedance of the thin loop with thickness factor of 12.76. Any increase in W_2 of the nonuniform loop reduces thickness factor of the antenna and antenna impedance approaches the impedance of thick loop with thickness factor 7.26.

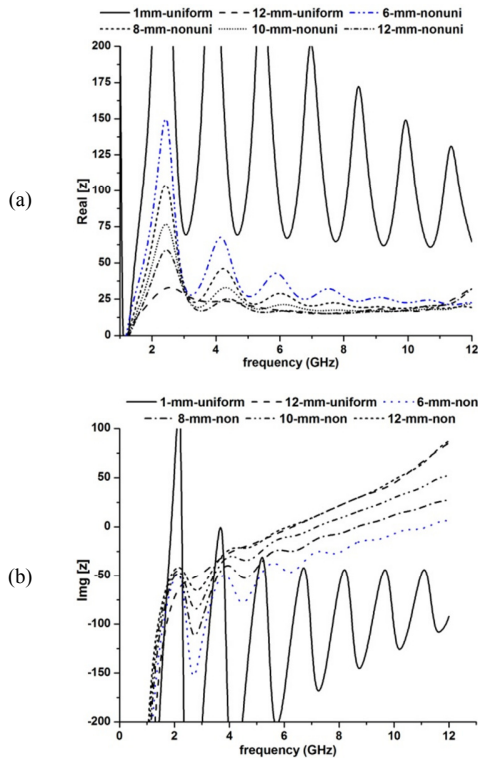


Fig. 3. Comparison of the reactance of uniform and nonuniform loop when feed is applied at wide width W_2 .

C. Feed Impact at Narrow Width W_1 with Varying Width W_1

Now the feed is placed at W_1 and width W_2 is kept at 6mm. W_1 varies from 1mm to 2mm. The result of this nonuniform loop is compared with the uniform loop of 24mm outer radius with 6mm width. The outer radius of the nonuniform loop is kept at 24mm in order to keep the same maximum dimension of uniform and nonuniform loop. The uniform antenna of 6mm width with an outer radius of 24mm has uniform resistance less than 50Ω from 3.3GHz and onwards as shown in Figure 4(a). The nonuniform loop with W_2 of 6mm and varying width W_1 from 1mm to 2mm shows that antenna resistance decreases with increase in W_1 . Any increase in W_1 leads to uniformity in the structure of the loop and also causes a drop in the thickness factor of the proposed antenna. Therefore the resistance of the nonuniform loop antenna decreases as shown in Figure 4(a). The antenna with uniform width of 6mm resonates at 11GHz. It is capacitive from 1GHz to 11GHz and then switches to inductive reactance. On the other hand, the reactance of the nonuniform loop is larger and capacitive from 1GHz to 12GHz and above. As W_1 increases from 1mm to 2mm, the antenna reactance reduces for obvious reasons as shown in Figure 4(b).

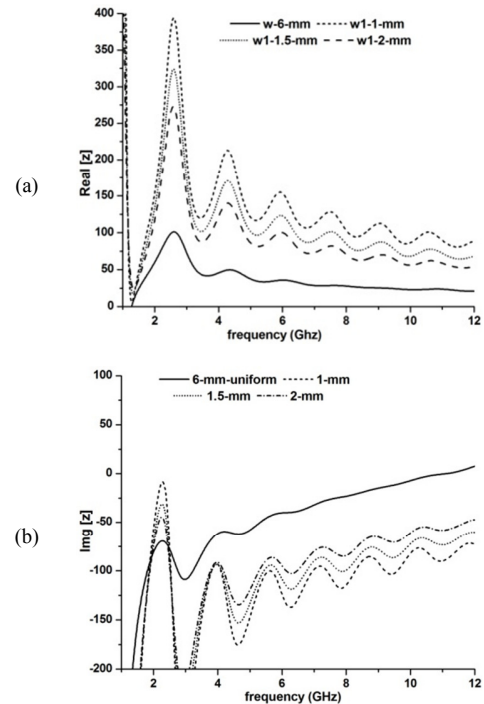


Fig. 4. (a) Resistance and (b) Reactance comparison of uniform and nonuniform loop when feed is applied at varying narrow width W_1 .

D. Feed Impact at Wide Width W_2 with Varying Width W_1

Now the feed is located at wide width W_2 and the width W_1 varies from 1mm to 2mm. W_2 is kept constant to 6mm. When the feed is shifted to W_2 end, there is a huge difference observed in the reactance of the nonuniform loop antenna. In the uniform antenna, the shift in feed location does not influence the characteristics of the antenna as the dimension seen by the two terminal sources triggering the antenna is uniform. This is not the case with the nonuniform loop for the same two terminal sources. The nonuniform loop with thin dimension W_1 of 1mm shows larger resistance. There is a continuous decrease in the resistance with increase in W_1 as this leads to uniformity of the proposed structure. The variation in resistance is shown in Figure 5(a). Larger resistance is observed from 2GHz to 2.6GHz for W_1 variation from 1mm to 1.5mm. The variation in resistance for W_1 of 2mm is very small and is well aligned with the resistance variation of the uniform loop of width 6mm from 2.7GHz onwards. It can be observed in Figure 5(b) that the reactances of uniform and nonuniform loop are well aligned from 3GHz and above. The two antennas, uniform and nonuniform, differ in their reactance from 2.45GHz to 3GHz. Table I summarizes the impedance behavior of the loop with different W_2 of 8mm and 10mm along with the earlier case of width W_2 of 6mm. Width W_1 ranges from 1mm to 2mm for all three cases. It can be concluded that for a feed at W_1 antenna impedance decreases significantly as W_2 increases. A huge fall in antenna impedance is observed when the loop is fed at W_2 . Therefore antenna impedance is a strong function of the feed location. Furthermore, the antenna impedance can be varied by changing W_1 and W_2 . This property of the proposed loop is not available in any other loop antenna available in the literature.

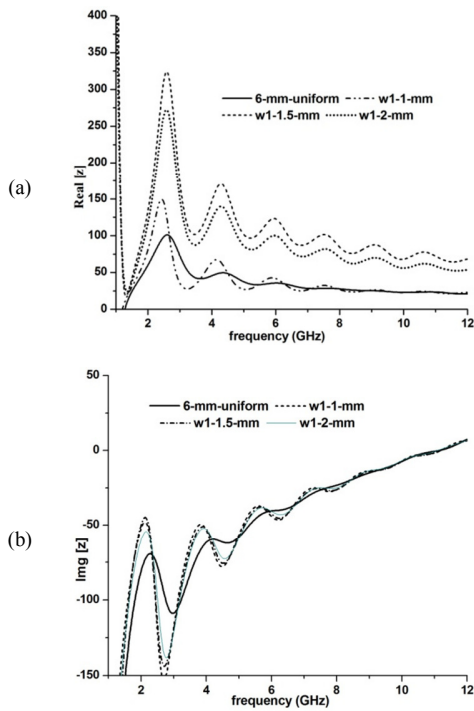


Fig. 5. (a) Resistance and (b) reactance comparison of uniform and nonuniform loop when feed is applied at wide width W2.

TABLE I. BEHAVIOUR OF PROPOSED NONUNIFORM LOOP ANTENNA

W2 (mm)	W1 (mm)	R/X (Ω) (4GHZ to 5GHz)		R/X (Ω) (8GHZ to 9GHz)		R/X (Ω) (11GHZ to 12GHz)	
		Feed at W1	Feed at W2	Feed at W1	Feed at W2	Feed at W1	Feed at W2
6	1	219/-134	49/-77	102/-87	23/-18	87/-77	21.3/4
	1.5	170/-124	52/-75	77/-80	24/-19	64/-66	21.6/3
	2	140/-113	52/-72	62/-69	23/-19	52/-54	21.7/3.4
8	1	183/-148	41/-51	97/-93	19/-105	87/-79	19/25
	1.5	146/-134	41/-49	76/-82	19/-1.7	66/-65	18/25
	2	122/-122	40.5/-47	63/-72	19/-1.5	53/-52	18/25
10	1	178/-144	31/-34	102/-100	17/13	88/-76	19/48
	1.5	140/-132	31/-33	80/-88	17/13	63/-64	19/47
	2	117/-120	30/-32	65/-74	16/13.8	51/-52	19/46

R-Resistance, X-Reactance

IV. LOCATING FEED FOR OPTIMUM BANDWIDTH

From the analysis above, it is concluded that antenna impedance is a function of the feed location. This section is dedicated to finding a suitable location of the feed to have the maximum bandwidth. The feed is applied from W1 end at 0° and is shifted to W2 end at 180° as shown in Figure 6(a). The reflection coefficient for all cases is compared in order to find the optimum feed location. Since the loop is a balanced antenna, it cannot be excited directly with SMA connector or coaxial cable. In order to excite the proposed loop with the help of SMA connector or any other unbalanced line, a coplanar strip line (CPS) is added to the loop as shown in Figure 6(b). For the simulations the outer radius of the nonuniform loop is kept at 24mm, the inner radius is 17.75mm with W1 of 2mm and W2 of 12mm. The inclusion of the CPS line converts the unbalanced field distribution from the SMA feed connector to a balanced field distribution at the loop [10]. The CPS feed line

is placed at different locations and the results are compared in Figure 7. The detailed dimension of the CPS line is included in Figure 6(b).

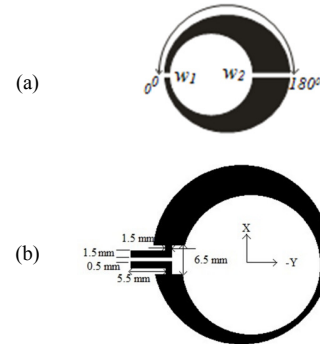


Fig. 6. The proposed nonuniform (a) showing various feed locations from W1 to W2 (b) loop with CPS feed line.

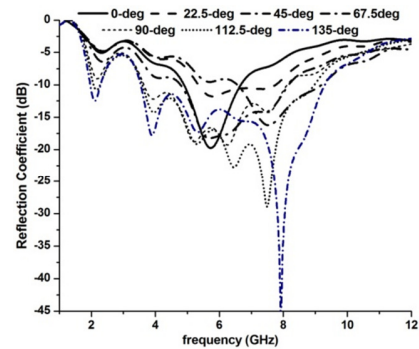


Fig. 7. Comparison of the reflection coefficient of the nonuniform loop for different feed locations.

It can be observed that the shift in the location of the feed influences the bandwidth of the antenna since the antenna impedance changes due to the change in the location of the feed as observed above. Table II summarizes the performance of the proposed loop in terms of % bandwidth of the loop with respect to different feed locations. It can be observed that the antenna gives the highest bandwidth when the feed is applied at 135°. The available bandwidth is 91.4%. The band has lower cut off frequency of 3.54GHz and higher cut-off frequency of 9.5GHz. Table III compares the proposed nonuniform loop antenna with other existing loop antennas. It can be observed that the proposed loop has the highest electrical and radiation bandwidth. Figure 8 shows the radiation patterns in the range of 3.54GHz to 9.5GHz. The loop antenna is placed in X-Y plane as shown in Figure 6(b). The radiation pattern is of end fire type and is available along -Y axis, opposite to the feed of the loop antenna. It was observed that the pattern is always available opposite to the feed of the loop for all cases listed in Table II. It is important to note here that when the proposed loop is compared with the loop proposed in [7], there is very little improvement in the antenna bandwidth. The advantages of the proposed loop over the earlier are summarized in Table IV. The earlier loop requires BALUN transformer but the loop presented in this paper does not require it, so it occupies a smaller area on PCB. In addition, the size of the presented loop

is almost half the size of the earlier loop whose outer dimension was 45mm. There are only three distinct locations for feed in the earlier loop: a) on the wide arm of the loop, b) on the thin arm of the loop, and c) between the interface of wide and thin arm of the loop. The loop in this paper has theoretically infinite locations to feed the antenna.

TABLE II. LOOP PERFORMANCE COMPARISON FOR DIFFERENT FEED LOCATIONS USING CPS.

Sr. No.	Feed Locations	f1-f2	% Bandwidth
1	0°	4.9-6.7	31
2	22.5°	5.4-7.6	34
3	45°	6.5-9.2	34
4	67.5°	4.8-8	50
5	90°	3.58-6.7	60.7
6	112.5°	3.7- 8.8	81.6
7	135°	3.54-9.5	91.4

f1, f2- lower and upper cut off frequency

TABLE III. PROPOSED AND OTHER LOOP ANTENNAS COMPARISON

Sr. No.	%Bandwidth	Reference	Year
1	88.6	[7]	2016
2	67	[11]	2015
3	40.7	[12]	2012
4	70	[4]	2010
5	48.8	[2]	2005
6	91.4	Proposed	-----

TABLE IV. PROPOSED LOOP AND EARLIER LOOP COMPARISON

	Property			
	Size	% Bandwidth	Feed Locations	Radiation Pattern
Proposed Loop	Smaller	91.4	Infinite	Stationary
Earlier Loop	Larger	88.6	Three	Not available

V. MEASUREMENTS AND DISCUSSION

Figure 9 shows a photograph of the proposed antenna. The proposed nonuniform loop is excited with a SMA connector directly. Figure 10 shows the measured and simulated reflection coefficient for the loop with CPS line feed at 135°. The measured result is in good agreement with the simulated one and ensures 91.4% bandwidth. The outer dimension of the loop is 24mm i.e. the antenna diameter is 48mm. The significant observation is that the loop antenna with outer dimension of 24mm and thickness factor of 12.76 resonates at around 1.9GHz. It resonates at about 6GHz when thickness factor changes to 7.26 as discussed earlier. The proposed loop is a combination of thin and thick loop with resonant frequency falling between 1.9GHz and 6GHz. The lowest cutoff frequency of the proposed loop is nearly 3.54GHz for which the antenna dimension should be smaller than 48mm. Therefore this technique can be useful for designing very high frequency antennas such as Ka band and higher where the dimension of the antenna becomes too small and a special lab is required for the manufacturing of the antenna.

VI. CONCLUSIONS

The proposed nonuniform loop antenna has the unique property of having infinite possibilities to feed the antenna. The

antenna offers different electrical properties for different feed locations. This property is not available in the conventional structure of loop antenna.

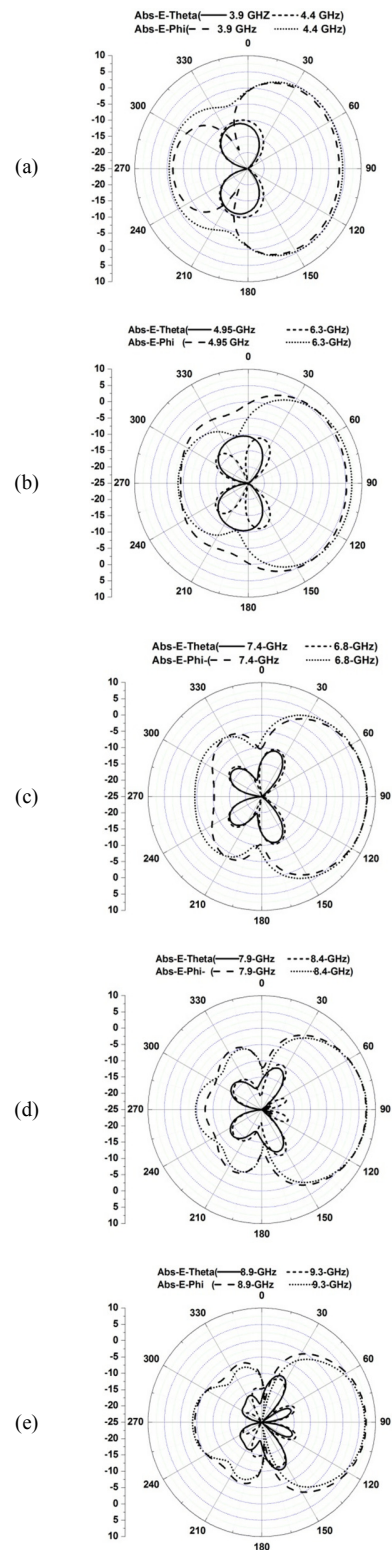


Fig. 8. Radiation pattern of the nonuniform loop at different frequencies.

The proposed structure with the CPS feed line can be excited with a coaxial SMA connector. The combination of thin and thick loop offers a wide bandwidth of 91.4%. The proposed dimension of the loop is expected to cover the lowest frequency of 2GHz but the lowest frequency obtained is 3.54GHz. This leads to an increase in the antenna dimension.

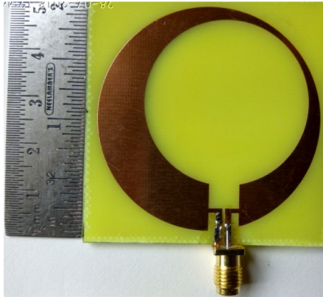


Fig. 9. Photograph of the proposed nonuniform loop antenna.

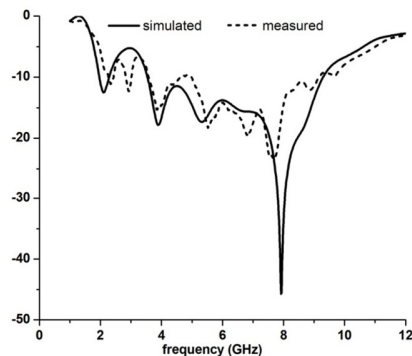


Fig. 10. The measured and the simulated reflection coefficient of the nonuniform loop antenna.

This approach can be used to design an antenna for Ka band applications or higher than Ka band where the antenna size becomes so small that a special lab is required to manufacture it. If this technique is used to design antennas at such a high frequency, the dimension of the loop will be sufficiently larger and simple pcb design technique can be used to manufacture the antenna at low cost. The proposed antenna shows wider % bandwidth than any other printed wideband loop antenna. The simulated and measured bandwidth of the loop is 91.4% with unidirectional radiation pattern oriented opposite to the feed. Since the pattern is available in the opposite side of the feed, the proposed antenna can have multiple feed points and pattern reconfigurability can be achieved.

REFERENCES

- [1] T. K. Roshna, U. Deepak, P. Mohanan, "A coplanar stripline fed compact UWB antenna", *Procedia Computer Sciences*, Vol. 46, pp. 1365-1370, 2015
- [2] K. Y. Yazdandoost, R. Kohno, "Design and Analysis of an Antenna for Ultra-Wideband System", 14th IST Mobile and Wireless Communication Summit, Dresden, Germany, June 19-23, 2005
- [3] T. A. Denidni, H. Lee, Y. Lim, "Wide-Band High-Efficiency Printed Loop Antenna Design for Wireless Communication Systems", *IEEE Transactions On Vehicular Technology*, Vol. 54, No. 3, pp. 873-878, 2005

- [4] F. M. Tanyer-Tigrek, I. E. Lager, L. P. Lighthart, "A CPW-Fed Printed Loop Antenna for Ultra-Wideband Applications and its Linear-Array Performance", *IEEE Antennas and Propagation Magazine*, Vol. 52, No. 4, pp. 31-40, 2010
- [5] R. L. Li, G. DeJean, J. Laskar, M. M. Tentzeris, "Investigation of Circularly Polarized Loop Antennas with a Parasitic Element for Bandwidth Enhancement", *IEEE Transactions On Antennas And Propagation*, Vol. 53, No. 12, pp. 3930-3939, 2005
- [6] Q. Balzano, K. Siwiak, "The Near Field of Annular Antennas", *IEEE Transactions on Vehicular Technology*, Vol. 36, No.4, pp. 173-183, 1987
- [7] R. R. Singh, S. P. Diwakar, S. Shastri, "Design of circular loop antenna with step change in loop width", 2016 International Conference on Signal Processing, Communication, Power and Embedded System, Paralakhemundi, India, October 3-5, 2016
- [8] R. L. Li, V. F. Fusco, H. Nakano, "Circular Polarized Open-Loop Antenna", *IEEE Transactions On Antennas And Propagation*, Vol. 51, No. 9, pp. 2475-2477, 2003
- [9] C. A. Balanis, "Small Circular Loop: Loop Antennas", in: *Antenna Theory: Analysis and Design*, John Wiley & Sons, 2010
- [10] K. Wei, Z. Zhang, Z. Feng, "Design of a Wideband Horizontally Polarized Omnidirectional Printed Loop Antenna", *IEEE Antennas And Wireless Propagation Letters*, Vol. 11, pp. 49-52, 2012
- [11] K. Xu, F. Liu, L. Peng, W. S. Zhao, L. Ran, G. Wang, "Multimode and Wideband Printed Loop Antenna Based on Degraded Split-Ring Resonators", *IEEE Access*, Vol. 5, pp. 15561-15570, 2017
- [12] J. Wu, Z. Zhao, Z. Nie, Q. H. Liu, "A broadband unidirectional antenna based on closely spaced loading method", *IEEE Transactions on Antennas and Propagation*, Vol. 61, No. 1, pp. 109-116, 2012

Multiband Printed Loop Antenna for UWB Applications

^{*1}Shailendra Shastri, ²Ravish R. Singh, ³K.V. Ajetroa

¹Pacific Academy of Higher Education and Research University, Udaipur, India

²Thakur Educational Trust, Mumbai, India

³K.J. Somaiya College of Engineering, Mumbai, India

Email: shastri_shailendra@rediffmail.com, ravishrsingh@yahoo.com, kiran_ajetroa@rediffmail.com

Received: 9th April 2018, Accepted: 14th May 2018, Published: 30th June 2018

Abstract

A printed loop antenna is designed to produce three distinct bands to cover six different frequency bands from UWB groups. Loop is fed using a printed BALUN transformer. The first band is available from 3.09 GHz to 4.44 GHz, the second band is available from 6.11 GHz to 7 GHz and the third band is available from 8.85 GHz to 10.5 GHz. The measured results are in good agreement with the simulated results. Frequency band from 3.0 GHz to 4.44 GHz covers UWB BAND-1 and BAND-2, the frequency band from 6.11 GHz to 7 GHz covers UWB BAND-7 and the last band from 8.85 GHz to 10.5 GHz covers UWB BAND-12, BAND-13, and BAND-14. Antenna rejects IEEE 802.11 Wi-Fi / WLAN band at 5.8 GHz.

Keywords: BALUN Transformer, Coplanar Stripline, Loop Antenna, Ultra Wideband, Wavelength.

1. Introduction

There is a continuous increase in the demand for more and more band with high data rate; therefore, UWB antennas have dragged attention of antenna researchers. Ultrawideband technology occupies a very large bandwidth and thus ensures the transmission of the larger data rate in the range of Gbps. In order to cover larger bands researchers have proposed different antennas to cover UWB frequency range from 3.1 GHz to 10.6 GHz. An UWB antenna senses all the frequency falling in its band but in order to reject busy channel and receive only free channels, multiband UWB antennas are preferred. Multiband antennas are antennas which generates multiple bands of interest. There can be different approaches to generate multiple bands: a) it is well known that the resonant frequency depends on impedance which in turn depends on the distribution of current in the antenna. Therefore multiband antennas can be designed using current reconfiguration techniques. Antenna current can be reconfigured by using electronic or electromechanical switches. b) Every antenna resonates at the designed fundamental frequency and its multiple frequencies.

This approach can be used to design a multiband antenna and is simpler than the approach (a). There are several approaches available in the literature to generate multiple bands in the loop antenna. A 3-D

loop antenna with three tuning strips produces five different bands for the application in smartphones. These bands are considered for -6 dB reflections coefficient [1]. A similar loop antenna is proposed to cover GSM 850/900, DCS 1800, PCS 1900, UMTS 2100 and LTE 2300/2500 bands by introducing reconfigurability technique. These bands are generated with the help of RF switch which is connected to reactive elements to influence the bands [2]. Dual asymmetric Loop antennas are integrated to work on WLAN/WiMAX. To have a larger impedance bandwidth a nonuniform loop width is used along with ground traces [3]. Loop antenna with outer SRR and inner strip can be operated as multi-mode and wideband antenna. Outer SRR loop radiates for odd modes and inner Loop radiates for even modes thus the multimode operation is achieved [4]. A loop antenna added with capacitive gaps and a passive strip along with a passive loop of smaller dimension than the main loop improves the gain and bandwidth of conventional loop antenna. By optimizing the gap between the main loop and passive strip and passive loop the upper cut-off frequency can be improved [5]. A small non-planar dual-meander folded loop antenna along with a disc loaded monopole produces omnidirectional radiation pattern with radiation efficiency of 65% and bandwidth of 10.8%. Bandwidth is enhanced due to proximity coupling between meander loop and monopole [6]. All the antennas proposed in these literatures either have complicated 3-D shape of loop or array of the loop and other passive structures are used to generate multiple bands.

In this paper, we are proposing a simple and planar structure of loop antenna which covers six different bands from UWB frequency range listed in figure 1. All the bands are generated without using any array or switch.

Entire work is divided into four sections, section 2 covers the design of loop for a reference impedance of 125 Ω and development of folded CPS (coplanar strip line) line to feed balanced loop antenna. Section 3 covers interfacing of proposed antenna with BALUN transformer and finally section 4 covers the measurement of proposed antenna.

2. Antenna Configuration and Design Consideration

Figure 1 shows the distribution of frequency spectrum of UWB. Each band is of 528 MHz wide, the centre frequency of each band is shown in the figure.

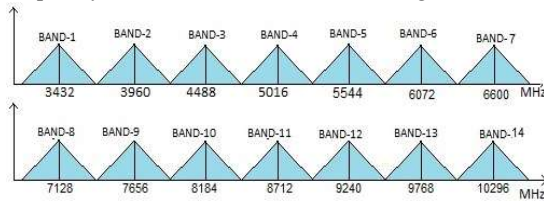


Figure 1: Band Group Allocation for UWB.

In order to cover UWB, printed circular loop is chosen. UWB ranges from 3.1 GHz to 10.6 GHz, therefore, the dimension of the loop is chosen to cover this band. Theory suggests that a large loop antenna when operated at a wavelength near to the circumference of the loop, first resonance occurs at the chosen wavelength and other resonance occurs at multiple of this wavelength. Loop antenna with different wire radii offers different impedances [7]. Loop with circumference much lesser than wavelength typically $\lambda/10$ is treated as the small loop and is not a good radiator [8].

Simulation is performed using IE3D simulation software. The final antenna is also simulated using CST STUDIO SUITE for comparison sake. Theory suggests that the electrical characteristic i.e. impedance of wire loop antenna is the function of the thickness of the wire. This relation between the thickness of wire $2b$ and radius of the loop is referred as thickness factor (Ω).

$$\Omega = 2 \ln \left(\frac{2\pi r}{b} \right) \quad (1)$$

Where Ω is thickness factor, r is the radius of the loop.

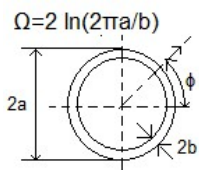


Figure 2: Loop Antenna showing the Relation between Wire Radius and Loop Radius.

Figure 2 shows the graphical significance of thickness factor. Loop antenna is also categorized as a thin and a thick loop. The thin antenna has Ω larger than 9 and resonates at more than one frequency. The thick antenna is capacitive in nature with the advantage of having almost uniform resistance. Since antenna impedance depends on the thickness factor of the loop by varying thickness of loop, antenna bandwidth can be varied easily.

The proposed antenna is a large loop as it is a good radiator. Least frequency of interest is 3 GHz in order to cover UWB range of 3.1 GHz to 10.6 GHz. The

circumference of the loop is calculated using the following relation:

$$C = 2\pi r = \frac{c}{f} \quad (2)$$

Where C is the circumference of the loop antenna in m, r is the radius of the loop in m, c is the speed of light in free space in m/s, f is the least frequency of loop in Hz.

Considering the fact that multiband antenna resonates at multiple frequencies, the thin loop antenna is chosen for the proposed design. For conversion from wire to the printed antenna, wire thickness is changed into the width of the printed antenna using relation given in [9]:

$$b = \frac{w}{4} \quad (3)$$

Where w is the width of printed loop and b is the radius of the wire, Figure 2.

In order to design printed loop, free space wavelength at 3 GHz is calculated and is 100 mm so the radius of the loop is approximately 15.9 mm, using relation (2). For the design of antenna Duroid 5880 with the dielectric constant of 2.2 and thickness of 0.787 mm is chosen. To find out the optimum radius of the printed loop on Duroid 5880 to cover the least frequency of 3 GHz, the loop is simulated for different widths ranging from 0.4 mm to 0.8 mm. Loop radius is chosen as 13.2 mm only after multiple simulations. Ω ranges from 12.05 to 13.44 for the specified widths and radius of 13.2 mm. Thus the loop remains a thin loop antenna for all the widths considered and resonates at more than one frequency [7]. Variation in resistance and reactance w.r.t. to loop width is shown in Figure 3. Simulated results for printed loop are well in accordance with the theoretical results of wire antenna. Loop with the radius of 13.2 mm and width of 4 mm is also simulated to show the characteristics of the thick loop antenna. Ω calculated is 8.8 and so the loop falls into the category of the thick loop. It can be observed in figure 3 that the resistance of the loop is uniform and is near to 60 Ω . Similarly, antenna reactance is capacitive and is nearly -100 Ω for a larger band.

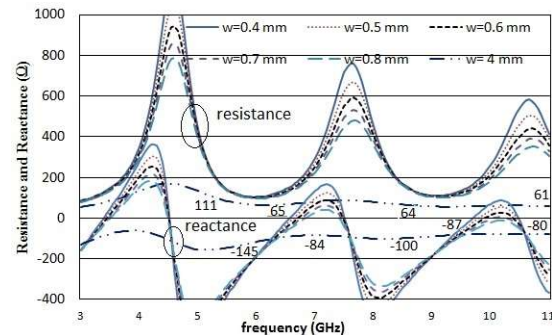


Figure 3: The Simulated Result of Frequency V/S Resistance for the Printed Loop Antenna.

So far it is observed that for a loop antenna under the category of the large loop as the width increases resistance and reactance of the loop decreases, figure 3. This characteristic of the loop can be used to control the bandwidth of the antenna. To verify this property, the loop is also simulated for reflection coefficient for different widths ranging from 0.4 mm to 0.8 mm. The simulated result is shown in Figure 4 and the result is

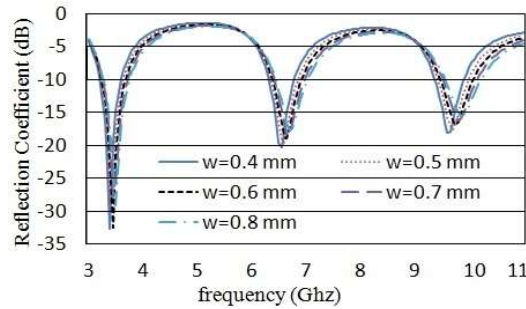


Figure 4: S_{11} V/S Frequency of Printed Loop Antenna for Various Widths.

Table 1: Loop Antenna Showing Start and End Frequency.

Width of loop(mm)	f_1 - f_2 GHz / BW (MHz)	f_1 - f_2 GHz / BW (MHz)	f_1 - f_2 GHz / BW (MHz)
0.4	3.23-3.60 (370)	6.31-6.79 (480)	9.4-9.9 (500)
0.5	3.22-3.63 (410)	6.33-6.85 (520)	9.42-9.98 (560)
0.6	3.26-3.71 (450)	6.41-6.96 (550)	9.46-10.1 (600)
0.7	3.3-3.77 (450)	6.4-6.9 (550)	9.5-10.148 (638)
0.8	3.27-3.74 (470)	6.44-7.03 (590)	9.56-10.2 (650)

f_1 -lower cut off, f_2 -upper cut off in GHz

tabulated in table 1. It confirms that there is an increase in the -10 dB bandwidth of the loop antenna for an increase in antenna width.

Reference impedance of 125 Ω is used to find -10dB bandwidth. Figure1 shows that each application band in UWB is of 528 MHz wide. Our aim is to choose a loop satisfying this requirement of the wide band.

Table 2 (a) and 2 (b) tabulates the impact of the width of loop antenna on resonant frequency and resistance at the resonant frequency. The loop of width 0.6 mm produces a band of 550 MHz and 600 MHz and impedance ranges from 132 Ω to 182.56 Ω , Table 1 and Table 2(a) respectively. Ω calculated using (1) for $w = 0.6$ mm is 12.63. Other widths of 0.7 mm and 0.8 mm also fulfil the requirement of the bandwidth of 528 MHz but the impedance is larger at the higher frequency, Table 1 and Table 2 (b) respectively. Larger impedance introduces difficulty in impedance matching. Therefore lower reference impedance is chosen which satisfies both the requirement of 528 MHz bandwidth and impedance matching. Therefore result in figure 4 is produced w.r.t. reference impedance of 125 Ω . Further reduction in reference impedance of 125 Ω does not fulfil the requirement of the minimum bandwidth of 528 MHz. Other widths of 0.4 mm and 0.5 mm give smaller band than 528 MHz, Table1, except 560 MHz bandwidth for 0.5 mm width. Therefore only single band is available and cannot fulfil the requirement of multiband antenna.

These comparisons show that loop with the width of 0.6 mm can be a good candidate for the UWB multiband applications. Band-7 ranges from 6.336 GHz to 6.864GHz and is not covered by the loop of width 0.6 mm as the start frequency at second resonance is 6.41 GHz, table1. The upper band for this width is from 9.46 GHz to 10.1 GHz and covers Band-13. There is a third band available from 3.26 GHz to 3.71 GHz with a bandwidth of 450 MHz. But this band is not suitable for the application. Increase in the loop

Table 2(a): Resonant Frequency and Resistance of Loop for Various Widths.

Width	0.4 mm		0.5 mm		0.6 mm	
	Resonant Frequency(GHz)	Resistance (Ω)	Resonant Frequency(GHz)	Resistance (Ω)	Resonant Frequency(GHz)	Resistance (Ω)
1	3.39	125.36	3.5	128.5	3.47	132
2	6.57	155	6.62	159.2	6.69	164
3	9.7	167.7	9.78	176.7	9.87	182.56

Table 2(b): Resonant Frequency and Resistance of Loop for Various Widths.

Width	0.7mm		0.8 mm	
	Resonant Frequency(GHz)	Resistance (Ω)	Resonant Frequency(GHz)	Resistance (Ω)
1	3.477	132.8	3.49	133.5
2	6.76	170	6.83	176.11
3	10.04	209.4	-----	-----

Table 3 Analysis of Effect of Feed Line on Bandwidth

Folded feed→	Case-1 (2.6mm)			Case-2 (3.1 mm)			Case-3 (3.6 mm)		
Length of main feed (mm)↓	f_1-f_2 GHz / BW (MHz)								
3.625	3.21-3.64 (430)	6.34-6.95 (610)	9.35-10.135 (785)	-----	-----	-----	-----	-----	-----
4.125	3.23-3.66 (430)	6.32-6.95 (630)	9.33-10.37 (1040)	3.21-3.65 (440)	6.29-6.91 (620)	9.25-10.29 (1040)	3.21-3.64 (430)	6.26-6.89 (630)	9.19-10.21 (1020)
4.625	3.22-3.65 (430)	6.3-6.95 (650)	9.35-10.52 (1172)	3.21-3.64 (430)	6.27-6.92 (650)	9.27-10.44 (1169)	3.21-3.63 (420)	6.26-6.9 (650)	9.19-10.33 (1140)
5.125	3.21-3.64 (430)	6.29-6.98 (690)	9.4-10.67 (1270)	3.20-3.63 (430)	6.26-6.95 (688)	9.31-10.56 (1250)	3.2-3.62 (420)	6.24-6.97 (670)	9.27-10.48 (1230)
5.625	3.2-3.64 (440)	6.28-7 (720)	9.46-10.7 (1240)	3.19-3.63 (440)	6.26-6.97 (720)	9.38-10.6 (1220)	3.2-3.62 (420)	6.24-6.95 (710)	9.31-10.52 (1210)
6.125	-----	-----	-----	3.19-3.62 (430)	6.26-7.02 (760)	9.46-10.58 (1124)	3.18-3.61 (430)	6.24-6.99(750)	9.37-10.5 (6(1190))

h= 0.25 mm, s = 0.36mm, f_1 -lower cut off, f_2 -upper cut off in GHz

radius reduces the resonant frequency therefore by increasing the radius of the loop; lower cut off frequency of the second band can be reduced to cover band-7. But this leads to shifting of other bands and also causes an increase in the size of the loop. In order to improve the antenna performance to cover the two bands with the same radius a new feed is proposed and is shown in Figure 5 (a).

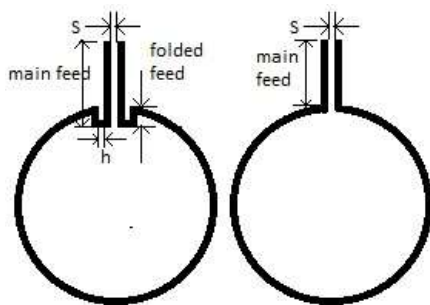


Figure 5: Loop Antenna with (a) Proposed Feed and (b) Conventional Feed.

New feed is the conventional CPS (coplanar stripline) only but with little modification in shape. Total length of the feed can be divided into i) folded length which is referred as folded feed and ii) main CPS feed referred as main feed, Figure 5(a). Table 3 summarizes the effect of main feed for three different lengths of folded feed. It can be seen that for all feed lengths, lower frequency band remains almost same

and is less than 500 MHz. Therefore this band is not useful. It is also observed from Table 3 that the middle band increases with increase in main feed line for all the cases. Third band increases with increase in the main feed line until feed length of 5.125 mm and then decreases as the feed length increases. The middle band for all the cases is more than 528 MHz and the third band is more than 1.056 GHz for most of the cases; therefore a total of three bands can be covered. In order to keep the antenna size as compact as possible, the total length of the modified feed can be chosen from one of the three cases.

Table 3 shows that the middle band covers BAND-7 for all lengths from 4.125 mm to 6.125mm. BAND-13 has lower cut off frequency of 9.504 GHz and upper cut off frequency at 10.032 GHz whereas BAND-14 has the lower cut off frequency at 10.032 GHz and upper cut off frequency at 10.56 GHz. These ranges of frequencies are well covered by loop when main feed line is 5.125 mm. There is always a possibility that the measured result of implemented antenna deviates little from the simulated results. Therefore the feed lengths are chosen in such a way that the simulated bands are larger than the expected bands. As far as the size of the proposed loop is concerned, both the feed lengths (total length) with the main feed of 5.125 mm and 5.625 mm occupy the same area for the folded feed of 2.6 mm (case-1) and 3.1 mm (case-2) respectively. Since the folded feed for case-2 is larger by 0.5 mm w.r.t. 2.6 mm folded feed of case-1, it penetrates more into the loop by 0.5 mm, Figure 5. Therefore the feed

location of main feed from the loop is at the same distance (2.525 mm) for both the cases when main feed is 5.125 mm and 5.625mm. The proposed feed length is chosen from case-1 of Table 3 and is of 5.125 mm. For this particular case, the third band is wider than the third band of main feed of 5.625mm.

Other than this total physical length of the feed for case-1 is smaller than the total physical length of feed (main feed + folded feed + h) of case-2 and is (5.125 + 0.25 + 2.6) 7.975 mm. Thickness factor Ω of this loop is 12.63. The first band is of 430 MHz and is not useful since it is less than 528 MHz, Table. 3.

In order to compare folded feeding technique with the conventional straight feed line, a printed loop of radius 13.2 mm with different lengths of straight feed line with a feed gap 'S' of 0.36 mm is simulated, Figure 5. It can be observed that the entire feed remains outside the loop and thus the overall antenna occupies larger space than the proposed feed since the proposed feed has half of the length inside the loop and half outside it. Various bands generated by the loop with straight feed for reference impedance of 125 Ω are tabulated in Table 4. It can be observed that when the feed length is 7.975 mm which is kept equal to the total feed length from proposed folded feed technique for optimum result, there are three -10 dB bands available. The first band is of 420 MHz wider and is not useful for the application. The second band is less than 1 GHz so covers a single band BAND-8. The third band covers BAND-14. Hence a total of two bands are covered which is less than the number of bands covered by the folded feed technique with loop of same radius of 13.2 mm. Larger length of the feed causes antenna to occupy larger area therefore to reduce the antenna area feed length is further reduced to 5.125 mm which is equal to the length of main feed from proposed feeding technique under the optimum result. For reduced feed length, first band remains almost similar to the earlier case, but the second band drops to 690 MHz and covers BAND-7. The upper band is increased and covers BAND-13 and BAND-14. Since antenna with feed 5.125 mm still occupies a larger area than the antenna with proposed feed, straight feed length is further reduced to 4.625 mm. For this feed length, antenna covers BAND-7, BAND-13, and BAND-14. But the antenna area is still larger and it can also be observed in Table 4 that the lower and upper cut off frequencies are very much close to the recommended cut off frequencies. Hence any manufacturing limitation may shift the measured cut off frequencies lesser than the expected one. Further reduction in feed length leads to the reduction in the number of bands covered and only band BAND-7 and BAND-13 are covered. The last case of the length of 2.525 mm is included here purposely since for this case area occupied by the loop with straight feed and folded feed are same. But loop with the straight feed of 2.525 fails to cover any of the bands. It can also be observed from Table 4 that the pattern of variation of

all the three bands is similar to the pattern of variation of all the bands of Table 3 for the increasing feeding

Table 4 Loop Antenna Showing Different Bands for the Straight Feed Line.

Length of main feed (mm)	f_1-f_2 GHz / BW(MHz)	f_1-f_2 GHz / BW(MHz)	f_1-f_2 GHz / BW(MHz)
7.975	3.18-3.6 (420)	6.49-7.44 (950)	9.81-10.6 (790)
5.125	3.21-3.64 (430)	6.3-6.99 (690)	9.48-10.8 (1320)
4.625	3.23-3.65 (420)	6.32-6.96 (640)	9.42-10.58 (1160)
4.125	3.23- 3.66(430)	6.33-6.96 (630)	9.4-10.44 (1040)
2.525	3.26-3.7 (440)	6.4-6.96 (560)	9.48-10.23 (750)

f_1 -lower cut off, f_2 -upper cut off in GHz.
length.

The first band remains almost constant w.r.t. any increase in the feed line, second bandwidth increases with length and the third one first increases then decreases with increase in length.

3. Interfacing Loop with BALUN

Loop antenna is a balanced antenna and must be fed with a balanced feed. Since connectors available to feed any antenna are unbalanced in nature, a BALUN (balanced to unbalanced) transformer is required. There are different BALUNs available to feed balanced antenna such as taper BALUN [10] and compact BALUN [11]. Since the length of tapered BALUN is dependent on the mismatch between the reference impedance and the load impedance i.e. antenna impedance, BALUN is very large in size. In order to have a compact size of the antenna, instead of taper BALUN compact BALUN is used here. The structure of the BALUN is shown in Figure 6 along with the proposed loop. It can be observed in Figure 6 that the BALUN comprises of three sections: microstrip line MS which is unbalanced in nature, coupled microstrip line, then coplanar stripline which is balanced in nature. The width of the microstrip line is 2.42 mm for 50 Ω . Length of the microstrip line is chosen to accommodate SMA connector and is 5 mm. Length of the middle section is about one-fourth of the wavelength of the central frequency of 3.1 GHz - 10.7 GHz. Length of the coupled microstrip line after multiple simulations is taken as 8 mm with a gap of 3.3 mm between them. Coplanar stripline is designed to have a characteristic impedance of 125 Ω . Length of the coplanar line is chosen to have smallest possible length while keeping loop antenna away from the ground plane. Length of the coplanar line is 10 mm. The gap between the coplanar lines is 0.2 mm. The smaller length of CPS brings antenna closer to the ground plane and the antenna loses its desired characteristics. Loop antenna is connected at the port

(2) of the printed BALUN transformer. Figure 7 shows the bandwidth of the BALUN when the impedance is 50Ω at the port (1) and 125Ω at the port (2). It can be observed in Figure 7 that the BALUN covers a band from 2.66 GHz to 10.2 GHz.

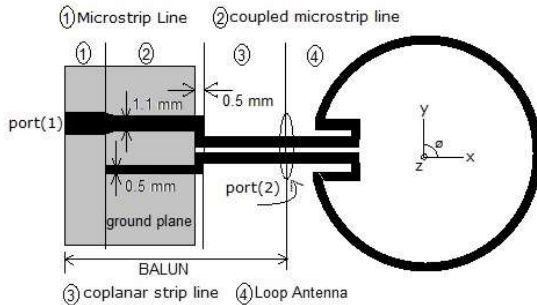


Figure 6: Compact BALUN Transformer Interfaced With the Loop at Port 2.

It also includes the simulated result of the reflection coefficient of the loop connected with BALUN transformer and loop without BALUN transformer. It can be observed that the loop antenna without BALUN produces three bands as discussed earlier but when it is connected with BALUN it produces 4 different -10 dB bands and covers seven different bands. The first band extends from 1.7 GHz to 1.85 GHz to cover GSM, the second is from 3.03 GHz to 4.34 GHz and covers BAND-1 and BAND-2. The third band ranges from 6.17 GHz to 7.02 GHz and covers BAND-7, the fourth ranges from 8.89 GHz to 11 GHz and it covers BAND-12, BAND-13, and BAND-14. When the loop is interfaced with BALUN three additional bands are generated. These bands are centred at 1.8 GHz, 3.9 GHz and 9.2 GHz. These bands are not present when the loop is not interconnected with BALUN. Possible reasons for the presence of these bands are discussed in next section.

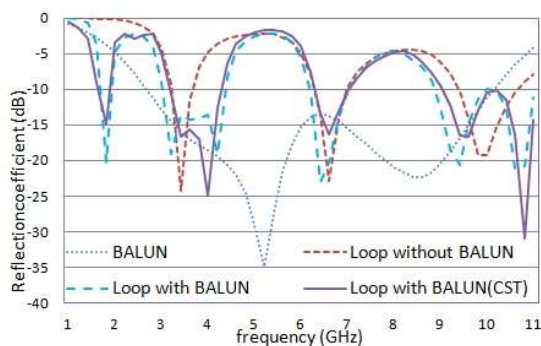


Figure7: S_{11} v/s Frequency Response of Loop, Loop Interfaced with BALUN along with BALUN response.

4. Measurement of Loop with BALUN

To check the validity of the proposed method loop is manufactured on Duroid 5880 and is tested using

Agilent Technologies: N9916A VNA. The measured result is reproduced along with the simulated one in figure 9. Figure 8 shows the photograph of the manufactured antenna.

It can be observed in Figure 9 that four distinct -10 dB bands are available. the first one is available from 1.7 GHz to 1.85 GHz, the second from 3.094 GHz to 4.44 GHz, the third is available from 6.11 GHz to 7 GHz and the final is available from 8.85 GHz to 10.5 GHz.

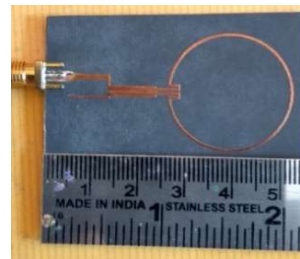


Figure 8: Photograph of the Manufactured Proposed Loop Antenna.

The measured and the simulated results are in close agreement. Loop antenna, when added to the BALUN, gives additional bands. In order to find out the possible reasons for the presence of these additional bands, current distribution along the loop with BALUN and wherever required loop without BALUN is analyzed and compared. The simulated result of current distribution along the loop is reproduced.

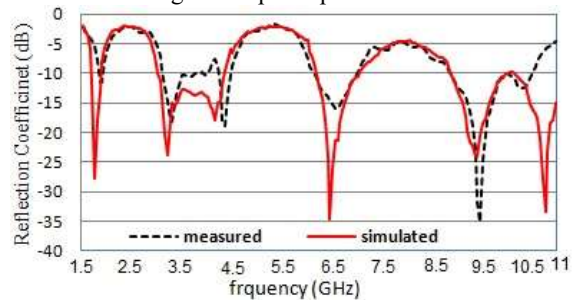


Figure 9: Measured and Simulated Result of the Proposed Loop Antenna.

Current distribution is presented in two different ways: a) distribution of current along circular loop with feed points 1, 2. b) same current distribution is reproduced along a straight line whose length equals to the length of the loop when it is open and made straight.

First band available is at 1.8 GHz when the loop is interconnected with BALUN. Figure 10 (a) shows the current distribution in the loop when it is not interfaced with BALUN. A varying dotted line represents a varying magnitude of current and solid line with the arrow represents the direction of the current.

Segment "a" and "b" contain current distribution in the same direction. Segment "a" acts as simple dipole of very small length w.r.t. free space wavelength of 166.67 mm at 1.8 GHz. Segment "a" is excited with source and segment "b" acts like a passive reflector as

it is not directly connected with the source. Length of this reflector is almost of length $\lambda/2$ due to half-length current distribution as shown in Figure 10(a). This arrangement leads to radiation towards feed only i.e. in $-x$ direction. Distribution of current shows that the current is very small at feed point 1, 2. This small current leads to the poor match with the source and there is no band available when the loop in not connected with BALUN transformer.

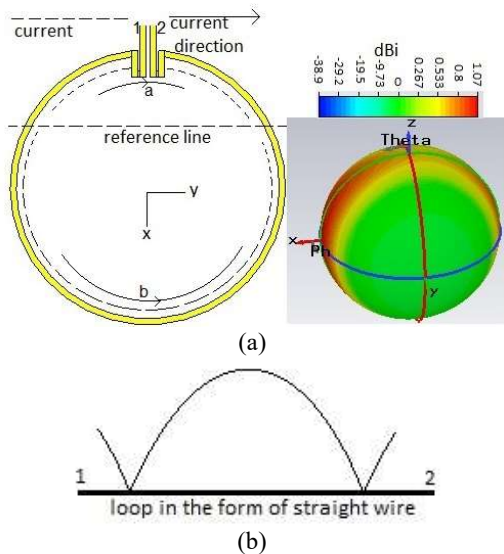


Figure10. (a) Simulated Current Distribution along Loop. (b) Radiation Pattern at 1.8 GHz without BALUN.

Free space wavelength at 1.8 GHz is 166.67 mm. When the loop is interfaced with BALUN, overall length of the loop increases by BALUN length. BALUN length is 18.5 mm and since it is balanced in nature, current travels from MS line into one arm of the BALUN then into loop and from the loop it goes

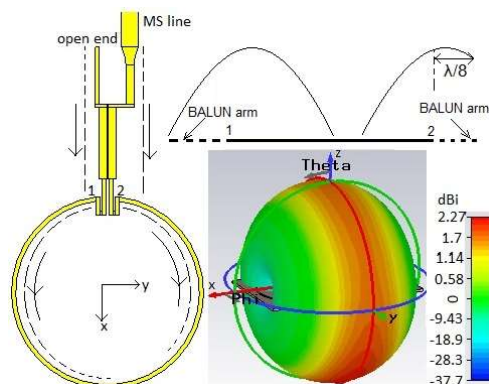


Figure11. Radiation Pattern and Current Distribution Along Loop at 1.8 GHz with BALUN.

into the second arm of the BALUN. Therefore current can see twice of 18.5 mm length. Thus overall length of this entire structure becomes 37 mm + 95.95 mm

(loop length with folded feed) = 132.95 mm, figure 11. This length is almost equal to one wavelength at 1.8 GHz if effective dielectric constant of Duroid is taken into consideration. It is well known that loop with a circumference equal to one wavelength resonates at this wavelength and produces a band.

Alternately it can also be explained w.r.t. current distribution. It can be observed that the current at point 2 is larger than the earlier case of the loop without BALUN, Figure 10. BALUN length is 18.5 mm and is nearly $\lambda/8$ at 1.8 GHz. BALUN arm connected to point 2 shifts the phase of the current by 45° . Therefore the magnitude of the current at point 2 and at MS feed is equal and large enough to establish matched condition. Other than this shift in current distribution shifts the orientation of the radiation pattern by 90° . Current distribution confined to loop is similar to simple dipole but of curved shape, therefore, the radiation is omnidirectional and is aligned along the y-axis, figure 11.

In the earlier case, the loop circumference was nearly half of the wavelength at 1.8 GHz. Free space wavelength at 3.4 GHz is almost equal to the circumference of the loop of 83 mm. Distribution of current along the loop is equal to one wavelength, Figure 12 (a). Current at point 1, 2 is weak and the inclusion of the BALUN at feed point 1, 2 improves the current distribution at MS feed. Current distribution around the reference line can be viewed

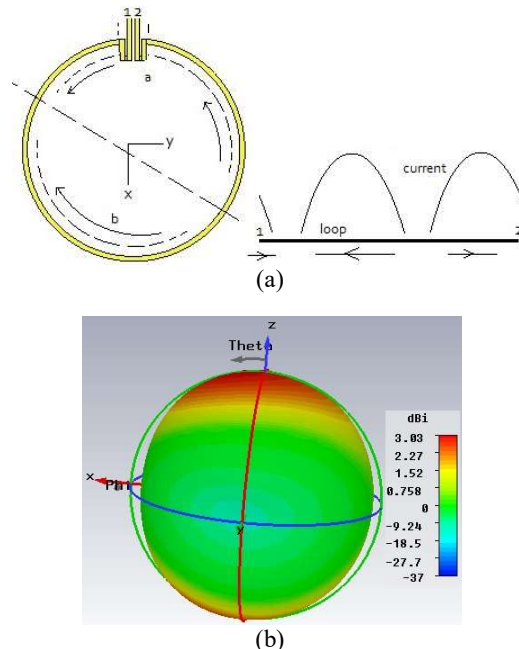


Figure12. (a) Simulated Current Distribution along the Loop. (b) Radiation Pattern at 3.4 GHz with BALUN.

as if a folded dipole is formed. This leads to an omnidirectional pattern with improved gain, Figure 12 (b). The loop without BALUN does not produce any

band at 3.96 GHz. Free space wavelength at 3.96 GHz is 76 mm and loop circumference is 83 mm, therefore, the loop is larger than the wavelength and current distribution is more than two half wavelengths as shown in Figure 13 (a). Length $\lambda/4$ is 19 mm and this length is close to the length of the BALUN. This quarter length shifts the phase of the low current available at point 2 by 90° to match the antenna with MS line. Current distribution along the loop can be divided in two parts "a-b" and part "c". Current distribution in part "a-b" is in the same direction but asymmetric w.r.t. feed at point 1, 2. When entire current distribution is viewed w.r.t. reference line it appears similar to the current distribution in a folded dipole. Radiation should be along $\pm z$ axis. But unequal current distribution in "a - b" segments of loop deviates the radiation away from $\pm z$ -axis, Figure 13 (b). It is also observed in Figure 13 (b) that there is radiation in (x, -y) direction. This is due to the asymmetric distribution of current in part "a - b". Part "b" is larger than "a" and contains larger current so the radiation is tilted more towards part "b". This gives radiation along $\pm z$ -axis and also in (x, -y) direction.

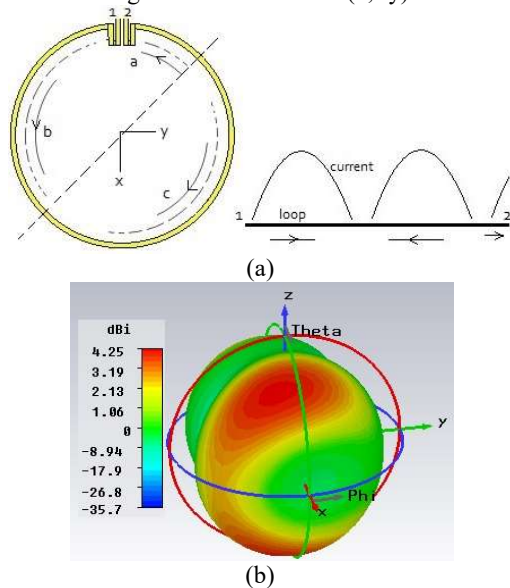


Figure13. (a) Simulated Current Distribution along the Loop. (b) Radiation Pattern at 3.96 GHz with BALUN.

Free space wavelength at 6.6 GHz is 45.45 mm. The circumference of the loop without the folded feed is 83 mm. Therefore it can be observed that there are more than three half cycles of current distribution along the loop. Radiation pattern can be explained w.r.t. the reference line passing through the centre of the loop. Part "a" and "b" can be viewed as folded dipole and similarly "d" and "c". These dipoles are formed along the reference line, Figure 14 (a). This current distribution is similar to the earlier case of 3.96 GHz except for one more current component along the loop. The reference line is shifted in clockwise direction

w.r.t. to the earlier current distribution. This shift in current

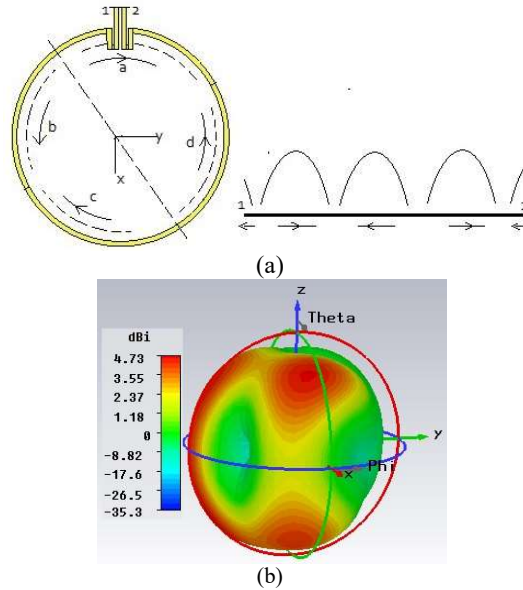


Figure14. (a) Simulated Current Distribution along the Loop. (b) Radiation Pattern at 6.6 GHz with BALUN.

distribution shifts the pattern in the clockwise direction. It is well known that the radiation along the axis of the dipole is zero and this can be observed in the radiation pattern of the loop. Similarly, radiation between part "b" and "c" and between "a" and "d" is

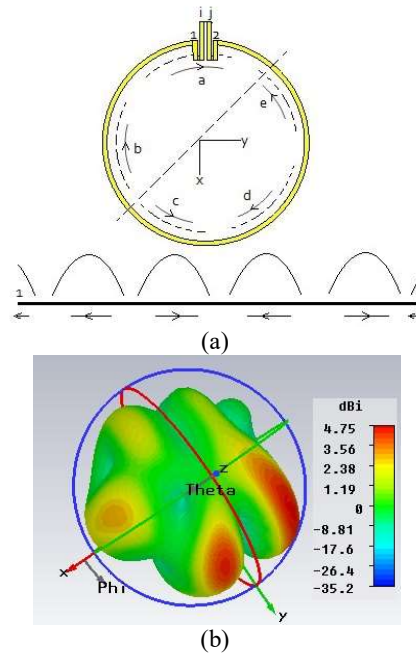


Figure15. a) Simulated Current Distribution along the Loop. (b) Radiation Pattern at 9.2 GHz with BALUN.

absent as there is no current between part "b" and "c" and between "a" and "d", Figure 14 (b).

The band at 9.2 GHz is available only if the loop is connected to the BALUN. Free space wavelength at this frequency is 32.6 mm. Loop circumference is 83 mm so able to accommodate more than two full wavelength current distributions and is clearly evident in the current distribution, Figure 15 (a).

Current distribution along the loop is viewed around the reference line as shown in Figure 15 (a). Currents in part "a"- "b" and "c"- "e" can be viewed as array of folded dipole and in phase. This arrangement of currents should give radiation along the $\pm z$ axis but the involvement of "d" component alters the pattern and the radiation is available in (-x, y) and (x, y) directions as shown in radiation pattern, Figure 15 (b). Nulls exist along the reference axis and between "a" -"b", "c"- "d" and "d"- "e".

It can be observed that the current at point 2 on the loop is very small. Folded feed whose length is 7.975 mm is approximately $\lambda/4$ in length and it transforms the current to maximum value at point j in Figure 15 (a). Length of the BALUN is 18.5 mm and is close to $\lambda/2$ in length at 9.2 GHz. It is well known that a load seen through a line of length $\lambda/2$ remains unchanged. Therefore a current maximum available at point j is also available to MS line feeding the BALUN and hence matching is achieved and an additional band is available at 9.2 GHz.

When the frequency is further increased to 9.7 GHz free space wavelength drops to 30.9 mm. The loop of circumference 83 mm can accommodate more than 2.5 wavelength current distributions and is shown in Figure 16 (a). Current distribution is similar to that of the earlier case of 9.2 GHz except for one more component of current due to increase in the frequency. Now there are total three pairs of half wavelength current distribution available. Current pairs "a"- "f" and "c"- "d" radiates along $\pm z$ axis as they are in phase but the additional pair "b"- "e" is opposite in phase and alters the pattern. The presence of current pair "b"- "e" improves the radiation in (x, y) direction compared to the earlier case of 9.2 GHz. The nulls are available along reference axis and between the two consecutive current components.

Current distribution at 10.3 GHz is similar to that of current distribution at 9.7 GHz, Figure 17 (a). The only difference is that the current distribution is shifted in clock-wise direction w.r.t. the earlier current distribution. The impact of this rotation in current distribution is clearly visible in the radiation pattern, Figure 17 (b). Current component "a" and "d" is in opposite direction as compared to the remaining current components. This pair is responsible for deviating the radiation from $\pm z$. Maximum radiation is available in (x, y) direction due to rotation of current

components. Nulls are present along the reference axis and between all the consecutive current components.

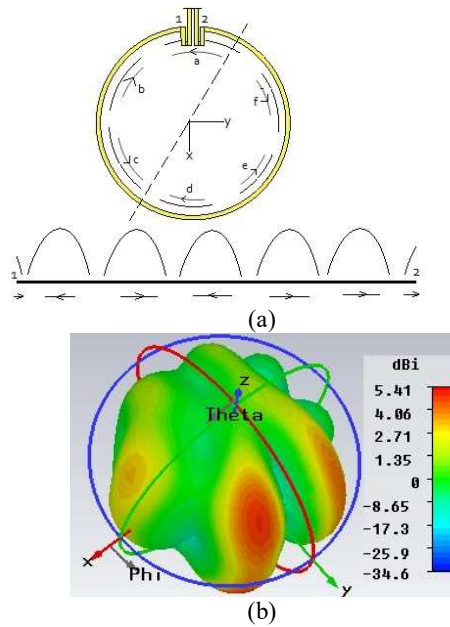


Figure16. a) Simulated Current Distribution along the Loop. (b) Radiation Pattern at 9.7 GHz with BALUN.

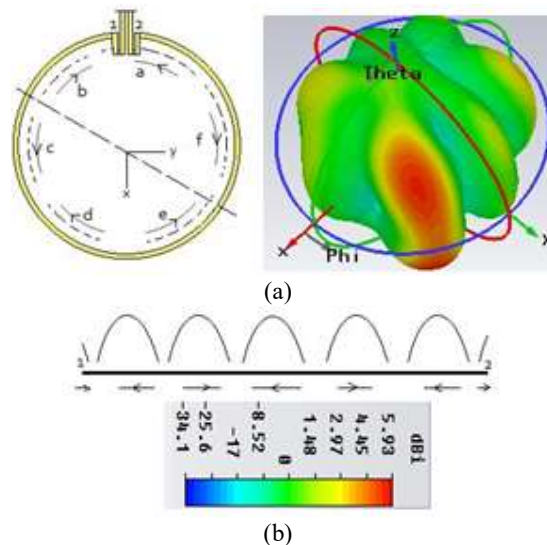


Figure17: (a) Radiation Pattern at 10.3 GHz (b) Simulated Current Distribution along Loop with BALUN.

Conclusion

It is shown that multiple bands can be achieved using simple printed loop antenna without using the reconfigurable technique. A new folded feed is proposed to feed the balanced loop. This feed can be applied to any balanced antenna. The advantage of the feed is that it reduces onboard space. The proposed multi-band loop is capable to generate four distinct

bands which cover six different bands from UWB group and one GSM band when interfaced with broadband printed BALUN transformer. The first band is available from 1.7 GHz to 1.85 GHz and covers upper GSM. The second band is from 3.09 GHz to 4.44 GHz and covers BAND-1 and BAND-2. The third band ranges from 6.11 GHz to 7 GHz and covers BAND-7, the fourth band ranges from 8.85 GHz to 10.5 GHz and it covers BAND-12, BAND-13, and BAND-14.

It is also found that the antenna rejects IEEE 802.11 Wi-Fi / WLAN at 5.8 GHz. Complete analyses of the current distribution along the loop reveal that at higher frequencies antenna current does not remain uniform and the radiation pattern fluctuates. Therefore the proposed antenna cannot be used for all the six bands at a time but can be used only for three different bands at a time i.e. from 3 GHz to 7 GHz together and from 8.85 GHz to 10.5 GHz together as the second group. To improve the antenna performance to have constant radiation pattern, RIS (reactive impedance surface) or other metamaterials can be introduced along with the proposed loop antenna.

Acknowledgement

Authors would like to express their thanks to Dr. Rajiv Gupta of Terna College of Engineering, Navi Mumbai, Maharashtra, India to provide support for the measurement of antennas. Authors are also very much grateful to the ROGERS Corporation for providing Duroid substrate.

References

- [1] C.W. Chiu and C.H. Chang, Multi Folded Loop Antenna For Smart Phones, Progress In Electromagnetics Research, PIER 102, 213-226, 2010.
- [2] Hao Wang et.al. Small Size Re-configurable Loop Antenna for Mobile Phone Application, <https://www.researchgate.net/publication/305523436>.
- [3] Chia-Mei Peng, I-Fong Chen, and Ji-Wei Yeh, Printed Broad Asymmetric Dual-Loop Antenna for WLAN/Wi MAX Applications, IEEE Antennas And Wireless Propagation Letters, VOL. 12, 2013.
- [4] Kuiwen Xu et.al., Multi-mode and Wide Printed Loop Antenna Based on Degraded Split-Ring Resonators, Journal of Latex Class Files, Vol. 14, No. 8, August 2015.
- [5] Jiangniu Wu et.al., A Printed Unidirectional Antenna With Improved Upper -Edge Selectivity Using a Parasitic Loop, IEEE Transactions On Antennas And Propagation, Vol. 63, No. 4, April 2015.
- [6] Wang-Table Hsieh and Jean-Fu Kiang, Small Broad Antenna Composed of Dual-Meander Folded

Loop and Disk-Loaded Monopole, IEEE Transactions On Antennas And Propagation, Vol. 59, No. 5, May 2011.

[7] Quirino Balzano and Kezimierz Siwiak, The Near Field of Annular Antennas, IEEE Transaction on Vehicular Technology, Vol. VT-36, No.-4, November 1987.

[8] Constantine A. Balanis, Loop Antennas, in Antenna Theory: Analysis and Design, 3rd ed, Hoboken, New Jersey, John Wiley & Sons, 2010, pp 257.

[9] Rong-Lin et. al., Circular Polarized Open-Loop Antenna, IEEE Transactions On Antennas And Propagation, Vol. 51, No. 9, September 2003.

[10] Wen-Hua Tu, and Kai Chang,, Wide-microstrip-to-Coplanar Stripline/Slot line Transitions, IEEE Transactions On Microwave Theory And Techniques, Vol. 54, No. 3, March 2006.

[11] Teck Beng Lim and Lei Zhu, Compact Microstrip-to-CPS Transition for UWB Application, 2008 IEEE MTT-S International Microwave Workshop Series on Art of Miniaturizing RF and Microwave Passive Components.

Capacitive Gap Loaded Dual, Triple and Wide Band Loop Antenna

^{*1}Shailendra P. Shastri, ²Ravish R. Singh, ³Sandeep Y. Pawar

¹Pacific Academy of Higher Education and Research University, Udaipur, India

²Thakur Educational Trust, Mumbai, India,

³Vidyavardhini's College of Engineering and Technology, Vasai, Maharashtra, India.

Email: ^{*1}shailendra.shastri@thakureducation.org, ²ravishrsingh@yahoo.com, ³sandeep.pawar@vcet.edu.in

Received: 15th September 2018, Accepted: 15th October 2018, Published: 31st October 2018

Abstract

In this paper, a printed loop antenna with current reconfiguration technique is proposed to improve the usability of the loop as a multiband antenna for UWB applications ranging from 3.1 GHz to 10.6 GHz. The current reconfiguration is achieved using a capacitive gap along the circumference of the loop antenna. The shift in the location of the capacitive gap changes the current distribution in the antenna and new bands are generated. It is found that using a single capacitive gap along the loop, the antenna can be operated as a wide band antenna whose frequency ranges from 6 GHz to 10.8 GHz with % bandwidth of 57. The proposed loop can also be used as dual and triple band antenna in the frequency range from 6 GHz to 10.8 GHz by simply switching ON and OFF the switches. The proposed antenna generates the highest numbers of bands at the minimum expense of switches. The proposed loop without capacitive gap is capable of covering only 24% out of the 3.1 GHz-10.6 GHz range. The range of band can be varied from 24% to 57% using the switches. The proposed antenna very well rejects the WLAN and WiMAX bands.

Keywords

Capacitive Gap, Current Reconfiguration, Loop Antenna, Multiband, Wide Band

Introduction

Reconfigurable antennas are required for the better selectivity of the desired band of operation. These are also used to have desired radiation pattern at different frequencies of operation. The reconfigurability in any antenna is achieved by introducing physical changes in the antenna structure. These changes in antenna structure bring change in antenna current distribution which changes antenna impedance. The performance of antenna changes as the antenna impedance changes. There are several techniques to achieve reconfigurability features in antenna. These techniques use electronic switches, optical, mechanical and electromechanical switches (Mohamed Nasrun Osman et.al, 2015). The change in current is introduced either in the antenna itself or in the ground plane (DGS: defected ground structure) as shown in (Mohammed Al-Husseini et. al., 2010) and (Xuelin Liu et. al., 2015). The structural modification in the antenna is used to control the orientation of the current in the antenna to generate different bands (Sonia Sharma and Chandra C. Tripathi, 2015).

Limitations and Solution to the Existing Multiband Loop Antenna

It is shown (S. P. Shastri, R. R. Singh, K.V. Ajetroa, 2018) that a printed loop antenna can be used to generate multiple bands to cover various bands under UWB applications ranging from 3.1 GHz to 10.6 GHz. Figure 1 is reproduced from (S. P. Shastri, R. R. Singh, K.V. Ajetroa, 2018) to show the multiband printed loop antenna. The loop is fed with a compact BALUN which is a compact size BALUN. This leads to the reduction in the overall dimension of the loop antenna. The loop antenna is interfaced with a printed BALUN and is simulated using CST STUDIO. The material used is DUROID 5880 with a thickness of 0.787mm.

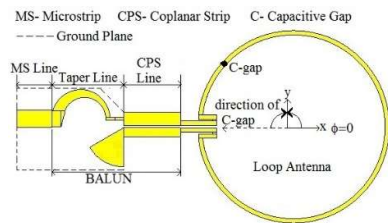


Figure 1: The Printed Loop Antenna Interfaced with a BALUN Transformer

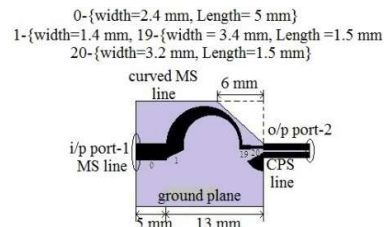


Figure 2: Dimensional Details of the Compact Printed BALUN Transformer

The loop radius is 13.2 mm with a width of 0.6 mm. This dimension of the loop is taken to cover the least frequency of UWB band which is 3.1GHz. The dimensional information of the BALUN is shown in Figure 2. The electrical characteristics of the loop are shown in Figure 3. The antenna generates three distinct bands from 3.1 GHz to 11 GHz.

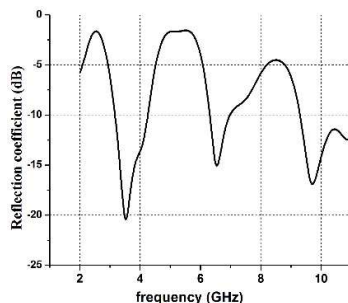


Figure 3: Reflection Coefficient v/s Frequency of Loop Antenna without Capacitive Gap

In order to claim the multiband property of the antenna, it is important to analyze the radiation patterns of the loop antenna at the claimed bands. The first band is available from 3.1 GHz to 4.2 GHz. The second band is available at 6.6 GHz with a bandwidth of 528 MHz. The last two bands are available at 9.77 GHz and 10.3 GHz with same bandwidth. It can be observed in Fig. 4 (a) and (b) that out of the three bands, the radiation patterns of the first band are uniform in θ -plane and are orthogonal to the plane of the loop, Figure 4(a).

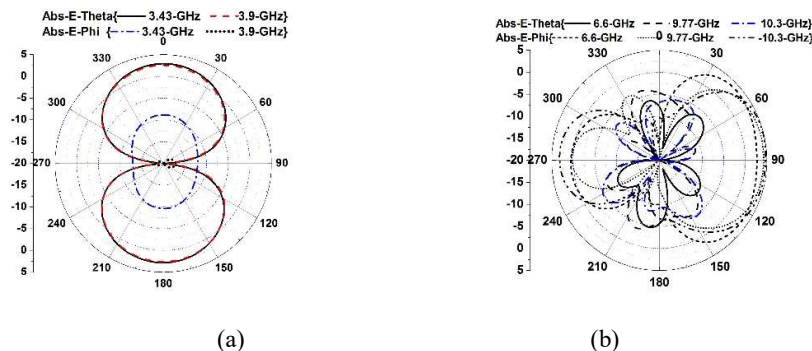


Figure 4: Radiation Pattern of Loop at 3.43 GHz, 3.96 GHz, 6.6GHz, 9.77 GHz, and 10.3 GHz.

But, the radiation patterns available for the last two bands are uniform in ϕ plane, Figure 4(b). Therefore the antenna can be claimed to have only dual band property. In order to increase the number of the bands and to claim the multiband feature of the antenna, a capacitive gap is introduced along the circumference of the loop as shown in Figure 1. The capacitive gap changes the current distribution along the loop. This change in the current along the antenna changes the input impedance of the antenna. A loop antenna of circumference equals to one wavelength is shown with input point marked as 1 and 2 in Figure 5(a). Figure 5(b) shows the current distribution in the same antenna at wavelength λ . It can be observed that a current maximum occurs at the feed points 1 and 2. Figure 5(c) shows the same antenna with a capacitive gap opposite to the feed point i.e. at the mid of the antenna. The current distribution throughout the antenna changes when excited at the wavelength λ . A current minima exists at the capacitive gap and the current is distributed in such a way that the current minima exists at the feed points. This leads to poor antenna impedance. This shows that the introduction of a capacitive gap at different locations, along the circumference of the loop, will lead change in the antenna impedance and this technique can be used to generate different bands from the loop antenna.

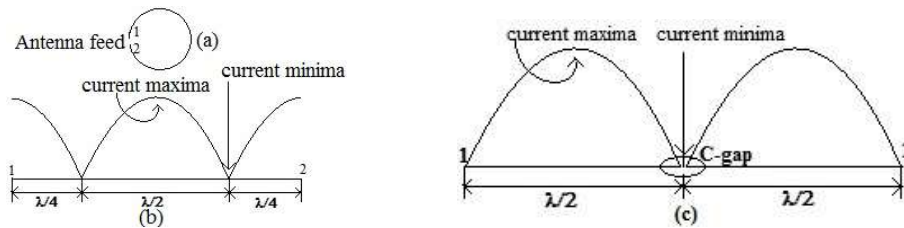


Figure 5: (a) Loop Antenna with Feed Point, (b) Current Standing Wave Along Loop with No Capacitive Gap, and (c) Current Standing Wave Along Loop with Capacitive Gap

Research Method

In order to generate more bands with a stable radiation pattern, a capacitive gap is added to the loop antenna and its impact on reflection coefficient and the radiation pattern is analyzed. The capacitive gap can be created by switching a diode ON or OFF at desired locations. In this paper the capacitive gap is realized using short and open circuit along the circumference of the loop. The capacitive gap is added to the loop from feed end and the location of the feed is augmented by 10^0 as shown in Figure 1. There is no useful band available till 40^0 , therefore, the electrical characteristic and the radiation patterns are not taken into consideration. Figure 6 shows that when the gap is created at 45^0 , the antenna generates a very wide range of frequency. This band ranges from 6.23 GHz to 10.2 GHz with a % bandwidth of 48.

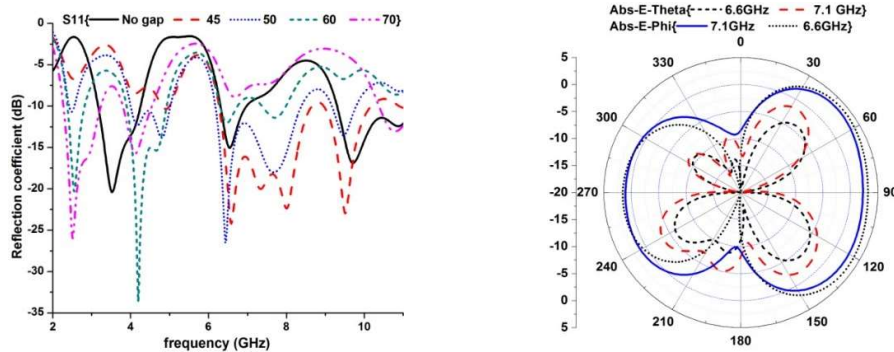


Figure 6: Reflection Coefficient v/s Frequency of the Loop Antenna Without and With Capacitive Gaps at Different Locations

The radiation patterns for this band are analyzed in order to verify the availability of the wide range of the frequency. It can be observed in Figure 7 that the radiation pattern is uniform for $\theta=90^0$ and $\Phi = 0^0$ which is the plane of the loop as shown in the Figure 1. So a wideband operation can be claimed when the capacitive gap is introduced at 45^0 .

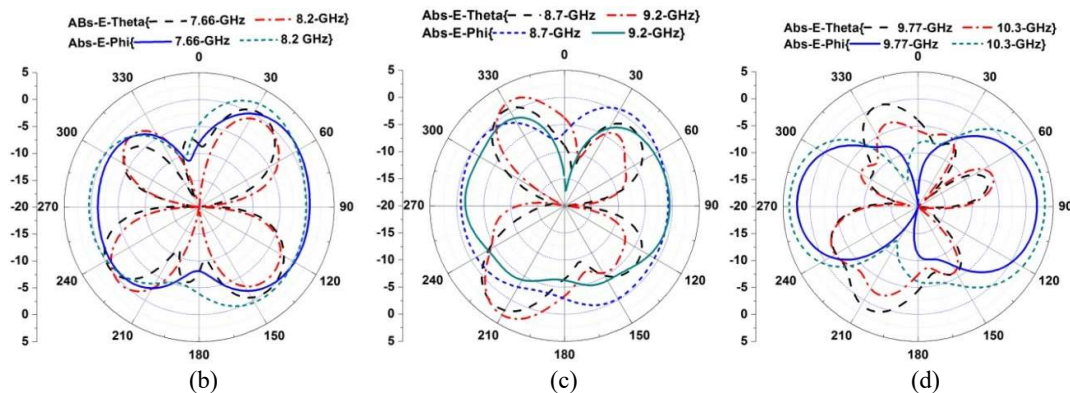


Figure 7: Radiation Pattern of Loop at (a) 6.6 GHz and 7.1 GHz, (b) 7.66 GHz and 8.2 GHz, (c) 8.7 GHz and 9.2 GHz, (d) 9.77 GHz, and 10.3 GHz for Capacitive Gap at 45^0 .

The loop responds in a similar way when it is added with a capacitive gap at 50° with a little drop in the reflection coefficient from 8.6 GHz to 8.9 GHz. The loop produces a new band from 4 GHz to 5 GHz. But a better response is observed for a capacitive gap at 60° as shown in Figure 6. The new bands available are from 2.36 GHz to 2.83 GHz, 3.8 GHz to 4.95 GHz and 7.34 GHz to 8 GHz. In order to verify the multiband operation of the loop with a capacitive gap at 60° , the radiation patterns are analyzed. It can be observed from Figure 8 that the radiation pattern at 2.4 GHz is orthogonal to the plane of the loop and is little inclined at 4.48 GHz since the two electric fields are comparable with each other. The radiation at 7.66 GHz is oriented in the horizontal direction. Therefore it can be claimed that when there is no gap and when gap is at 60° , there are total 3 bands with radiation patterns orthogonal to the plane of the loop. The first band is available at 2.4 GHz, the second is at 3.6 GHz and the third is at 4.2 GHz. The same antenna can be used to cover other 3 bands with the first band at 6.5 GHz, the second at 7.66 GHz and the third band at 10 GHz. The radiation for these bands are in the plane of the loop and is oriented at $\Phi = 0^\circ$. Therefore even though there are six distinct bands available for when the loop is operated with a capacitive gap (C-gap) at 60° and the loop with no C-gap. Therefore, only three bands can be claimed, i.e, three bands below 6 GHz or three bands above 6 GHz.

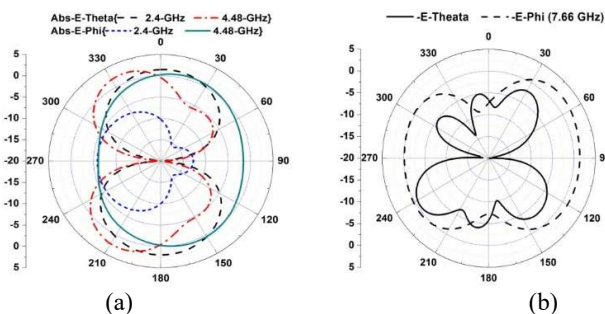


Figure 8: Radiation Pattern of Loop at (a) 2.4 GHz, 4.48 GHz and (b) 7.66 GHz for Capacitive Gap at 60° .

There is no fruitful result when the capacitive gap is at 70° , 80° and 90° . When a capacitive gap is created at 100° and shifted at 110° , the response of the antenna is almost the same for both the cases but is better when the C-gap is at 110° . The new bands generated under this case are from 7.27 GHz-8.5 GHz, and from 8.97 GHz to 10 GHz. So it can be concluded that the loop for this particular case works as dual band antenna. Therefore, when the loop loaded with a capacitive gap at 110° and the loop with no gap are considered, a total of four bands are generated to cover six different bands at 7.66 GHz, 8.2 GHz, 9.2 GHz and 6.6 GHz, 9.7 GHz and 10.3 GHz respectively. But the second band from the loop with C-gap at 110° and the first half of the second band from the loop with no C-gap are overlapped therefore the antenna can be claimed to cover only three bands. The details of the electrical and radiation pattern characteristics are shown in Figure 9 and Figure 10.

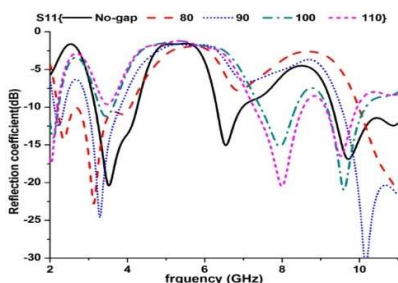


Figure 9: Reflection Coefficient v/s Frequency of the Loop Antenna without and with Capacitive Gaps at Different Locations.

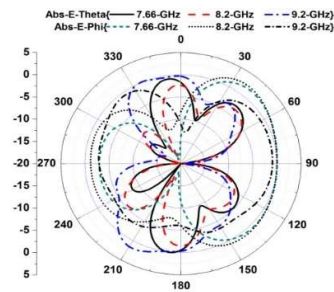


Figure 10: Radiation Pattern of Loop at 7.66 GHz, 8.2 GHz and 9.2 GHz for Capacitive Gap at 110° .

The capacitive gap is further shifted till 310° with a step shift of 10° and the reflection coefficient for all the cases are compared in Figure 11. It can be observed that there is no new band available for any of the cases. Nevertheless, the two cases of the capacitive gap at 130° and 250° are worth to consider as these cases generate a wide band, ranging from 6.4 GHz to 8.4 GHz. Out of these two cases, the reflection coefficient is better for when the gap is at 130° . Once again the antenna with C-gap at 130° and with no gap can be used as triple-band loop antenna covering a band from 6.2 GHz to 8.3 GHz and from 9 GHz to 10.6 GHz as observed in Figure 12.

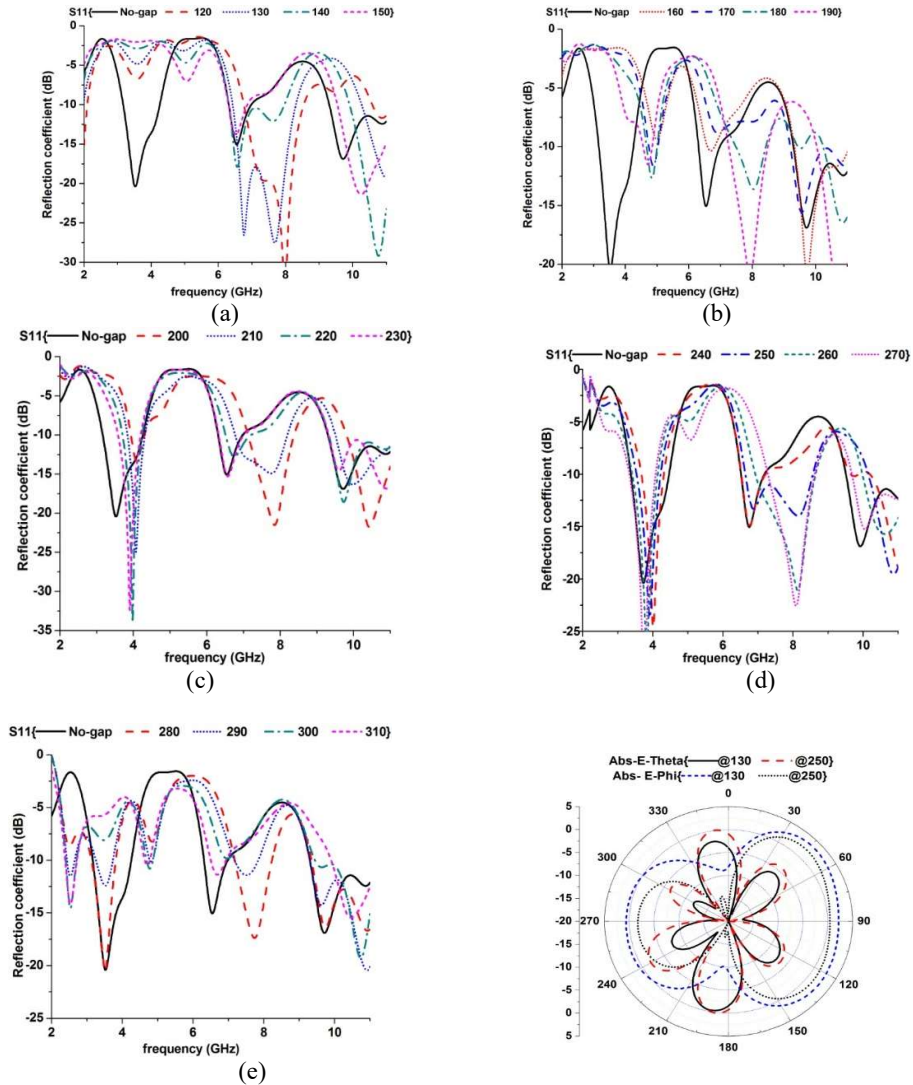


Figure 11: Reflection Coefficient v/s Frequency of the Loop Antenna without and with Capacitive Gaps at Different Locations

Figure 12: Radiation Patterns at 7.1 GHz for Capacitive Gaps at 130° and 250°.

It can be concluded that the capacitive gap introduced in the loop antenna by using a switch, reconfigures the antenna bands. The orientation of the radiation pattern of the loop can be categorized as orthogonal and parallel to the plane of the loop antenna. It is observed that the antenna radiates in the orthogonal direction when the frequency is less than 6 GHz and it is parallel to the plane of the loop and uniform along $\Phi=0$ direction above 6GHz. Table 1 summarizes the significant characteristic of multiband operations using a capacitive gap. The loop antenna with no capacitive gap generates three bands. The introduction of capacitive gap along the circumference of the loop generates new bands listed in Table 1. f_c is the center frequency of the listed band.

Gap Location	No gap		45°	60°		110°	130°/250°
f_c GHz	3.6	6.5, 10	6.2-10	2.4, 4.48	7.66	8, 9.5	7.6
Number of bands	1	2	Single wide band	2	1	2	Single wide band
Orientation of Radiation	Orthogonal to loop plane	Along the loop plane	Along the loop plane	Orthogonal to loop plane	Along the loop plane	Along the loop plane	Along the loop plane

Table 1: Summary of Different Bands Generated Using Capacitive Gap at Different Locations

The maximum number of bands is available when the switch is placed at 110° . The loop with no C-gap and gap at 110° together generates three distinct bands and covers BAND -7, BAND-9-10 and BAND-12-13-14 as shown in Figure 13. Thus the loop can cover 6 different bands using a single switch.

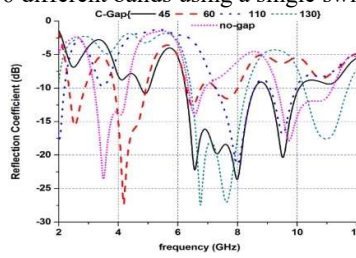


Figure 13: Various Bands Covered by C-Gap Loaded Loop Antenna

It can be observed in Figure 13 that the loop added with the capacitive gap covers all the bands from 3.1 GHz to 10.6 GHz. The band below 3 GHz is not taken into consideration. Figure 13 also shows that the antenna rejects WLAN and WiMAX bands. Figure 14 shows the band distribution for UWB band ranging from 3.1 GHz- 10.6 GHz as given in (S. P. Shastri, R. R. Singh, K.V. Ajetroa, 2018) and is used here for reference purpose. The loop antenna added with C-gap at 45° produces a very wide band of frequency when compared with the other cases of the loop antenna added with C-gap. This technique can be used to enhance the bandwidth of the loop antenna. In order to verify this band enhancement technique, other loops with different dimensions are simulated and the bandwidth of each antenna is compared. A summary of the comparison is given in Table 2.

Location of C-gap	Radius of Loop (mm)	f_1 - f_2 (GHz)	% Bandwidth
45°	13.2	6.27-10	45.9
51°	19	3.5-5	35
65°	9.5	8.7-10.5	20
f_1 - f_2 - lower and upper cut off frequencies			
Table 2. Bandwidth Enhancement Using C-Gap			

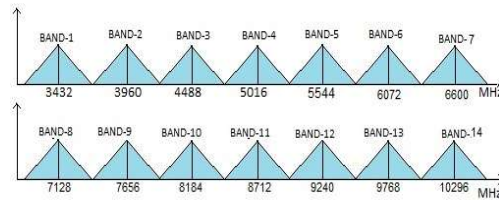


Figure 14. Band Allocation from 3.1 GHz - 10.6 GHz.

The bandwidth is larger for when the loop radius is of 13.2 mm and is minimum when the radius if 9.5 mm. The proposed technique is a simple technique to improve the antenna bandwidth. In order to find out the usefulness of the proposed technique, the result of the loop with capacitive gap is also compared with the loop with no capacitive gap and the comparison is shown in Figure 15. It can be observed that the center frequency of the obtained wide band using a capacitive gap is almost twice of the center frequency of the lowest band obtained when there is no capacitive gap for all the three cases compared in Table 2.

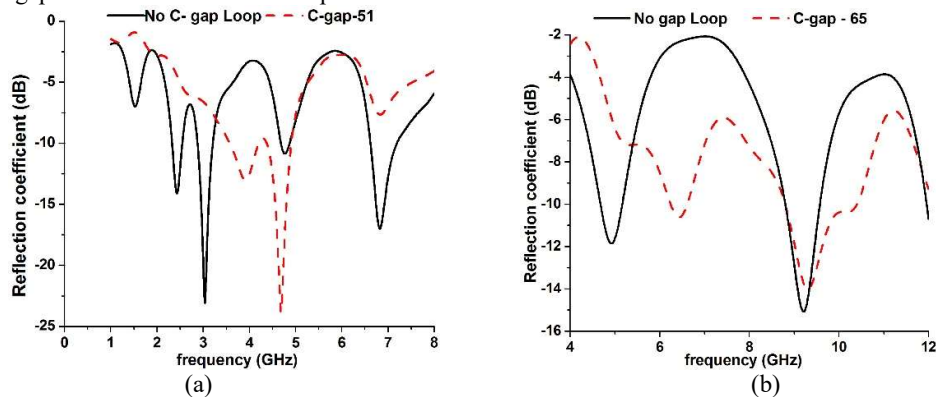


Figure 15. Reflection Coefficient of the Loop with C-Gap at (a) 51° and at (b) 65° for Loop with Radius 19 mm and 9.5 mm respectively.

Results and Discussion

In order to verify the proposed technique of generating different bands from a printed loop antenna, the antenna is manufactured and tested using VNA of series N9926A from Keysight Technologies. Figure 16 shows the photograph of the manufactured antenna.

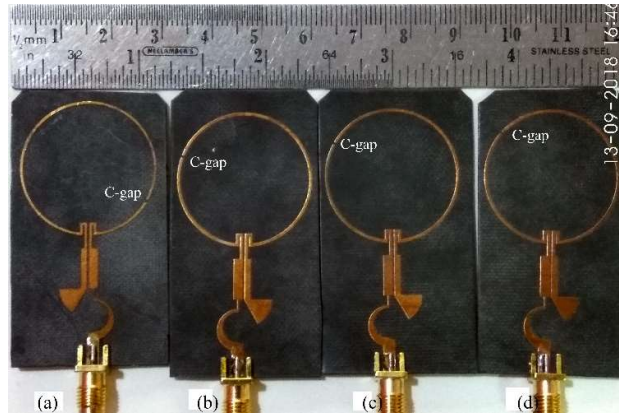
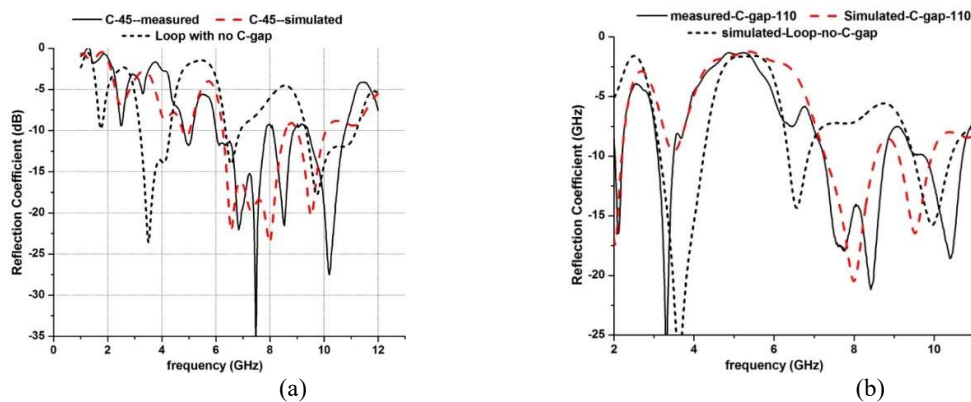


Figure 16. The Loop Antenna with C-Gap at: (a) 45° (b) 110° , (c) 120° , (d) 130° .

The measured result is compared with the simulated one and is shown in Figure 17. It can be observed that the measured results are in good agreement with the simulated result. The switch is realized using open and short circuit along the loop. The open gap is of 0.5 mm width and can be seen in Figure 16.

It can be observed here that the capacitive gap along the circumference of the loop indeed improves the usefulness of the loop as a multiband antenna. It can be observed in Figure 17 (a) that the loop, when added with the C-gap at 45° , produces a wide band from 6 GHz to 10.8 GHz. When there is no gap, the antenna covers an additional band from 3 GHz to 4.2 GHz. Therefore a total of two bands are available using a single switch. When the switch is at 110° , the antenna produces two distinct bands from 7 GHz to 8.4 GHz and from 10 GHz to 10.8 GHz. The loop with no C-gap already covers two different bands as shown in Figure 17 (b). When a single switch is used at 110° , the antenna produces total four distinct bands depending on the ON and OFF state of the switch. When the switch is at 120° , the antenna can produce three distinct bands as shown in Figure 17 (c). The performance of the loop loaded with C-gap at 130° is similar to the performance of the loop loaded with C-gap at 120° and is shown in Figure 17 (d). Since the radiation pattern of the loop is orthogonal to the plane of the loop below 6 GHz and along the loop plane above 6 GHz, the multiband can be claimed either for frequency below 6 GHz or above 6 GHz. The actual bands of operation using C-gap are listed in Table 3.



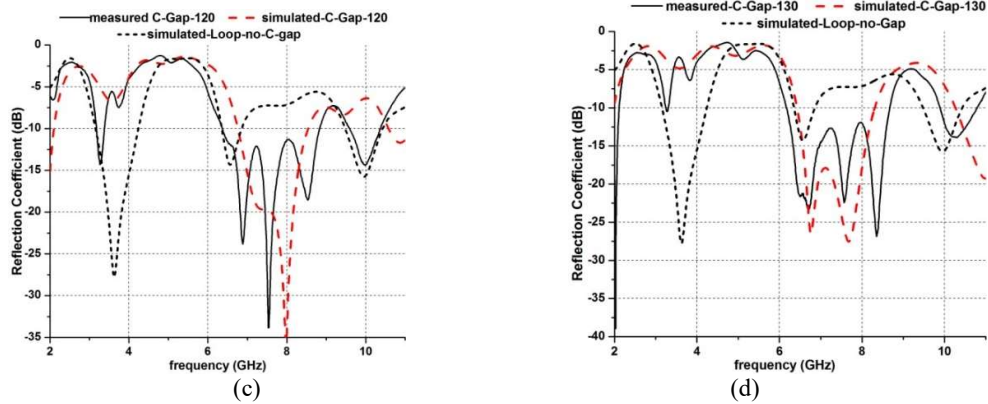


Figure 17. Proposed Loop Antenna with C-Gap at (a) 45° (b) 110°, (c) 120°, (d) 130°.

A comparison of the proposed loop is done with the other recent existing reconfigurable antennas. The summary of the comparison is shown in Table 4.

Switch location	Switch State	Bands (GHz)	Application Band	Mode
45°	ON	6.27-7, 9.45-10.5	BAND-7, BAND-12-13	Dual or single wide band
	OFF	6-10.8	BAND-7-14	
110°	ON	6.27-7, 9.45-10.5	BAND-7, BAND-12-13	Triple
	OFF	7.2-8.8, 9.4-10.7	BAND-9-11, BAND-13-14	
120°	ON	6.27-7, 9.45-10.5	BAND-7, BAND-12-13	Dual
	OFF	6.2-8.8	BAND-8-10	

Table 3. Different Modes of Operation of C-Gap Loaded Loop Antenna

R	B	Frequency (GHz)	Number of switches	Number of Antenna
[6]	2	1.8, 2.4	8	1
[7]	2	8.2, 10.4	1, MEM capacitor	1
[8]	2	15.95, 17.1	1, MEM capacitor	1
[9]	2	2.4, 5.8	Motor	2
[10]	3	1.58, 2.38	2	1
	5	1.51, 2.28	4	1
[11]	5	2.16 - 9	4	1
[12]	3	2.4, 3.5, 2	6	1
[13]	4	2.45, 3.49, 5.13, 5.81	2	1
P	1	6-10.8	1	1
	2	6.27-7, 9.45-10.5	0	1
	2	6.27-7, 6.27-8.8, 9.45-10.5	1	1
	3	6.27-7, 7.2-8.8, 10-10.5, 9.45-10.5	1	1

R-Reference, B-number of bands, P-Proposed work

Table 4: Comparative Analysis of the Proposed Antenna with the Other Existing Antennas

The antenna given by authors in (P.Tilanth, P. C. Sharma, 2014) generates two distinct bands centered at 1.8 GHz and 2.4 GHz. These two bands are generated using eight different switches. The antenna proposed by the authors in (K. Topalli et.al., 2007, 2009) are multiband antenna generating two bands at 8.2 GHz, 10.4 GHz and 15.95 GHz and 17.1 GHz respectively. Both the antennas use MEM switch for the reconfiguration. There are four antennas proposed by authors in (F. Alsharif et.al., 2016). The two antennas are used to generate the two different bands and others are used to change pattern and polarization. The two antennas used to generated different bands are selected using a rotating mechanism so the reconfiguration is controlled mechanically. The antenna proposed by authors in (S. Sharma, C. C. Tripathi, 2015) is operated with two switches and depending on the ON and OFF state of diodes, the antenna generates three different bands from 1.58 GHz to 2.38 GHz. When the same antenna is added with four diodes and is made ON or OFF in a particular sequence then it generates five different bands from 1.51 GHz to 2.28 GHz. The antenna proposed by the authors in (X. Liu, X. Yang, F. Kong, 2015) uses 4 switches and depending on the ON and OFF state of switches, it is operated as single, double and triple band antenna and generates a total 5 different bands. The antenna proposed by authors in (H. I. Idris et.al., 2014) uses 3 pairs of the diode and generates three different bands under single, dual and triple band modes. A single monopole antenna with two optical switches generates four different bands as shown in (S.A.A. Shah et.al., 2017).

The proposed antenna uses a single switch and can produce up to three different bands. The number of bands listed in Table 4 also includes the bands generated by the proposed loop when there is no C-gap added to the antenna. It can be observed that the maximum number of bands obtained from a single antenna is five given in (S. Sharma, C. C. Tripathi, 2015) and (X. Liu, X. Yang, F. Kong, 2015) but there are four switches to generate these bands. The proposed antenna can generate three different bands using only a single switch. Though the bands generated are only three but are wide enough to cover every band given in Figure 14 from 6 GHz onwards. Therefore the proposed technique improves the usefulness of the loop antenna as a multiband loop.

Conclusion

A single loop antenna is not capable of generating multiple bands which restricts the wide application of loop antenna. The proposed method of current reconfiguration in the loop antenna using switches improves the number of bands. The proposed technique successfully demonstrates the enhancement of loop bandwidth using a single switch and can be extended to any dimension of the loop. It is also found that the antenna can be used as a dual or triple band antenna using a single switch at different locations. Therefore it can also be concluded that the location of the switch not only generates different bands but also influences the bandwidth of the produced bands. The proposed loop without a switch is capable of covering only 24% of the entire band of UWB ranging from 3.1 GHz to 10.6 GHz due to the unstable radiation pattern. The range of band can be varied from 24% to 57% using the switches.

Acknowledgment

Authors are very much grateful to the ROGERS Corporation for providing Duroid substrate.

References

1. Mohamed Nasrun Osman et.al., 2015. An Electronically Reconfigurable Patch Antenna Design for Polarization Diversity with Fixed Resonant Frequency, RADIOENGINEERING, Vol. 24, No. 1.
2. Mohammed Al-Husseini et. al., 2010. A Reconfigurable Frequency-notched UWB Antenna with Splitting Resonators, Proceedings of Asia-Pacific Microwave Conference.
3. Xuelin Liu, Xiaolin Yang, and Fangling Kong. 2015. A Frequency-Reconfigurable Monopole Antenna with Switchable Stubbed Ground Structure, RADIOENGINEERING, Vol. 24, No. 2.
4. Sonia Sharma and Chandra C. Tripathi. 2015. Frequency Reconfigurable U-Slot Antenna for SDR Application, Progress in Electromagnetics Research Letters, Vol. 55, 129–136.
5. S. P. Shastri, R. R. Singh, K. V. Ajtrao. 2018. Multiband Printed Loop Antenna For UWB Applications, Helix Vol. 8(4), pp. 3481- 3490.
6. P. Tilanth, P. C. Sharma. 2014. A New Frequency Reconfigurable Antenna, J. of Active and Passive Electronic Devices, Vol. 9, pp. 133–140.
7. K. Topalli, E. Erdil, O. A. Civi, S. Demir, S. Koc, T. Akin. 2009. Tunable dual-frequency RF MEMS rectangular slot ring antenna, Sensors and Actuators A: Physical, Vol. 156, pp.373-380.
8. K. Topalli, E. Erdil, O. Aydin Civi. 2007. Reconfigurable Antenna Structures Using MEMS Technology, IEEE Transactions on Antennas and Propagation, Vol. 55, Issue: 4, pp. 392-395.
9. F. Alsharif, S. Safi, T. AbouFoul, M. Abu Nasr, S. A. Nasser. 2016. Mechanical Reconfigurable Microstrip Antenna, International Journal of Microwave and Optical Technology, Vol.11, No.3, pp. 153-160.
10. S. Sharma, C. C. Tripathi. 2015. Frequency Reconfigurable U-Slot Antenna for SDR Application, Progress in Electromagnetics, Research Letters, Vol. 55, pp.129–136.
11. X. Liu, X. Yang, F. Kong. 2015. A Frequency-Reconfigurable Monopole Antenna with Switchable Stubbed Ground Structure, Radioengineering, Vol. 24, No. 2, pp. 449-454.
12. H. I. Idris, M. R. Hamid, M. H. Jamaluddin, M. K. A. Rahim, J. R. Kelly, H. A. Majid. 2014. Single-, Dual- and Triple-band Frequency Reconfigurable Antenna, Radioengineering, VOL. 23, NO. 3, pp. 805-811.
13. S.A.A. Shah, M.F. Khan, S. Ullah, A. Basir, U. Ali, U. Naeem. 2017. Design and Measurement of Planar Monopole Antennas for Multiband Wireless Applications, IETE Journal of Research, pp. 1-11.